ASPECTS OF COLLISION-INDUCED ABSORPTION OF HYDROGEN AND DEUTERIUM

PAUL G. GILLARD

CANADIAN THESES ON MICROFICHE

I.S.B.N.

THESES CANADIENNES SUR MICROFICHE

National Library of Canada
Collections Development Branch

Canadian Theses on
Microfiche Service

Ottawa, Canada
K1A 0N4

Bibliothèque nationale du Canada
Direction du développement des collections

Service des thèses canadiennes
sur microfiche

NOTICE

The quality of this microfiche is heavily dependent upon the quality of the original thesis submitted for microfilming. Every effort has been made to ensure the highest quality of reproduction possible.

If pages are missing, contact the university which granted the degree.

Some pages may have indistinct print especially if the original pages were typed with a poor typewriter ribbon or if the university sent us a poor photocopy.

Previously copyrighted materials (journal articles, published tests, etc.) are not filmed.

Reproduction in full or in part of this film is governed by the Canadian Copyright Act, R.S.C. 1970, c. C-30. Please read the authorization forms which accompany this thesis.

THIS DISSERTATION
HAS BEEN MICROFILMED
EXACTLY AS RECEIVED

AVIS

La qualité de cette microfiche dépend grandement de la qualité de la thèse soumise au microfilmage. Nous avons tout fait pour assurer une qualité supérieure de reproduction.

S'il manque des pages, veuillez communiquer avec l'université qui a conféré le grade.

La qualité d'impression de certaines pages peut laisser à désirer, surtout si les pages originales ont été dactylographiées à l'aide d'un ruban usé ou si l'université nous a fait parvenir une photocopie de mauvaise qualité.

Les documents qui font déjà l'objet d'un droit d'auteur (articles de revue, examens publiés, etc.) ne sont pas microfilmés.

La reproduction, même partielle, de ce microfilm est soumise à la Loi canadienne sur le droit d'auteur, SRC 1970, c. C-30. Veuillez prendre connaissance des formules d'autorisation qui accompagnent cette thèse.

LA THÈSE A ÉTÉ
MICROFILMÉE TELLE QUE
NOUS L'AVONS REÇUE

Canada

NL-339 (r. 82/08)

ASPECTS OF COLLISION-INDUCED ABSORPTION OF HYDROGEN AND DEUTERIUM

BY

Paul G. Gillard, M.Sc.

A thesis submitted to the School of Graduate Studies in partial fulfillment of the requirements for the degree of Doctor of Philosophy

Department of Physics
Memorial University of Newfoundland

April 1983

St.John's Newfoundland

ABSTRACT

Induced infrared absorption spectra of hydrogen in the fundamental and second overtone regions and of deuterium in the fundamental and first and second overtone regions were investigated over a wide range of gas densities. The spectra were recorded using a 2 m high-pressure low-temperature absorption cell which was modified by the addition of a vacuum jacket to allow the cell to be cooled by immersion in liquid nitrogen. Many of the spectra were recorded with a microprocessor-controlled data acquisition system designed specifically for this purpose. This device transmitted the data to one of the larger computers on campus for further analysis.

The hexadecapole-induced U-transitions corresponding to a change of 4 in the rotational quantum number which occur in the high wavenumber wing of the hydrogen fundamental band were studied at a temperature of 77 K over a density range 500 - 900 amagat and an analysis of the absorption profiles was carried out.

In the fundamental band of deuterium, the weak S + S type double transitions arising from the anisotropy of the polarizability were studied at 77 K. Induced spectra of deuterium in the first overtone region were studied at 77, 201 and 295 K at gas densities in the range 100 - 450 amagat. The spectrum appears to have no contribution from the short-range electron overlap interaction, and the observed and theoretically predicted intensities

for the individual components of the spectrum are not in good agreement. However, an "improvement factor" proposed for the available theoretical matrix elements of the quadrupole moment of deuterium produces good agreement between the observed and calculated profiles. The anisotropic S + S type transitions in the first overtone region were also studied at 77 K for densities in the range 500 - 850 amagat. A distinct narrowing of the halfwidth of the spectral lines as a function of density was observed for the transitions of the main band as well as for the S + S transitions for densities greater than 300 amagat at 77 K.

Induced spectra of both hydrogen and deuterium in the second overtone regions were recorded at 77 K at densities in the range 500 - 930 amagat. In these spectra there is clear evidence of the contribution from the short-range overlap interaction. Transitions of the S + S type were also observed in the region of the 3-0 band of hydrogen. In the spectral region of the 3-0 bands the agreement between the observed intensities and the corresponding theoretically calculated values was rather poor.

ACKNOWLEDGEMENTS

It is with pleasure that I express my gratitude to my supervisor, Professor S. P. Reddy, for his encouragement and assistance throughout all stages of the work presented in this thesis.

I wish particularly to thank Mr. T. van Nostrand for his assistance with the experimental work, and for many discussions about the analysis.

I thank the members of my supervisory committee, Dr. C. W. Cho, Dr. N. Foltz and Dr. J. Lewis for their encouragement. I also thank Dr. J. Lewis for many useful and stimulating conversations.

I wish to thank Mr. L. Feltham, Mr. G. Power and Mr. L. Spurrell for their assistance in the construction of the cooling jacket for the high pressure cell. I also thank Mr. T. White and Mr. M. Ryan for much valuable technical assistance. As well, I thank to Mr. D. Seymour, Mr. T. Perks and Mr. M. Hatswell for their skilful glassblowing.

I am also grateful to my colleagues in the Computer Science Department, especially Mrs. J. Foltz, for their support and encouragement.

Finally, I wish to express my sincere appreciation to my wife, Gayle, for her encouragement and patience, without whose support this work would not have progressed so well.

CONTENTS

CHAPTER 1

INTRODUCTION

1.1. Induction mechanisms in molecular collisions

Symmetric diatomic molecules like hydrogen and deuterium have no permanent electric dipole moments in their ground electronic states, and therefore do not have allowed molecular absorption spectra in the infrared. Short-lived dipole moments can be induced in such molecules, however, by collisions with other molecules giving rise to "collision-induced absorption". The dipole moments so induced may be modulated by the internal rotation, vibration and relative translational motion of the colliding molecules. The induced dipole moments can interact with the electromagnetic field from an appropriate radiation source, and the colliding molecules absorb radiation in the spectral regions corresponding to vibration-rotation, pure rotation and translation. The interacting molecules may be identical as in the present work where aspects of the vibration-rotation collision induced spectra have been studied in both hydrogen and deuterium.

The phenomenon of collision-induced absorption, also known as pressure-induced absorption, was first discovered in compressed oxygen and nitrogen in their fundamental vibrational regions by Crawford et al. (1949). The collision induced absorption spectrum of the fundamental vibrational band of gaseous hydrogen was first observed by Welsh et al. (1949) and that of gaseous deuterium was observed by Reddy and Cho (1965) at room temperature, and by Watanabe and Welsh (1965) at temperatures between 24 and 77 K. Welsh (1972) has given a detailed review of the work done until 1971. A comprehensive bibliography of work in collision induced absorption

has been compiled by Rich and McKellar (1975). For more recent work, the reader is referred to Reddy et al. (1977), Sen et al. (1980), Reddy et al. (1980), Birnbaum et al. (1982), Penney et al. (1982) and the references therein.

The collision induced first overtone absorption band of hydrogen has been observed by Welsh et al. (1951). In the case of hydrogen, the observed spectrum was found to consist of a pure overtone band in which one molecule of the colliding pair makes a vibrational transition from $v = 0$ to $v' = 2$, and a double vibrational band in which each molecule of the pair simultaneously makes the transition $v = 0$ to $v' = 1$. Absorption in the first overtone region of hydrogen was further investigated by Hare and Welsh (1958) at very high densities at room temperature. Watanabe et al. (1971), Watanabe (1971) and McKellar and Welsh (1971) investigated this region at low temperatures. Recently, Silvaggio et al. (1981) have made measurements in the same region. Reddy and Kuo (1971) observed the collision-induced absorption of deuterium in the first overtone at room temperature.

Herzberg (1952) observed collision-induced absorption of hydrogen in the second overtone region. This absorption has been found to consist of a pure second overtone band in which one of the colliding molecules makes a vibrational transition from $v = 0$ to $v' = 3$, and a double vibrational band in which one molecule makes a transition from $v = 0$ to $v' = 2$ while its partner simultaneously makes a transition from $v = 0$ to $v' = 1$. A quantitative measurement of the absorption spectrum of the hydrogen second overtone region at 85 K was made by McKellar and Welsh (1971).

Collision induced spectra have a number of striking features not seen in other types of spectra. Perhaps the most striking feature is the very broad lines associated with collision induced absorption, due to the short interaction time of the colliding molecules. Because of the Maxwellian distribution of the velocities of the colliding molecules, there is a characteristically asymmetric lineshape associated with the individual lines (Chisolm and Welsh, 1954). Collision induced spectra exhibit not only single transitions in which one of the colliding molecules changes its vibration-rotation energy state, but also double transitions in which both molecules may simultaneously change their vibration-rotation energy states.

The theory of collision induced absorption was given by Van Kranendonk (1957, 1958, 1959). The dipole moment induced in a pair of colliding molecules was represented by the "exponential -4" model, in which the induced dipole moment arises from two effects, the overlap of the electron clouds of the colliding molecules, and the polarization of one molecule by the quadrupole field of another. The contribution to the dipole moment resulting from the short-range electron overlap interaction is usually called the "overlap contribution" to the induced dipole moment. The overlap contribution to the induced dipole moment decreases exponentially with intermolecular separation, R. The overlap contribution gives rise mainly to the broad $Q_{overlap}$ ($\Delta J = 0$) transitions, J being the rotational quantum number. The overlap contribution to the spectrum has a characteristic "dip" in the Q branch at the position of the corresponding free-molecular transition. This effect was explained by Van Kranendonk (1968) as an intercollisional interference effect. The intensity of the overlap contribution relative to the quadrupolar contribution is strongly dependent on temperature.

The quadrupole interaction of the colliding molecules is a relatively long range effect, and the resulting induced dipole moment is usually called the "quadrupolar contribution" to the induced dipole moment. The quadrupolar contribution to the dipole moment is anisotropic, and varies as R^{-4}. It gives rise to relatively less broad O ($\Delta J = -2$), Q ($\Delta J = 0$) and S ($\Delta J = 2$) transitions. Both single and double transitions may occur. The total polarizability consists of an isotropic part denoted by α and an anisotropic part denoted by γ. The anisotropic part of the polarizability is responsible for the S + S type double transitions, and also makes a small contribution to the other quadrupolar transitions. Thus, in the exponential -4 model the total induced dipole moment is the sum of the overlap and quadrupolar contributions.

The exponential -4 model essentially considers only asymptotic interactions: that is the effects of the short-range and long-range interactions which can induce a dipole moment in a colliding pair of molecules. A number of refinements have been made to the original theory. The effects of intercollisional interference in the overlap component of the spectrum have been detailed by Van Kranendonk (1968) and Lewis and Van Kranendonk (1971,1972). An anisotropic contribution to the overlap component in the S lines of the collision-induced band of hydrogen in H_2 - He mixtures was treated by Poll et al. (1975). Additionally, values for the hydrogen and deuterium quadrupolar and polarizability matrix elements have been calculated by Birnbaum and Poll (1969), Poll (1971), and Poll and Wolniewicz (1978). The theory has been extended to include multipole induction, principally hexadecapole induction by Karl et al. (1975).

The theory of collision induced absorption described in the previous references deals for the most part with binary collisions, and describes the behavior of systems at low gas densities. At higher densities, ternary and higher order collisions may become important. De Remigis et al. (1971) observed a narrowing of the quadrupole-induced transitions as a function of density in the fundamental band of hydrogen in H_2 - Ar mixtures at high densities. Similar effects were observed in other H_2 - rare gas mixtures by Mactaggart and Welsh (1972) and Mactaggart et al. (1973). This pressure narrowing effect has been explained by Zaidi and Van Kranendonk (1971) as a diffusional effect. Recently van Nostrand (1983), in this laboratory, has found a similar effect for transitions in the first overtone of hydrogen in the pure gas, and this work presents similar results for deuterium. This effect is interesting in the pure gas because it may allow the calculation of the self-diffusion of the gas.

In addition to the overlap and quadrupolar induction mechanisms dipoles can also be induced in the colliding molecules by higher order multipole fields, notably the hexadecapolar field. The "hexadecapolar induction" contributes a term which varies as R^{-6} to the total induced dipole moment. It gives rise to U (Δ J = 4) transitions.

1.2. Expressions for the absolute intensities in multipole induction

The absorption coefficient $\alpha(\nu)$ at wavenumber ν (cm^{-1}) for a sample of material with optical path length l is defined as

$$\alpha(\nu) = (1/l) \ln \left[\frac{I_0(\nu)}{I(\nu)} \right] \qquad (1.1)$$

where $I_0(\nu)$ is the intensity of radiation incident on the sample, and $I(\nu)$ is

the intensity of radiation which is transmitted through the sample. It is convenient to define the integrated absorption coefficient $\int\alpha(\nu)d\nu$ for collision-induced spectra. This integrated absorption coefficient can be expanded as a power series in density as

$$\int\alpha(\nu)d\nu = \alpha_1\rho^2 + \alpha_2\rho^3 + \ldots \tag{1.2}$$

where α_1 and α_2 are the binary and ternary absorption coefficients, respectively. The dependence of the integrated absorption coefficient on the square of the density, at low densities, is a characteristic property of collision induced absorption.

For comparison with theory, we define the integrated absorption as $\int\frac{\alpha(\nu)}{\nu}d\nu$. The integrated absorption can be calculated theoretically for certain mechanisms which give rise to collision-induced spectra: specifically the multipole-induced components of the collision-induced spectrum, where a dipole is induced in one molecule by the multipole field (quadrupole field, hexadecapole field, etc.) of its collision partner. The binary integrated absorption for a given molecular transition, in the case of multipole-induced absorption, can be calculated theoretically from the expression given by Poll (1971) and Karl et al. (1975) which can be written as

$$\bar{\alpha}_L^m = (1/\rho)^2\int\frac{\alpha^m(\nu)}{\nu}d\nu \tag{1.3}$$

$$= \frac{8\pi^3e^2}{3hc}n_0^2a_0^5J_L\chi_L^m \tag{1.4}$$

where

$$X_L^m = P_{J_1} P_{J_2} \left| C(J_1 L J'_1;00)^2 C(J_2 0 J'_2;00)^2 \right. \tag{1.5}$$

$$\left. \times \langle v_1 J_1 | Q_1^L | v'_1 J'_1 \rangle^2 \langle v_2 J_2 | \alpha_2 | v'_2 J'_2 \rangle^2 \right] + Y_L^m$$

and

$$J_L = 4\pi(L+1) \int_0^\infty x^{-2(L+2)} g(x) x^2 dx \tag{1.6}$$

In the above, m denotes a particular molecular transition, the subscripts 1 and 2 refer to the two interacting molecules, n_0 is the number density of the gas at NTP, e is the charge of an electron, a_0 is the first Bohr radius, the quantities $C(J L J';00)$ are the Clebsch-Gordan coefficients, the matrix elements involving Q^L are the matrix elements for L-pole inductions, the matrix elements involving α are the polarizability matrix elements, $g(x)$ is the pair correlation function for the gas and $x = R/a_0$ where R is the intermolecular separation. The quantities P_J are the Boltzmann factors and are defined as

$$P_J = Z^{-1} g_J (2J+1) \exp\left[-\frac{E_J}{kT}\right] \tag{1.7}$$

where Z is a normalization factor such that $\sum_{J=1}^{\infty} P_J = 1$, E_J is the energy corresponding to rotational state J, and the g_J are the nuclear statistical weights for the rotational states. For hydrogen, g_J = 1, 3 for J even, odd respectively; and for deuterium, g_J = 6, 3 for J even, odd, respectively.

In Eq. (1.5), the term Y_L^m is included to account for the contribution due to the anisotropy of the polarizability. This contribution is given by (McKellar and Welsh, 1971)

$$Y_L^m = P_{J_1} P_{J_2} C(J_1 L J'_1 :00)^2 C(J_2 L J'_2 :00)^2$$

$$\times \left[\frac{2}{9} \left(\langle v_1 J_1 | Q_1^L | v'_1 J'_1 \rangle^2 \langle v_2 J_2 | \gamma_2 | v'_2 J'_2 \rangle^2 \right.\right.$$

$$\left.\left. + \langle v_2 J_2 | Q_2^L | v'_2 J'_2 \rangle^2 \langle v_1 J_1 | \gamma_1 | v'_1 J'_1 \rangle^2 \right) - \frac{4}{15} \langle v_1 J_1 | Q_1^L | v'_1 J'_1 \rangle \right.$$

$$\left. \times \langle v_2 J_2 | \gamma_2 | v'_2 J'_2 \rangle \langle v_2 J_2 | Q_2^L | v'_2 J'_2 \rangle \langle v_1 J_1 | \gamma_1 | v'_1 J'_1 \rangle \right]$$

The term Y_L^m is small compared to the term X_L^m, but accounts completely for transitions of type $S_{\Delta v}(J_1) + S_{\Delta v}(J_2)$.

For H_2 and D_2 at the present experimental temperatures, only the v = 0 state of the ground electronic state is populated. In the present work collision-induced spectra of deuterium in the fundamental, first and second overtone regions those of hydrogen in the fundamental and second overtone regions have been investigated. In the hydrogen fundamental band the effect of the hexadecapolar (L = 4) transitions has been reinvestigated. For all other spectra the quadrupolar (L = 2) transitions are of primary concern. In the second overtone bands of hydrogen and deuterium there is considerable contribution to the intensity from the short-range overlap induction. A computer program was written to calculate the intensities for the L-pole induced contribution to the bands; this program is listed in Appendix A.

Our primary interest is in the integrated absorption for either a particular transition or an entire band. We must therefore sum all possible contributions to obtain the intensity of the transition or the band. For a single transition, there may be a "cyclic term" (see Poll, 1971) which is arrived at by interchanging the subscripts 1 and 2 in Eq. (1.5). The program listed in Appendix A accomplishes this by generating all possible initial states and

combining all terms with equivalent initial and final states. In the case of transitions with $\Delta v = 0$ and $\Delta J_1 = 0$, or $\Delta J_2 = 0$, one molecule may make only an orientational transition, which practically involves no change in energy. Such transitions are summed together in the program.

1.3. Lineshapes

A number of empirical lineshapes have been used to describe quadrupole-induced transitions: Chisholm and Welsh, (1954) observed that the intensities of the low- and high- wavenumber wings of collision induced lines obey the Boltzmann relation

$$\alpha^-(\nu_m - \Delta\nu) = \alpha^+(\nu_m + \Delta\nu)\ exp-(hc\,\Delta\nu/kT)$$

where ν_m is the wavenumber of the free-molecular transition, $\alpha^-(\nu_m - \Delta\nu)$ and $\alpha^+(\nu_m + \Delta\nu)$ are the absorption coefficients at wavenumbers $\nu_m - \Delta\nu$ and $\nu_m + \Delta\nu$ respectively. Kiss and Welsh (1959) found that the dispersion lineshape fitted the high wavenumber wing of the $S_0(1)$ line of hydrogen, except at the extreme high wavenumber wing where it gave too large an intensity. Hunt and Welsh (1964) combined these observations and used the following "Boltzmann-modified dispersion lineshape" for the collision-induced components in the analysis of the fundamental band of hydrogen:

$$\alpha^+/\nu = \frac{1}{1 + (\Delta\nu/\delta_q)^2} \qquad \Delta\nu \geq 0$$

$$\alpha^-/\nu = (\alpha^+/\nu)\exp(-hc\,\Delta\nu/kT) \qquad \Delta\nu < 0$$

where α^+ and α^- are as defined previously, and $\Delta\nu'$ is defined such that $\Delta\nu = |\nu - \nu_m|$.

Following Van Kranendonk (1968), Mactaggart and Welsh (1973) used the "symmetrized" lineshape as follows

$$\propto A_n \times \frac{\bar{\alpha}_n^m}{1 + (\Delta\nu/\delta)^2} \times \frac{1}{1 + \exp(-hc\,\Delta\nu/kT)} \qquad (1.8)$$

This lineshape also does not fit the observed profiles well in the extreme high wavenumber wing. Reddy et al. (1980) included a $(\Delta\nu/\delta_4)^4$ term to account for the contribution of the quadrupolar wing in the region of the hydrogen hexadecapolar U-transitions in the fundamental band. To improve the fit in the high wavenumber wing, we use the "modified symmetrized lineshape" (Lewis, 1983)

$$A_n \times \frac{\bar{\alpha}_n^m}{1 + (\Delta\nu/\delta_2)^2 + (\Delta\nu/\delta_4)^4} \times \frac{1}{1 + \exp(-hc\,\Delta\nu/kT)} \qquad (1.9)$$

where $\bar{\alpha}_n^m$ is the value for the integrated absorption as calculated from Eq. (1.4), the subscript n is 1 and 2 for quadrupolar and hexadecapolar induction respectively, and m denotes the particular molecular transition; $\Delta\nu = \nu - \nu_m$ where ν_m is the wavenumber of the transition m for the free molecule. The term A_n is a normalization factor for the lineshape used.

We find that the modified lineshape fits the observed spectra considerably better in the high wavenumber tail of the quadrupole-induced transitions. We attribute little significance to the term $\Delta\nu/\delta_4$, other than that the lineshape represented by Expression (1.9) is a higher order rational function approximation to the true lineshape than Expression (1.8). The parameter δ_4 is not constant for varying densities, and δ_4 is usually two to four times larger than δ_2. This term is particularly useful when analysing

the weaker transitions in the high wavenumber tail of the main quadrupolar spectrum; e.g., the S + S type transitions in the fundamental and first overtone bands, and the U transitions in the fundamental band.

For the overlap transitions, Levine and Birnbaum (1967) have proposed a lineshape for the translational spectrum arising from the short-range overlap interaction. Their model used a Gaussian-type dipole moment, and assumed straight-line paths for the colliding molecules. The resulting lineshape, called the Levine-Birnbaum lineshape, is given as:

$$A_0 x \left[\frac{2\Delta\nu}{\delta_d}\right]^2 K_2\left(\frac{2\Delta\nu}{\delta_d}\right) x \left[1 - \frac{1}{1+(\Delta\nu/\delta_c)^2}\right] x \frac{\bar{\alpha}_0^m}{1+\exp(-hc\,\Delta\nu/kT)} \qquad (1.10)$$

where K_2 is a Bessel function of the second kind, order 2. This lineshape has been shown (Mactaggart and Welsh, 1973, Reddy et al. 1977) to adequately describe the overlap contribution to the hydrogen fundamental band. For the overlap transitions, theoretical absolute values for the integrated absorption $\bar{\alpha}_0^m$ are not available; however, relative values can be calculated, assuming that there is no J-dependence of the matrix elements, from the Boltzmann factors alone.

Birnbaum and Cohen (1976), using an empirical dipole moment correlation function, derived the following lineshape:

$$\frac{\tau_1}{\pi}\exp\left[\frac{\tau_2}{\tau_1}\right]\exp\left[\frac{hc\,\Delta\nu}{kT}\right]\frac{z\,K_1(z)}{1+(2\pi c\,\Delta\nu\,\tau_1)^2}$$

$$z = (1/\tau_1)\left[1+(2\pi c\,\Delta\nu\,\tau_1)^2\right]^{1/2}\left[\tau_2^2 + (h/(4\pi kT))^2\right]^{1/2}$$

where K_1 is a first order Bessel function of the second kind, τ_1 and τ_2

are characteristic times in the dipole moment correlation function. τ_1 and τ_2 can be chosen to produce a correct classical value for the first two moments of the lineshape for translational spectra. This lineshape can be applied to both overlap and quadrupolar transitions, but does not account for the dip in the overlap transitions due to the intercollisional interference effect mentioned earlier. Goorvitch et al. (1981) compared this lineshape with a modified form of the Boltzmann-modified dispersion lineshape in the fundamental band of gaseous hydrogen for temperatures in the range 100 - 273 K and found that both lineshapes produced equally good fits to the experimental profiles. Silvaggio et al. (1981) used this lineshape in the analysis of the first overtone collision-induced spectrum of hydrogen.

As mentioned earlier, the collision-induced absorption spectra of hydrogen in the fundamental and second overtone regions and of deuterium in the fundamental and first and second overtone regions were recorded over a wide range of high gas densities. Chapter 2 of this thesis describes the apparatus and the experimental techniques used in this work. In particular, the details of the modifications made to an existing 2 m high-pressure low-temperature absorption cell and of a microprocessor-controlled data acquisition system specially designed for the present work are included in this chapter.

Chapter 3 presents a reinvestigation of the hexadecapole-induced U-transitions occurring in the extreme high wavenumber wing of the hydrogen fundamental band at 77 K. New data were collected over a higher range of densities than had been used in earlier experiments (Sen et al., 1980), and an improved analysis was performed.

Chapter 4 details the first analysis of the S + S type transitions in the fundamental band of deuterium at 77 K. These relatively weak double transitions occur as a result of the anisotropy of the polarizability of the deuterium molecule. In the case of deuterium, these transitions are intermixed with stronger transitions due to the isotropic polarizability, and cannot be directly observed as individual components in the gaseous phase at 77 K.

Chapter 5 presents an analysis of the absorption profiles of the induced spectra of deuterium obtained in the first overtone region for gas densities in the range 100 - 450 amagat at 77, 201 and 295 K. It is found that there is no overlap contribution to the intensity of the band, in agreement with a similar observation in the first overtone band of hydrogen. It is also found that the observed and theoretically calculated intensities of the individual components of the spectrum are not in good agreement. An "improvement factor" proposed for the available theoretical matrix elements of the quadrupole moment of deuterium gives good agreement between the observed and calculated profiles. Chapter 5 also presents the absorption profiles of the S + S type transitions at 77 K occurring in the high wavenumber wing of the main components of the band, and their analysis. A distinct narrowing of the halfwidth of the quadrupolar lines as the density increases beyond about 300 amagat was observed.

Induced spectra of both of hydrogen and deuterium in the second overtone at gas densities in the range 500 - 930 amagat at 77 K are presented in chapter 6. The observed Q_P and Q_R maxima with the associated dip in the Q branches of the spectra of hydrogen and deuterium have given a positive indication of the contribution of the overlap interaction to the intensity. An analysis of the absorption profiles was attempted but the

agreement between the observed and calculated intensities was found to be rather poor.

CHAPTER 2

APPARATUS AND EXPERIMENTAL PROCEDURES

2.1. Introduction

Spectra of the collision-induced infrared absorption of H_2 and D_2 were recorded over a wide range of densities, up to 930 amagat, and at three temperatures, 77, 196 and 295 K. A 2 m high-pressure, low-temperature absorption cell, two infrared recording spectrometers, and a microprocessor controlled data acquisition system were used to record the experimental data. Spectra in the fundamental, first and second overtone regions of D_2, and in the fundamental and second overtone regions of H_2 were recorded. A description of the apparatus and the experimental procedure is presented in this chapter.

2.2. The 2 m Absorption Cell

Initial experiments were performed using a transmission type 2 m absorption cell which was originally designed for use at room temperature and pressures to 1000 atm (Reddy and Kuo, 1971) and subsequently modified for use at low temperatures (see for example Prasad, 1976). This modification enclosed the cell in a double-walled stainless steel jacket in which the space between the walls was filled with vermiculite which acted as an insulating material. This absorption cell was used without further modification for some deuterium first overtone experiments. Unfortunately, the consumption of liquid nitrogen, when used as a coolant, was unacceptably high. Extensive modifications were therefore made to the cell, replacing the vermiculite filled insulating jacket by a stainless steel vacuum jacket, as shown schematically in Fig. 2.1.

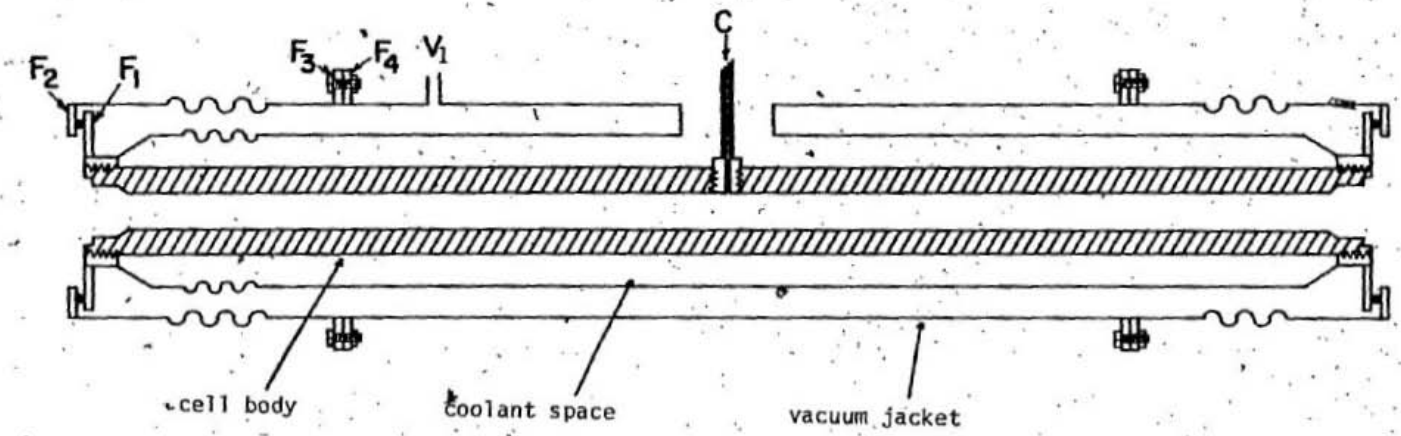

Figure 2.1 The 2 m absorption cell with vacuum jacket.

Figure 2.2 shows a cross sectional view of one end of the cell after these modifications. The high-pressure absorption cell A was constructed from a type 303 stainless steel cylinder, 2 m long and 7.62 cm in diameter, with a 2.54 cm hole bored through its centre. A polished stainless steel light guide L with a rectangular cross sectional aperture 0.50 cm x 1.00 cm was inserted into the bore to ensure good transmission of radiation through the cell. In the course of these modifications, the light guide shown in Fig. 2.2 was shortened by approximately 5 cm from its original length to allow the extension of the window seats further into the cooled region of the cell. A 1.00 cm thick sapphire window W_1 was attached with General Electric RTV-108 silicone adhesive sealant to a stainless steel window seat S having a circular aperture of 1.00 cm. The window seat S was pressed firmly against an Invar O-ring by a stainless steel retaining block R, which was held in place by eight 3/8 in. Allen head steel cap screws threaded into the face of the high-pressure cell. This produced a satisfactory high pressure seal at all temperatures.

A type 312 stainless steel nut N, about 7.62 cm in diameter and 1.5 cm long was threaded onto the ends of the cell. A solid stainless steel flange F_1 and a stainless steel cone C were welded to this nut, as illustrated in Fig. 2.2. The flange F_1 was drilled and tapped for eight 10-24 machine screws, which held the outer jacket end piece in place. A 10.2 cm diameter stainless steel bellows B_1 was welded to the stainless steel cone to allow for relative expansion and contraction of the cell and the vacuum jacket. The outer jacket end piece consisted primarily of flanges F_5, F_2 and F_3, and bellows B_2, approximately 16.5 cm in diameter, all of stainless steel. This end piece was attached to the outer jacket by eight 1/4 - 20

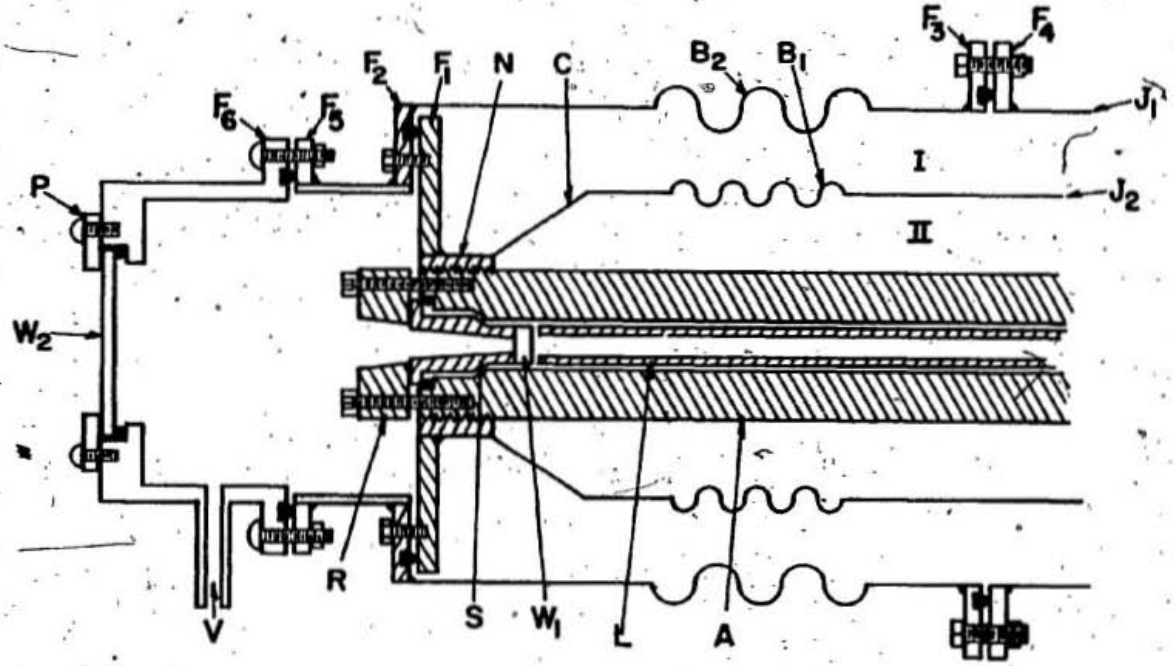

Figure 2.2 A cross-sectional view of one end of the 2 m absorption cell.

screws and nuts by flanges F_3 and F_4. Flanges F_1 and F_2 were held together by eight 10 - 24 machine screws. An RTV silicone rubber O-ring type seal was formed between F_1 and F_2. Attached to F_2 was a short stainless steel tube and another flange, F_5. Flange F_5 was sealed with a neoprene O-ring to the flange F_6 of an end cap made of Delrin which was normally evacuated through vacuum port V_1 to prevent condensation on window W_1. A sapphire window W_2, 5.08 cm in diameter and 0.30 cm thick was sealed to the end of the plastic end cap by a Plexiglas ring, P. Heating tapes were wrapped around the end of the cell near flange F_2 to keep the O-ring seal from freezing. Chamber I was normally evacuated through a vacuum port V (shown in Fig. 2.1). Chamber II was filled with a coolant, usually liquid nitrogen, through an opening in the central section of the jackets J_1 and J_2, as shown in Fig. 2.1. A gas inlet to the cell was provided by means of a 1.27 cm Aminco fitting.

Photographs of the assembled cell, a view of one end of the cell and a view of the internal structure of one of the outer jacket end pieces during assembly are shown in Fig. 2.3 (a), (b) and (c) respectively.

The modifications to the absorption cell considerably reduced the consumption of liquid nitrogen coolant, allowing the experiments to be carried out more economically and for longer periods of time. Also, virtually the entire length of the high pressure cell was in contact with the coolant, producing a more uniform temperature in the cell.

2.3. The Gas Handling System

Since many of the experiments required high pressures to be developed, up to 12,000 psi at liquid nitrogen temperatures, two large stain-

Figure 2.3 Photographs of the high-pressure low-temperature cell used in the experiments.

(a) An overall view of the cell.

(b) A view of one end of the cell (under construction) showing the cell body and the inner jacket.

(c) One end of the completed cell, showing the window mount and the Delrin end cap.

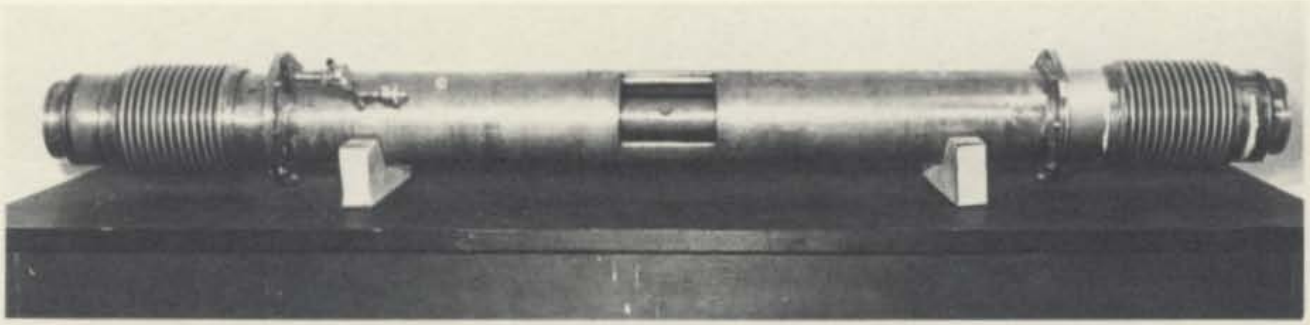

(a)

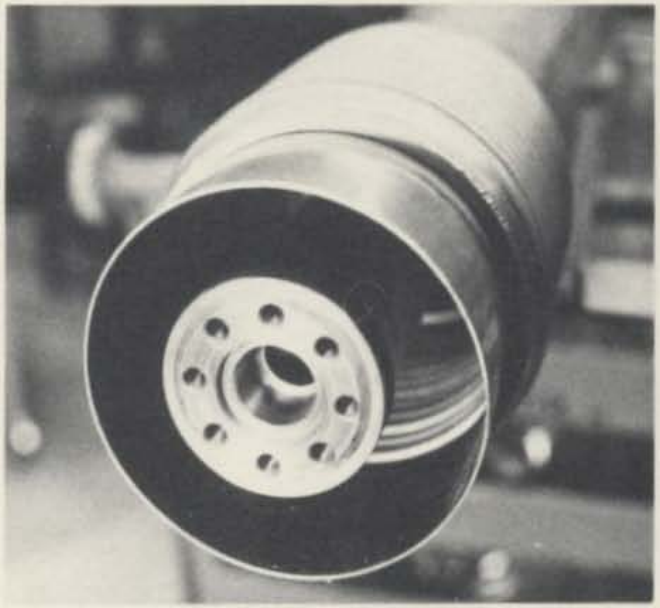

(b)

(c)

less steel reservoirs, each with a volume of about 0.5 litre were constructed to act as thermal compressors. Gas from a cylinder at room temperature and typically at about 1500 psi was alternately cooled to 77 K and warmed to room temperature in a series of reservoirs to generate the required pressures. A typical gas handling system is illustrated in Fig. 2.4. T_1 is a thermal compressor in which the first stage of compression was done. Gas from one of the cylinders was allowed to enter T_1 after passing through a copper coil, with both the copper coil and T_1 immersed in liquid nitrogen. The copper coil thus acted as a trap for any impurities in the gas. T_1 was then closed off from the cylinder,and allowed to warm. The gas from T_1 was then allowed to enter one of the large reservoirs, R_1 or R_2, which were also immersed in liquid nitrogen. This process was repeated until sufficient gas was collected in the reservoirs. One of the large reservoirs was then warmed, and the gas allowed to enter the other (cold) reservoir. This process could be repeated several times. If necessary, reservoirs R_1 and R_2 could be opened to the cell independently. The gas in the reservoir at the lower pressure was consumed first, and then sealed off. Gas was then taken from the higher pressure reservoir. T_2 was a high pressure, low volume thermal compressor, used to develop the highest pressures. This technique was advantageous when developing high pressures with a limited quantity of deuterium, and was much simpler than other techniques such as using an oil compressor.

In Fig. 2.4, G_1, G_2 and G_3 were Bourdon tube pressure gauges, manufactured by Ashcroft. They were calibrated against mirrored test gauges, which in turn were calibrated with a dead-weight pressure gauge. Gauges with ranges 0 - 5000 psi, 0 - 10,000 psi and 0 - 20,000 psi were

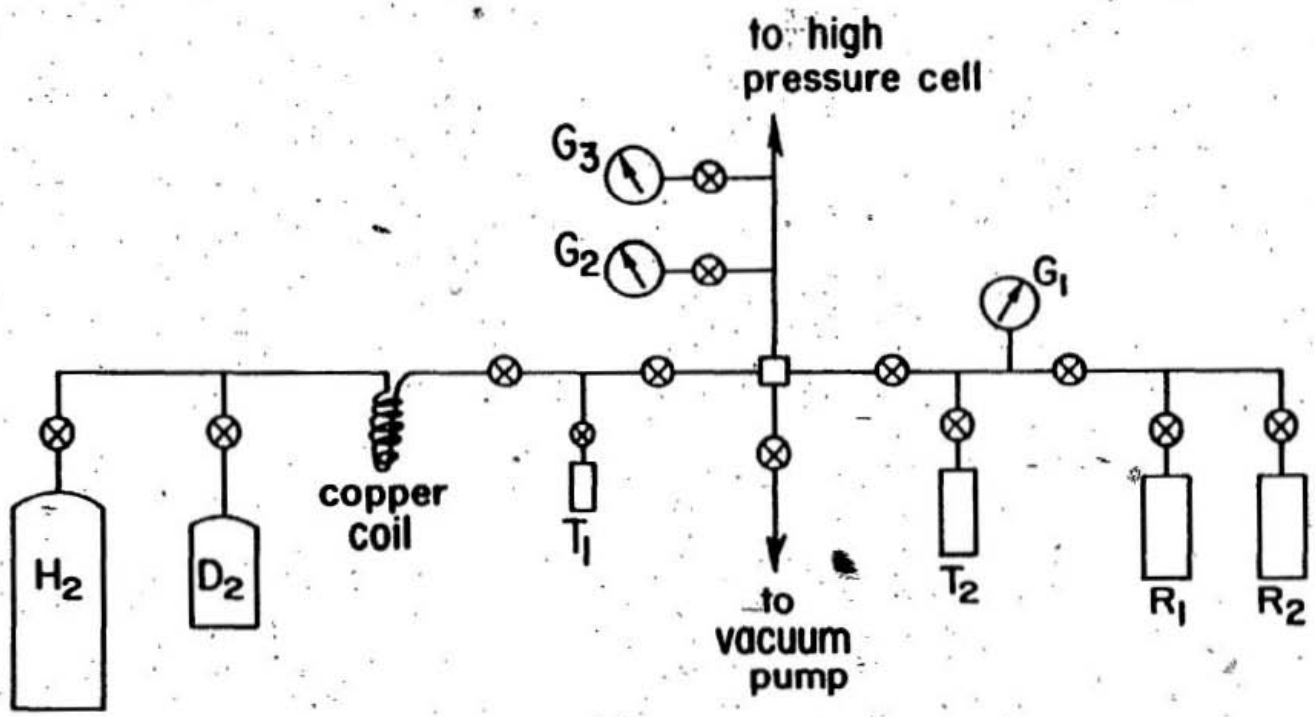

Figure 2.4 The gas handling system.

normally used. All fittings except those of the copper coil and the gas cylinder were Aminco stainless steel fittings, rated for pressures up to 60,000 psi.

For the experiments at 77 K, the level of liquid nitrogen surrounding the high pressure cell was maintained automatically by a Rochefort Liquid Nitrogen Level Controller which operated an ASCO 3/8 in. solenoid valve on a liquid nitrogen line from a 200 litre container. Pressure was maintained in the container by a compressed air line in the laboratory.

The "ultra high purity" grade hydrogen and "chemical purity" grade deuterium used in the experiments were supplied by Matheson of Canada Ltd.

2.4. Removal of Water Vapor From the Optical Path

Since some of the spectra of interest were in spectral regions of strong water vapor absorption, it was necessary to remove as much of the atmospheric water vapor as possible from the light path between the source and the optical detector. This was accomplished by enclosing the light source and its associated optics in an airtight Plexiglas box. This box was then attached to one end of the absorption cell by an airtight rubber seal. The spectrometer was placed in a similar box attached to the other end of the absorption cell. Dry nitrogen evaporating from a 200 litre container of liquid nitrogen was continually flushed through these boxes, and allowed to escape through one-way valves attached to each box. This arrangement typically reduced the intensity of water vapor absorption to a stable and acceptable level over a period of 3-5 days.

2.5. The Spectrometers and Optics

The optical arrangement, shown schematically in Fig. 2.5, was the same for all experiments. In all the experiments except those in the deuterium fundamental band, the light source L was a 600 W. General Electric FFJ Quartzline lamp, housed in a water cooled brass jacket and positioned close to the end of the absorption cell. The lamp was operated at a voltage between 60 - 90 V, depending on the spectral region. The voltage applied to the lamp was controlled by a Variac autotransformer which was connected to an a.c. voltage regulator. For the experiments in the deuterium fundamental band, the light source was a globar (silicon carbide rod) held in a water cooled metal housing and operated at a constant temperature of ~1500 K. Power was supplied to the globar from a Source Radiation Controller Model 10, supplied by Warner and Swansey Co., Flushing, N. Y. Radiation from the light source, L, was focused onto the entrance window of the cell A using a 15 cm diameter f/4 aluminized concave spherical mirror M_1. Light which passed through the absorption cell was focused by another similar mirror, M_2, onto the entrance slit of the spectrometer S. The spectrometer was inclined at an angle of approximately 30 degrees to the axis of the cell.

Two different spectrometers and detectors were used for the experiments. For the H_2 second overtone experiments, a Perkin-Elmer model 112G double pass grating spectrometer was used. This instrument contained a grating ruled with 300 lines/mm., blazed at an angle of $26^0 45'$. A Hamamatsu type R758 photomultiplier tube (PMT) was placed directly behind the exit slit of the monochromator, inside the spectrometer box. The PMT was mounted in a magnetic shield supplied by Hamamatsu and modified to

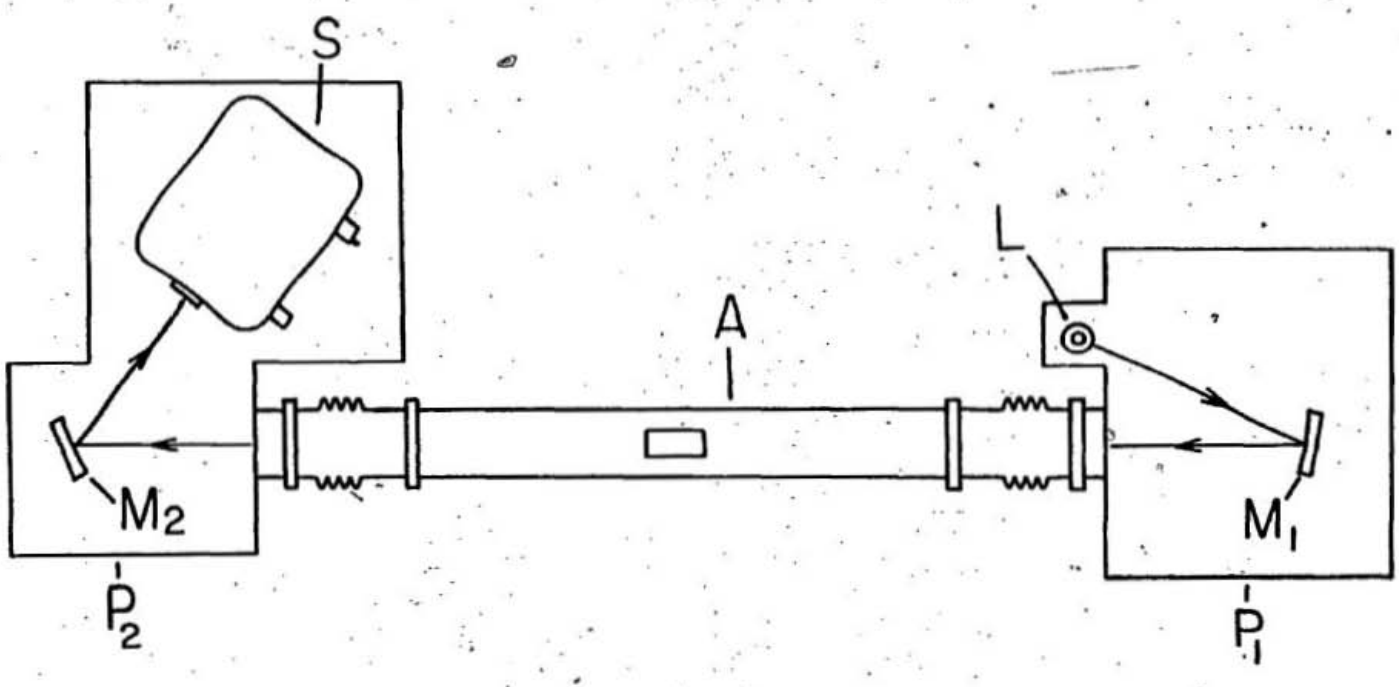

Figure 2.5 The optical arrangement: A - absorption cell, L - source lamp
M_1 and M_2 - spherical mirrors, S - spectrometer
P_1 and P_2 - plexiglas boxes

fit inside the spectrometer. A small light-tight box was constructed of brass shimstock to fit around the exit slit of the spectrometer and the PMT housing to keep stray light to a minimum. All such objects which were placed inside the spectrometer housing were painted flat black to reduce scattered light. A hole was bored in the cover of the spectrometer to allow the base of the PMT to protrude so that electrical connections could readily be made. This opening was made light-tight by a rubber gasket.

All other experiments were performed with a modified Perkin-Elmer model 112 double pass spectrometer using a lithium fluoride prism and an uncooled lead sulphide detector.

2.6. The Signal Recording System

Figure 2.6 shows a block diagram of the electronics for the signal recording system. After passing through the cell, the radiation which entered the spectrometer was dispersed by a dispersing element (prism or grating). This radiation was then chopped by a 260 Hz tuning fork chopper, reflected back to the dispersing element again, and was finally focused on the exit slit of the spectrometer. The radiation passing through the exit slit was either focused on a PbS detector by appropriate optics or allowed to fall directly on a photomultiplier tube which was housed immediately behind the exit slit. (See Prasad, 1976 for a further description.) The detector produced an output signal proportional to the intensity of the radiation incident on it. This signal was first amplified by a preamplifier and then by a lock-in amplifier. A reference signal was supplied to the lock-in amplifier from the power supply for the tuning fork chopper, and the in-phase component of the input signal was amplified.

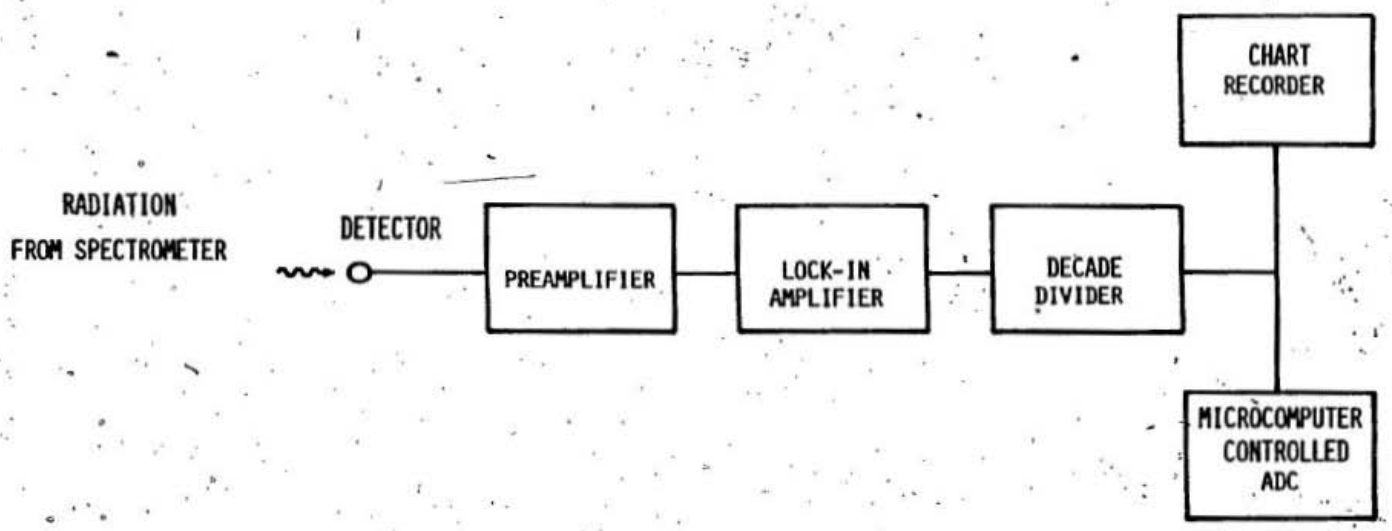

Figure 2.6 A block diagram of the signal recording system.

For the H_2 second overtone experiments, the signal from the Hamamatsu type R758 PMT, was amplified by a Princeton Applied Research model 184 current sensitive preamplifier and a PAR model 124A lock-in amplifier. For the experiments in the D_2 fundamental region a liquid nitrogen cooled PbS detector was used; for all other experiments, a PbS detector, operated at room temperature, was used; with both PbS detectors, a Brower Laboratories model 261 preamplifier and a Brower model LI-100 lock-in amplifier were used to amplify the signal. The remaining equipment was the same for all experiments.

A decade divider was required to attenuate the output of the lock-in amplifier (0 - 10 V) to a range acceptable to the analog-to-digital converter (ADC). The ADC accepted an input of 0 - 2 V, and produced a decimal number in the range 0 - 4000 as output. The strip chart recorder was a Hewlett-Packard model 7132A. The data from the deuterium first overtone experiments and the D_2 fundamental S+S experiments were analyzed completely from the chart recorder traces. Data from other experiments, however, were analyzed with the microprocessor controlled ADC system.

Figure 2.7 shows a block diagram of the microprocessor-controlled ADC system. This system was designed by the author to eliminate the time-consuming steps involved in manually reducing the experimental data and entering it into the computer for analysis. The system was designed to imitate the operation of the chart recorder. The ADC samples and digitizes the output of the lock-in amplifier at 0.5 second intervals, and sends the digital output to one of the large computers on campus, normally the VAX 11-780 system of the Computer Science Department.

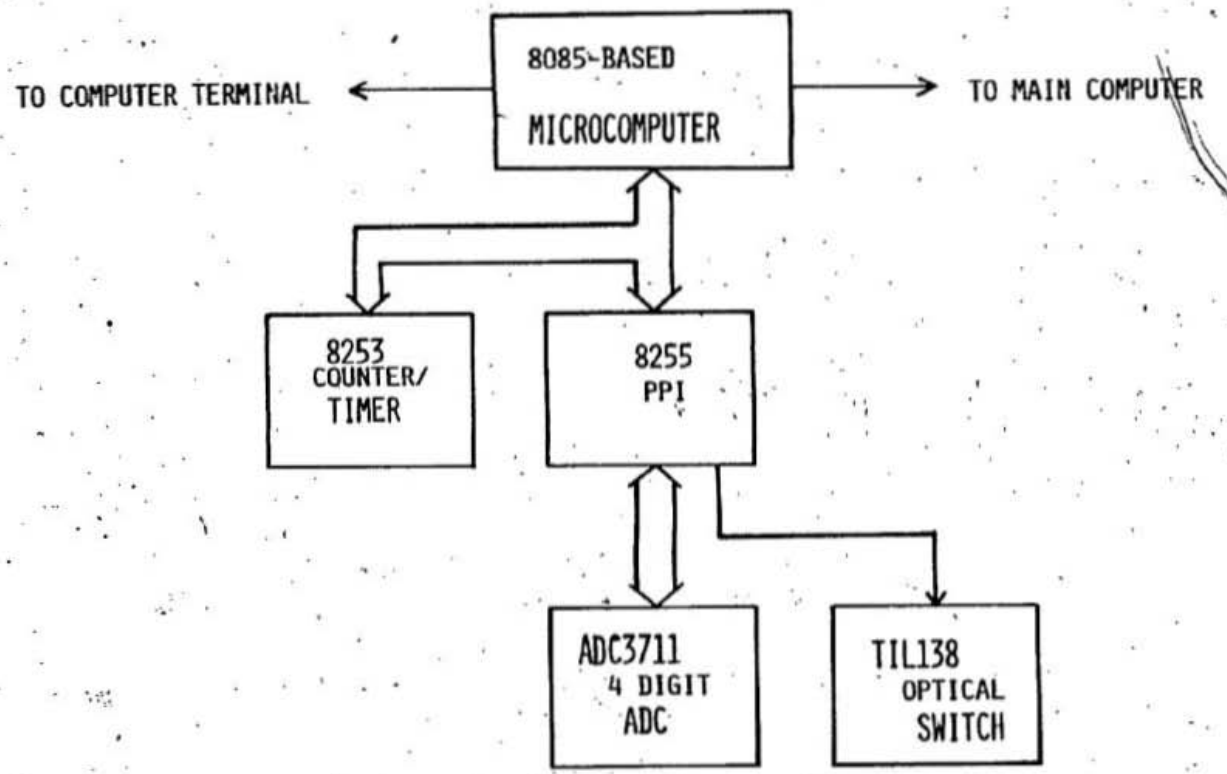

Figure 2.7 A block diagram of the microprocessor-controlled data acquisition system.

The microcomputer itself, which is based on the INTEL 8085 microprocessor, was supplied in kit form by Netronics R&D. Ltd. It incorporates the "standard" S-100 microcomputer bus, and therefore it is relatively a straightforward process to add additional components to the microcomputer system. The microcomputer contains an interpreter for the BASIC language, thus any programming required to control peripheral devices could be done in BASIC.

The ADC used in the present work is the model ADC3711 single chip A/D converter manufactured by National Semiconductor Corporation. It employs a pulse modulation technique, which averages the input voltage over the conversion time. The ADC is capable of performing at the rate of five conversions per second, and continually performs conversions at this rate internally. When the microcomputer requires a value from the ADC, it must wait until the current conversion is complete; this value is then provided as the output from the ADC. There is, therefore, an uncertainty of up to 0.2 second between the time a value is requested and the time it is made available to the microcomputer. The clock input to the ADC is derived by doubling the frequency of the microprocessor clock (3.072 MHz), and dividing this frequency by 10 to obtain a 614.4 KHz signal with a 50% duty cycle. The output of the ADC is a 4 digit decimal number in the range 0 - 4000. The reference voltage for the ADC is set at 2.000 V ,so the resolution of the ADC is 0.5 mV. The output from the ADC must be read one digit at a time, and each digit can be addressed separately.

Since the control functions required for the ADC are complex, the ADC is controlled by another programmable device, the INTEL 8255 Parallel Peripheral Interface (PPI). This device contains two 8-bit input/output ports and one 6-bit input/output port, all individually programmable. Two of these ports

are used to control the operation of the ADC and provide other functions.

The Intel 8253 counter/timer provides the critical timing signals for the data acquisition system. This device contains three programmable counter/timers, which can be individually programmed to operate in any of five modes. In the present application, counter 0 was programmed to produce a square wave output with a frequency of (1/24) x the input frequency. The input frequency was half the crystal-controlled clock frequency of the microcomputer of 3.072 MHz, or 1.536 MHz. Counter 0 therefore produced an output frequency of 64 KHz. This output was connected as the input to counter 1, which was programmed to produce a single pulse output whenever 32,000 input pulses had been received; thus it produced a single output pulse each half second. This output pulse was sent directly to the "start conversion" input of the ADC3711, and caused the ADC to respond with a "conversion complete" signal at the end of the current conversion cycle. The "conversion complete" signal was sent to the 8255 PPI, and was continually monitored by the microcomputer. When this signal was detected by the microcomputer, it read the data from the ADC3711 and sent the result to the main computer. The output of counter 1 was also used as an input to counter 2. Counter 2 was initialized at the beginning of each trace, and merely kept a record of the number of half second intervals from the start of the trace. The value of counter 2 was read whenever the ADC was read, and its value was also sent to the main computer.

In order to compare two traces, it was necessary to provide some reference position common to both traces. This was accomplished by attaching a thin brass disc with eight equally spaced radial slots milled in it to the drive shaft of the spectrometer. A TIL138 optical switch assembly,

consisting of a light-emitting diode (LED) and a phototransistor in a single plastic housing separated by a 0.318 cm air gap, was attached to the body of the spectrometer so that light from the LED was blocked by the brass disc. When the disc rotated to a point where light could pass through one of its slits, the phototransistor was turned on. The output of the transistor was connected to the input of a Schmitt trigger inverter, and then to one of the inputs of the 8255 PPI. An experiment was started by positioning the spectrometer drive shaft so that no light from the LED could pass through a slit in the brass disc; the spectrometer drive was then engaged. The microcomputer continually sampled the output of the phototransistor, and when the phototransistor was found in the "on" state, the microprocessor started the timers which controlled the sampling of the ADC. It was found that this technique worked quite well, with trace to trace registration usually within 0.5 second. In addition, a sharp reference line from either a mercury or neon lamp was recorded, to provide a reference position on the strip chart record.

Appendix A contains a copy of the BASIC program which controlled the ADC system.

2.7. Spectral Calibration and Absorption Coefficient Calculation

The spectrometers were calibrated in the regions of interest with the standard wavenumber measurements of the mercury emission lines (Zaidel et al. 1970) and the absorption lines of the water vapor spectrum (Humphreys, 1953 and Plyer et al., 1955). For the calibration of the H_2 second overtone region, standard wavelengths of neon and argon lines were used (C. R. C. Handbook of Chemistry and Physics, and the A. I. P. Handbook of Physics).

For the calibration of the D_2 fundamental region, absorption lines of water vapor (IUPC Tables of Wavenumbers for Calibration of Spectrometers, 1977), HCN, CH_4, HCl, and HBr (Rao et al., 1966) were used. A polynomial least squares fit of the observed wavenumbers against chart positions was performed. Polynomials up to fifth order were required for calibration of the prism instrument. For the grating instrument, a first order polynomial fit of wavelength against chart position was found to be adequate.

For data recorded by the microprocessor controlled data acquisition system, the quantity $ln(I_0/I)$ was calculated for each point by taking the logarithm of the ratio of the intensity I_0 transmitted by the evacuated cell to the intensity I transmitted by the cell filled with the experimental gas at a given density. Background traces, with the cell evacuated, were recorded at the beginning and end of each set of experiments. The initial and final background traces were compared, and if there were significant discrepancies the data were discarded. Additionally, the quantity $ln(I_0/I)$ was calculated using the initial and final traces separately, to ensure that the results were consistent. When the data were recorded using only the chart recorder, the quantity $\log_{10}(I_0/I)$ was obtained directly from the chart recorder trace for each experiment, using a standard logarithmic scale. These measurements were made at intervals determined by superimposing on the chart recorder trace a calibration chart with lines at fixed intervals of 5 cm^{-1} or 10 cm^{-1}, depending on the spectral region.

In both cases, the absorption coefficient $\alpha(\nu) = (1/l)ln(I_0/I)$, where l is the optical path length of the cell.

2.8. Isothermal Data and Density Calculation

The isothermal data required to calculate densities for hydrogen and deuterium at 201 and 295 K were obtained by linear interpolation of the data published by Michels et al. (1959) at temperatures 200 K and 225 K, and 275 K and 300 K, respectively. To obtain densities for pressures which were not tabulated, a least-squares polynomial was fitted to the tabulated data, and the resulting expression used to calculate the density at other pressures within the range of the tabulated data. For hydrogen at 77 K and for high densities, the data tabulated by McCarthy et al. (1981) was used.

For deuterium at 77 K and densities greater than 200 amagat, no isothermal data were available. However, if the pressure difference between H_2 and D_2 at a given density was plotted as a function of density, the resulting graph was found to be virtually independent of temperature. Figure 2.8 shows such a graph with data at several temperatures. The data used was obtained from the data of Michels et al. (1959). Since no points were available at 77 K, an experiment was performed to measure the density of D_2 at a pressure near the maximum density used in these experiments. This single point is also plotted in Fig. 2.8. This graph can therefore be used to relate the density of deuterium to that of hydrogen at any temperature from 77 K to 400 K, and very likely over a more extended temperature range. For our purposes, this graph allowed the calculation of deuterium densities from the available data for hydrogen.

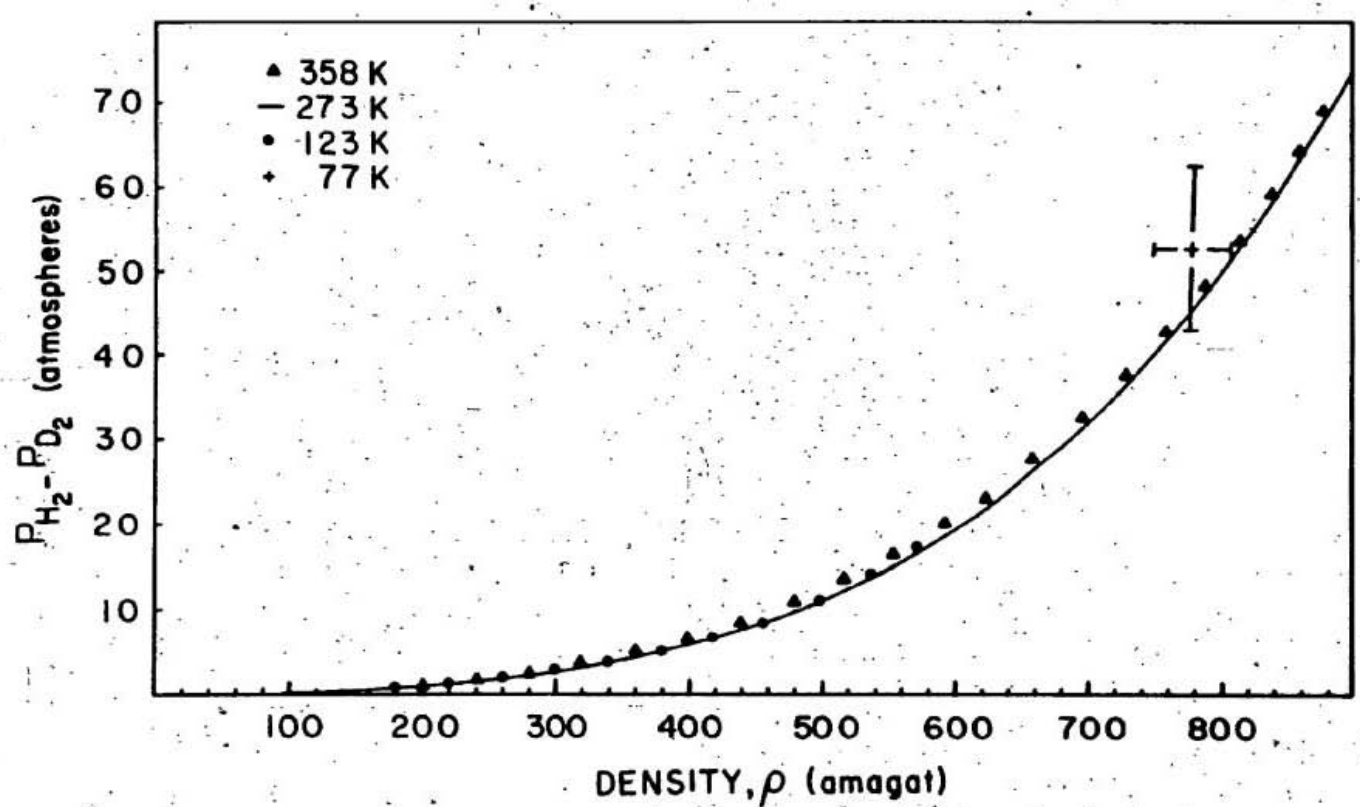

Figure 2.8 A plot of the difference in pressure of H_2 and D_2 against density at several temperatures.

CHAPTER 3

ABSORPTION SPECTRA OF THE U BRANCH TRANSITIONS OF THE FUNDAMENTAL BAND OF NORMAL H_2 AT 77 K

3.1. Introduction

The collision-induced absorption of the fundamental band of gaseous hydrogen has been the subject of numerous experimental and theoretical investigations for more than three decades. References to the earlier work on this band are given in Chapter 1. The induced electric dipole moment in a pair of colliding molecules is a function of the intermolecular separation R and the relative orientation of each molecule with respect to $\vec{R}$. As mentioned in Chapter 1, the dipole moment induced in one molecule by collision with another can be represented as the sum of several terms. In the induced fundamental band of hydrogen, a short range overlap term, a long range quadrupolar term and an intermediate range hexadecapolar term contribute to the intensity. Thus the total induced dipole moment can be written as

$$\mu_{ind}(R) = Ae^{-BR} + CR^{-4} + DR^{-6} \qquad (3.1)$$

where A, B, C and D are constants; Ae^{-BR} is the short-range electron overlap induced dipole moment, CR^{-4} is the long-range quadrupole-induced, angle-dependent dipole moment, and DR^{-6} is the intermediate-range hexadecapole-induced, angle-dependent dipole moment. The first term gives rise mainly to the broad $Q_{overlap}(J)$ single transitions with $\Delta J = 0$. The second term gives rise to $O(J)$, $Q(J)$ and $S(J)$ transitions with $\Delta J = -2, 0, 2$, respectively. In the quadrupolar induction mechanism, the isotropic

part of the polarizability contributes to the intensity of the single transitions $O_{\Delta v}(J)$, $Q_{\Delta v}(J \neq 0)$, $S_{\Delta v}(J)$, and the double transitions $O_{\Delta v}(J) + Q_{\Delta v}(J)$, $Q_{\Delta v}(J) + Q_{\Delta v}(J)$ and $Q_{\Delta v}(J) + S_{\Delta v}(J)$. The anisotropic part of the polarizability gives rise to the double transitions $S_{\Delta v}(J) + S_{\Delta v}(J)$ and makes a small contribution to the other quadrupolar transitions. The third term in Eq. (3.1) gives rise to the rotational selection rule $\Delta J = 0, \pm 2, \pm 4$. The hexadecapolar U transitions ($\Delta J = 4$) of the form $U_1(J)$ and $Q_1(J) + U_1(J)$ in the fundamental band of hydrogen have been observed in the gas by Gibbs et al. (1974) and in the solid by Prasad et al. (1978). Reddy et al. (1980) studied these transitions for densities in the range 300 - 500 amagat for a path length of 194.9 cm at 77 K and analysed the experimental profiles.

In Eq. (1.4) which gives the integrated binary absorption for various multipole-induced transitions, the quadrupole- and hexadecapole-induced transitions correspond to L = 2 and L = 4 respectively. The U transitions are in general much weaker than the quadrupole-induced transitions. This effect is seen in the configurational integral J_L (Eq. 1.6), which represents the average of the square of the L-pole induced dipole moment. For L = 2, J_L is proportional to $(a_0/\sigma)^5$ and for L = 4, J_L is proportional to $(a_0/\sigma)^9$, σ being the Lennard-Jones intermolecular separation.

In the present work the collision-induced absorption in the U branch of the fundamental band of hydrogen has been studied at gas densities in the range 500 - 900 amagat. The experiment was performed with a modified version of the 2 m absorption cell described in Chapter 2, and a Perkin-Elmer model 112 double pass spectrometer equipped with an LiF prism and an uncooled PbS detector. The spectrometer slit width maintained at 35 μm gave a spectral resolution of about 7.5 cm^{-1} at the position of the $U_1(1)$

line, 5696 cm^{-1}. This experiment also served as a test experiment for the performance of the microprocessor-controlled data acquisition system described in Chapter 2.

3.2. Experimental absorption profiles

Figure 3.1 shows four absorption profiles at various densities between 605 and 894 amagat in the region of the U transitions for the H_2 fundamental band. The positions of the $U_1(1)$, $U_0(1) + Q_1(1)$ and $U_0(1) + Q_1(0)$ transitions are marked on the wavenumber axis. The absorption profiles shown in the figure are taken directly from the microprocessor-controlled data acquisition system. Normally three traces obtained under identical conditions were averaged, but no attempt was made to further smooth or digitally filter the resultant profiles. The clear absorption peak (5740 cm^{-1}) corresponds to the transitions $U_1(1)$ (5695.4 cm^{-1}) and $Q_1(1) + U_0(1)$ (5776.9 cm^{-1}) although from the analysis six components (see Table 3.1) are found to contribute to the intensity of the absorption profiles at 77 K.

3.3. The profile analysis

The U transitions are relatively weak lines occurring on the high wavenumber tail of the main H_2 collision-induced spectrum, consisting of many relatively intense components. The tail of these intense components was modeled by a single line with the lineshape (see Reddy et al., 1980)

$$\bar{\alpha}(\nu) = \frac{\alpha(\nu)}{\nu} = \frac{a_1}{1 + (\Delta\nu/a_2)^2 + (\Delta\nu/a_3)^4} \qquad (3.2)$$

where a_1, a_2 and a_3 are parameters to be fitted, and $\Delta\nu = \nu - \nu_q$. ν_q is the position of the nearest strong quadrupolar component, $S_1(1) + S_0(1)$

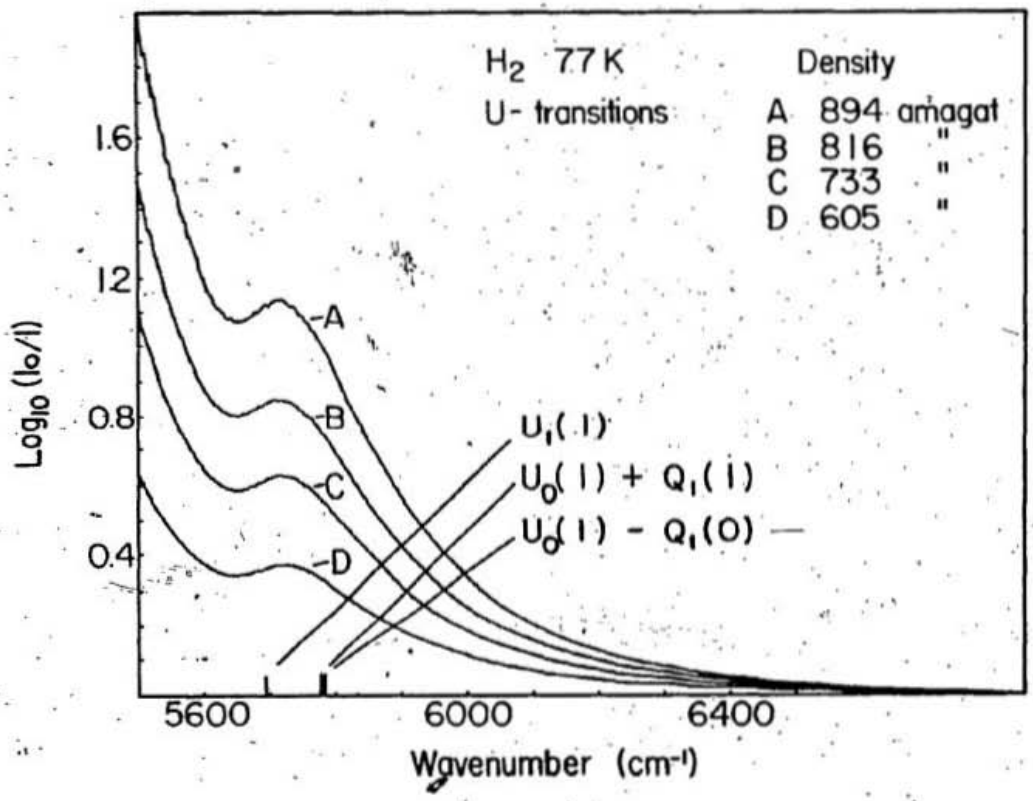

Figure 3.1 Absorption profiles in the region of the U - transitions in the fundamental band of H_2 at various densities.

(5399.1 cm^{-1}).

The lineshape adopted for the U transitions was the "symmetrized" dispersion lineshape (see, for example Mactaggart and Welsh, 1973), as follows:

$$\bar{\alpha}_h(\nu) = \frac{\alpha_h(\nu)}{\nu} = A_h \; x. \; \frac{\bar{\alpha}_h^m}{1 + (\Delta\nu/\delta_h)^2} \; x \; \frac{1}{1 + exp(-hc\,\Delta\nu/kT)} \qquad (3.3)$$

where $\bar{\alpha}_h^m$ is the intensity of a particular hexadecapolar component calculated from Eq. (1.4). δ_h is the characteristic halfwidth of the hexadecapolar component. $\Delta\nu = \nu - \nu_m$, where ν_m is the molecular wavenumber in cm^{-1} of the particular hexadecapolar component. This lineshape represents an empirical "broadening" function for the theoretical value calculated from Eq. (1.4): where A_h is defined so that the integrated absorption $(1/\rho^2)\int \alpha_h(\nu)/\nu d\nu$ is equal to the quantity $\bar{\alpha}_h^m$.

In this analysis, we assume that all the hexadecapolar components have the same halfwidth δ_h (Poll, 1960) which is to be fitted from the observed profiles. Also, although we calculate absolute intensities for each hexadecapolar component, we use only their intensities relative to the strongest U transition, $U_1(1)$ at 5695.4 cm^{-1} and leave the absolute intensity as an adjustable parameter. The theoretical value of this parameter can readily be calculated for each density and compared with the experimental result.

The absolute and relative intensities for the hexadecapolar transitions of the band at 77 K were calculated by the program given in Appendix A, using the matrix elements of Karl et al. (1975) and their values are listed in Table 3.1.

TABLE 3.1 Calculated Intensities for the H_2 U-transitions at 77 K

Transition	Wavenumber (cm^{-1})	Absolute Intensity (cm^{-1} $amagat^{-2}$)	Relative Intensity
$U_1(0)$	5271.4	.8195e-10	.6851e+00
$U_0(0) + Q_1(1)$	5324.0	.9351e-11	.7817e-01
$U_0(0) + Q_1(0)$	5330.0	.3088e-11	.2581e-01
$U_1(1)$	5695.4	.1196e-09	.1000e+01
$U_0(1) + Q_1(1)$	5776.9	.1612e-10	.1348e+00
$U_0(1) + Q_1(0)$	5782.8	.5324e-11	.4451e-01

The experimental profiles were analysed using the non-linear least squares lineshape program given in Appendix A, with the lineshape subroutine given in Appendix A. There are five parameters to be fitted, three of which characterize the high wavenumber wing of the main collision-induced absorption spectrum, corresponding to the parameters a_1, a_2 and a_3 in Eq. (3.2), and two of which correspond to the halfwidth δ_h and the intensity A_h of the hexadecapolar lines from Eq. (3.3). The latter two characterize the hexadecapolar components.

A total of 15 profiles was analysed, at densities ranging from 500 to 900 amagat. Figure 3.2 shows the relative intensities of each component in a typical observed profile; the agreement between the observed and fitted profiles was very good. The characteristic halfwidth δ_h obtained from the profile analysis and the corresponding collision duration τ_h are presented in Table 3.2. Also included in this table are the corresponding values obtained by Reddy et al. (1980). The values of the parameters a_2 and a_3 in Eq. (3.2) vary between 200 and 230 cm^{-1} and 300 and 330 cm^{-1} respectively for the profiles analysed.

The integrated absorption coefficient for the $U_1(1)$ transition was calculated from the area for the fitted profiles. A graph of $(1/\rho^2)\int\alpha(\nu)d\nu$ against ρ was plotted in Fig 3.3. A straight line was fitted to these points, and the binary and ternary absorption coefficients were calculated; the results are summarized in Table 3.3 and compared with the results of Reddy et al. (1980).

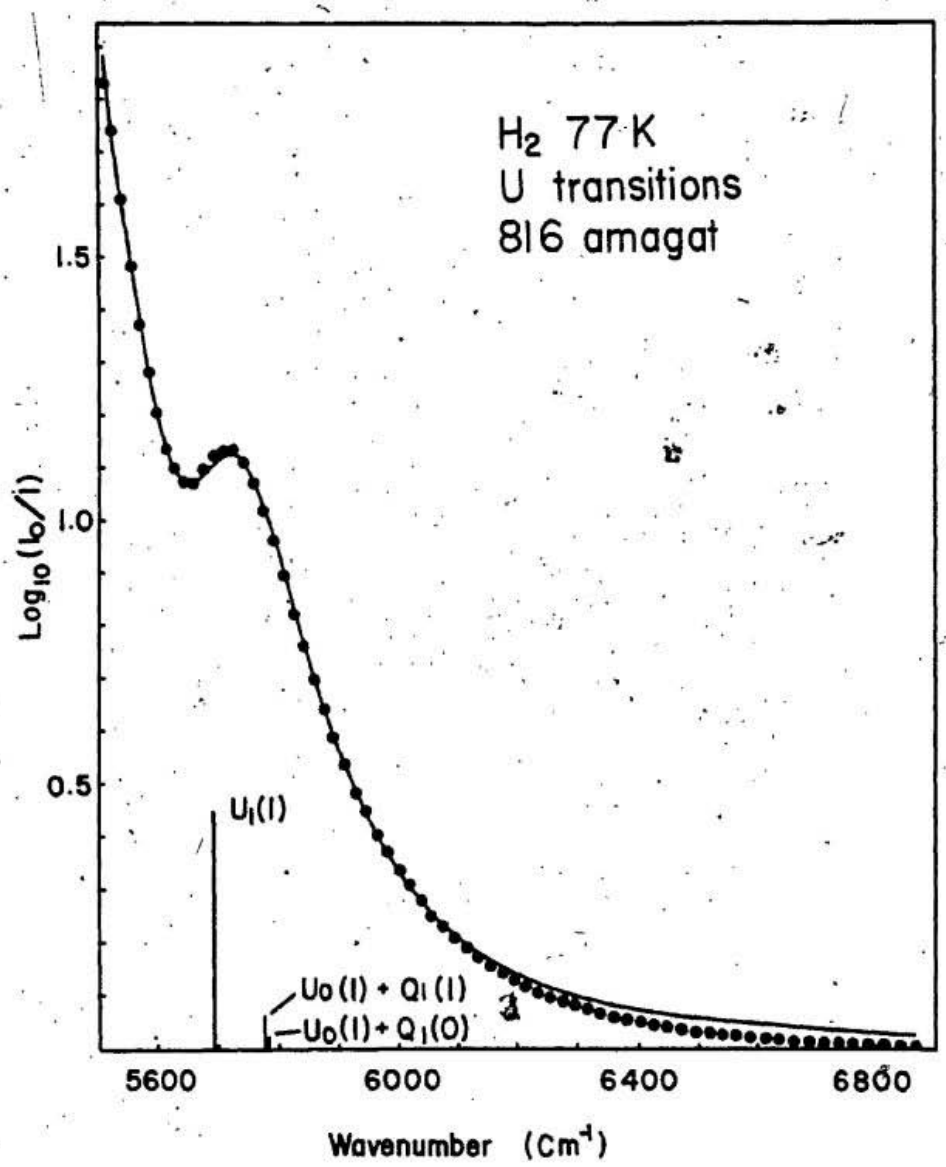

Figure 3.2 Analysis of an absorption profile of the fundamental band of H_2 at 77 K with an absorption path length of 187.1 cm. The dots are the experimental points; the solid curve is the fitted profile.

TABLE 3.2. Results of Profile Analysis of the H_2 U Transitions at 77 K

Hexadecapolar half-width δ_h (cm^{-1})	Collision duration* τ_h ($10^{-14}s$)	References
124 ± 2	4.3 ± .1	Present work
118 ± 8	4.5 ± .3	Reddy et al. (1980)

* $\tau_h = \frac{1}{2\pi c \delta_h}$

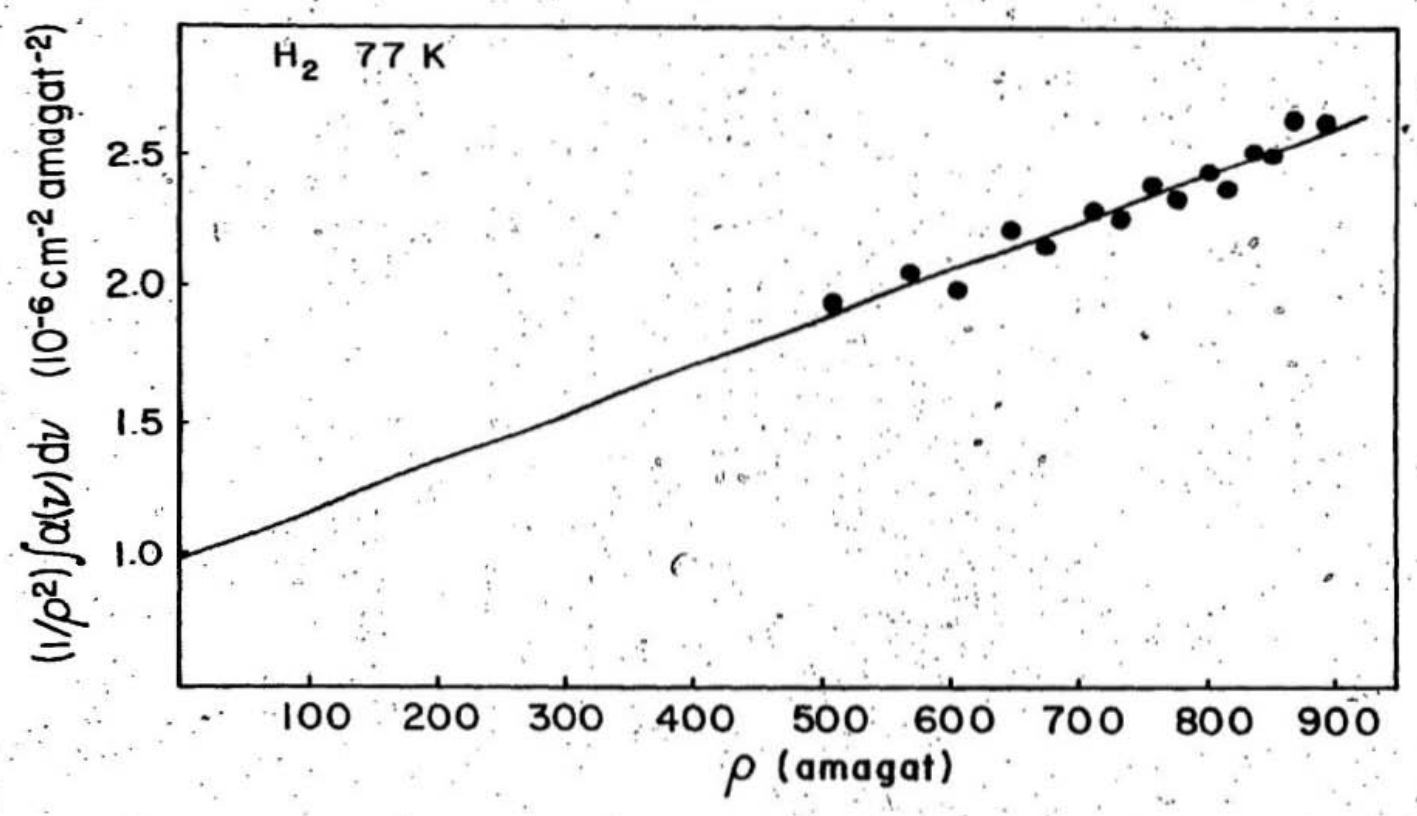

Figure 3.3 A plot of $(1/\rho^2)\int\alpha(\nu)d\nu$ against density ρ for the $U_1(1)$ transition.

TABLE 3.3 Absorption Coefficients of the $U_1(1)$ Transition at 77 K

Binary Absorption Coefficient			Ternary Absorption Coefficient	
Experiment		Theory		
α_{1a} (10^{-6} cm^{-2} $amagat^{-2}$)	$\bar{\alpha}_{1a}$ (10^{-38} cm^6 s^{-1})	$\bar{\alpha}_{1a}$ (10^{-38} cm^6 s^{-1})	α_{2a} (10^{-9} cm^{-2} $amagat^{-3}$)	
0.98 ± .09	0.69 ± .07	0.50	1.8 ± .13	(a)
1.38 ± .09	0.98 ± .06	0.50	0.17	(b)

(a) Present work

(b) Reddy et al. (1980)

3.4. Conclusions

The hexadecapolar U transitions in normal hydrogen at 77 K were analysed using the "symmetrized" dispersion lineshape function as a "broadening" function for the intensities calculated from the theory of Karl et al. (1975). The hexadecapolar-induced halfwidth for this lineshape was derived, and a value obtained for the binary and ternary absorption coefficients. There is, however, a considerable discrepancy in both the binary and ternary coefficients derived from this experiment, and those of Reddy et al. (1980). These earlier results were obtained with lower gas densities of H_2 than those used in the present work, and consequently the absorption spectra were weaker. Also, the number of data points used in fitting each profile was considerably less, about 50 points in the previous work compared with about 500 points in the present work. In both cases, however, it should be noted that for the calculation of the ternary coefficient, a separate, individual component could not be used; rather, a component derived from the preceding analysis based on the theory of Karl et al. (1975) which is valid only for binary collisions was used. Therefore the value of the ternary absorption obtained from this analysis is considered to be approximate.

The absolute intensity of the $U_1(1)$ transition calculated from Eq. (1.4) is 1.20×10^{-10} cm^{-1} $amagat^{-2}$ (Table 3.1). The corresponding experimental value obtained from the present work is $(1.67 \pm 0.16) \times 10^{-10}$ cm^{-1} $amagat^{-2}$, which exceeds the theoretical value by 40 ± 15 percent. For the quadrupolar $S_1(1)$ component the theoretical value for the absolute intensity is 0.43×10^{-7} cm^{-1} $amagat^{-2}$. The value obtained experimentally was $0.53 \pm 0.01 \times 10^{-7}$ cm^{-1} $amagat^{-2}$ (Reddy et al., 1977) which exceeds the theoretical value by 23 ± 2 percent.

CHAPTER 4

ABSORPTION SPECTRA OF S + S TYPE TRANSITIONS IN THE FUNDAMENTAL BAND OF NORMAL D_2

4.1. Introduction

Recently the collision-induced fundamental band of normal deuterium in the pure gas at 77, 196 and 298 K was studied in detail for a number of gas densities up to 60 amagat with 2 m and 2.1 m absorption cells in this laboratory by Penney et al. (1982). The experimental absorption profiles were analysed using the Levine-Birnbaum lineshape (Eq. 1.10) and a dispersion-type line shape proposed by Van Kranendonk (1968) for the intracollisional part and intercollisional part respectively of the overlap-induced Q components [$Q_{1\,overlap}(J)$], and the symmetrized dispersion lineshape for the quadrupole-induced single [$O_1(J)$, $Q_{1\,quad}(J \neq 0)$ and $S_1(J)$] and double [$Q_1(J) + Q_0(J)$ and $Q_1(J) + S_0(J)$] transitions. Similar work on the fundamental band of H_2 and HD was also reported by Reddy et al. (1977) and Reddy and Prasad (1977) respectively. Figure 4.1 shows the absorption profile of the fundamental band of deuterium at a gas density of 37.8 amagat at 77 K, from Penney et al. (1982). In the analysis of the absorption profiles in Fig. 4.1, transitions corresponding to J = 0, 1 and 2 were taken into account, although the weaker transitions with J = 2 are not shown in the diagram for the sake of clarity. The main contribution to the intensity of the quadrupole-induced transitions in Fig. 4.1 arises from the isotropic part of the polarizability of the colliding molecules. However, as mentioned in Chapter 1, the anisotropic part of the polarizability gives rise to the relatively weaker double transitions of the type $S_1(J) + S_0(J)$ which occur in

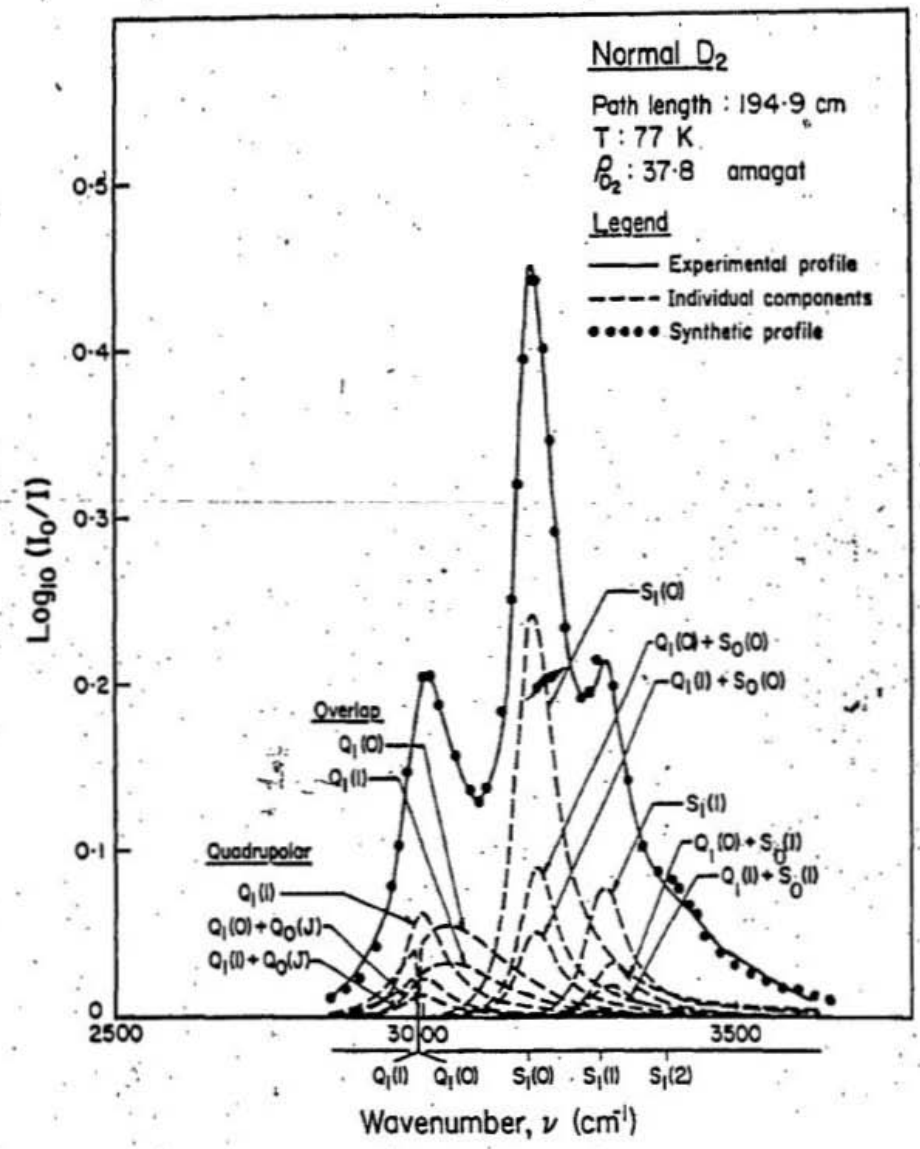

Figure 4.1 Absorption profile of the collision-induced fundamental band of normal D_2. The solid curve is the experimental profile, the dashed curves represent the computed individual overlap and quadrupole-induced components and the dots represent the sum of these components. The weaker components with J = 2 are not shown. (From Penney et al., 1982).

the high wavenumber wing of the main quadrupolar transitions shown in Fig. 4.1. A detailed study of the double transitions $S_1(J) + S_0(J)$ in gaseous hydrogen has been recently reported by Sen et al. (1980).

In the absorption spectrum of normal hydrogen, almost all transitions arise from the initial rotational levels J = 0 and J = 1, whereas in the spectrum of normal deuterium at 77 K transitions also arise from the level J = 2 with considerable intensity. In fact, the ratio of the intensities of the $S_1(1)$ and $S_1(2)$ components of normal hydrogen at 77 K is 0.01 whereas a similar ratio for normal deuterium is 4.34. Because of the negligible population of hydrogen in the J = 2 level at 77 K and the large value of its rotational constant, the $S_1(1) + S_0(1)$ component in its absorption spectrum at 77 K is reasonably well resolved (see Sen et al., 1980). However, the weak $S_1(J) + S_0(1)$ transitions in normal deuterium at 77 K are masked not only by the high wavenumber tail of the more intense transitions of the main band involving J = 0 and 1 but also transitions arising from J = 2, as will be seen in the next section.

4.2. Experimental absorption profiles

In the present work, the absorption profiles of the deuterium fundamental band in the region 3300 - 3700 cm^{-1} were recorded for densities in the range 80 - 140 amagat at 77 K with the 2 m absorption cell. The source of radiation was a globar held in a water cooled metal housing and operated at a constant temperature of ~ 1500 K. Details of the source, the spectrometer, the recording system and other experimental considerations are described in Chapter 2. The spectrometer slit width maintained at 65 μm gave a spectral resolution of about 3 cm^{-1} at 3345 cm^{-1}, the position of

the $S_0(0) + S_0(0)$ transition of D_2.

Several absorption profiles were recorded at various gas densities in the range 80 to 140 amagat. Absorption profiles for gas densities 97, 116 and 137 amagat in the spectral region 3300 - 3700 cm^{-1} are shown in Fig. 4.2. The positions of four transitions of the type $S_1(J) + S_0(J)$ with J = 0, 1 and 2 calculated from the molecular constants for the free D_2 molecule (McKellar and Oka, 1978) are shown along the wavenumber axis. Figure 4.2 also shows the location of the group of transitions corresponding to the transitions $S_1(2)$ and $Q_1(J) + S_0(2)$. Although there is some evidence of a broad peak at about 3580 cm^{-1} in the absorption profile at 137 amagat, the structure of the various $S_1(J) + S_0(J)$ components is masked by the high wavenumber wing of the main band. One of the aims of the present work is to extract the weak features of the $S_1(J) + S_0(J)$ transitions from the relatively strong background of the main quadrupolar components of the band.

4.3. The profile analysis

At 77 K there are four principal components which contribute to the S + S type double transitions. The absolute and relative intensities for the S + S type transitions were calculated by the program in Appendix A, using the matrix elements of the anisotropy of the polarizability of Poll (1983), and the quadrupolar matrix elements of Birnbaum and Poll (1969). Table 4.1 shows the relative and absolute intensities of the important S + S type transitions, together with those of other relatively intense transitions in the region.

The experimental profiles were fitted to all of the quadrupolar lines; the intensity was calculated for each line including any contribution from the

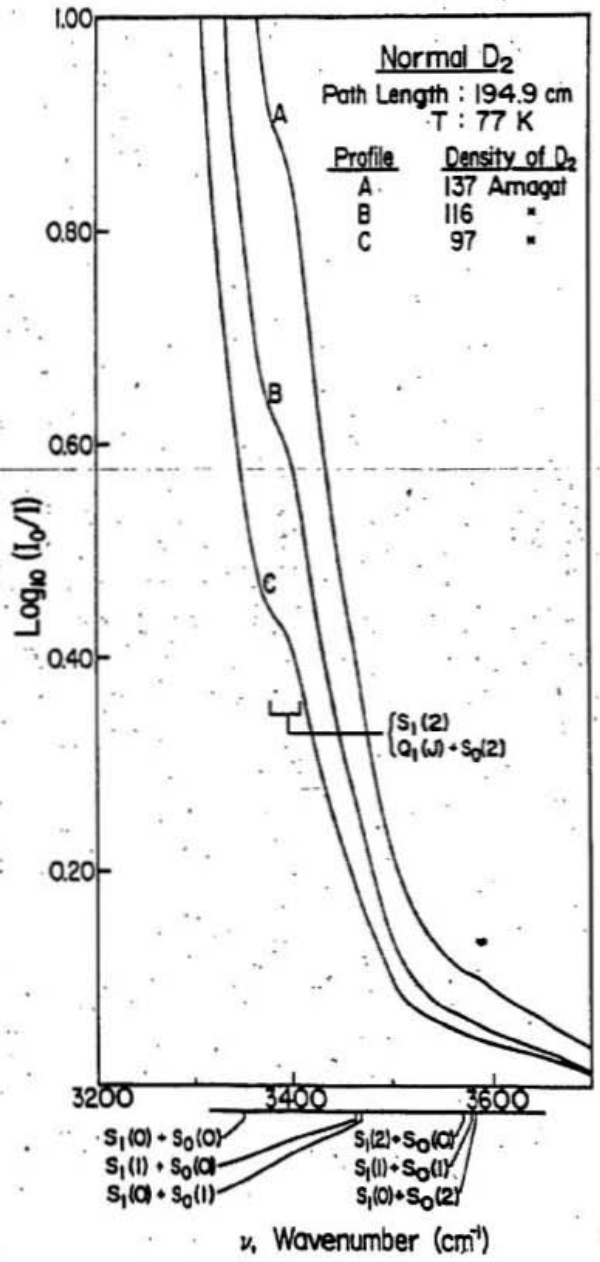

Figure 4.2 Absorption profiles of the collision-induced fundamental band of normal D_2 in the spectral region 3200 - 3700 cm^{-1} where there is significant contribution from S + S type transitions.

TABLE 4.1 Calculated Intensities of the transitions in normal D_2 at 77 K

Transition	Wavenumber (cm^{-1})	Absolute Intensity (cm^{-1} $amagat^{-2}$)	Relative Intensity
$Q_1(3) + S_0(0)$	3160.1	.9940e-10	.2006e-02
$S_1(0)$	3166.4	.4956e-07	.1000e+01
$Q_1(2) + S_0(0)$	3166.4	.3343e-08	.6745e-01
$Q_1(1) + S_0(0)$	3170.6	.1126e-07	.2271e+00
$Q_1(0) + S_0(0)$	3172.7	.1786e-07	.3604e+00
$S_1(1)$	3278.5	.1548e-07	.3124e+00
$Q_1(2) + S_0(1)$	3284.8	.1174e-08	.2370e-01
$Q_1(1) + S_0(1)$	3289.0	.3955e-08	.7979e-01
$Q_1(0) + S_0(1)$	3291.1	.6275e-08	.1266e+00
$S_1(2)$	3387.3	.3585e-08	.7233e-01
$Q_1(2) + S_0(2)$	3401.9	.3062e-09	.6179e-02
$Q_1(1) + S_0(2)$	3406.1	.1031e-08	.2081e-01
$Q_1(0) + S_0(2)$	3408.2	.1636e-08	.3301e-01
$S_1(3)$	3492.1	.8774e-10	.1770e-02
$S_0(0) + S_1(0)$	3345.4	.3054e-08	.6161e-01
$S_0(0) + S_1(1)$	3457.6	.1005e-08	.2028e-01
$S_0(1) + S_1(0)$	3463.9	.1073e-08	.2164e-01
$S_0(0) + S_1(2)$	3566.3	.2456e-09	.4955e-02
$S_0(1) + S_1(1)$	3572.1	.3532e-09	.7126e-02
$S_0(2) + S_1(0)$	3581.0	.2797e-09	.5643e-02
$S_0(1) + S_1(2)$	3684.8	.8627e-10	.1741e-02
$S_0(2) + S_1(1)$	3693.2	.9208e-10	.1858e-02

anisotropy of the polarizability. This profile analysis was carried out using the non-linear least squares lineshape program given in Appendix A. The lineshape chosen is a variant of the "symmetrized" dispersion lineshape as given in Eq. (1.9) and requires three parameters: namely, an intensity and two "halfwidth" parameters, δ_2 and δ_4 to be fitted. The analysis of a typical absorption profile is shown in Fig. 4.3. The fit of the synthetic profile to the observed profile was found to be satisfactory.

Small shifts of the S + S type double transitions from the positions of their free molecular wavenumber in the fundamental band of hydrogen at 77 K were observed (see Sen et al., 1980 and van Nostrand, 1983). A similar fit using a fourth, "shift", parameter corresponding to a shift from the free molecular wavenumber ν_m for each transition was attempted in the present analysis. This "shift" parameter was added to all the free molecular quadrupolar wavenumbers. The results of this analysis showed that the best fit was obtained when a shift of 8 cm^{-1} ± 6cm^{-1} was used. However, there was no significant improvement in the quality of the fit to the experimental profiles whether or not the shift parameter was used. There appears, therefore, to be no strong reason to conclude that these transitions are shifted from their free molecular positions. This conclusion is supported by the analysis of Penney et al. (1982) in their analysis of the fundamental band of deuterium.

The parameter δ_2 remained virtually constant over the entire density range, with an average value of 41.4 cm^{-1}, and values varying from 39 - 43 cm^{-1}. The corresponding value for the main band of deuterium measured by Penney et al.(1982) is 37 ± 1 cm^{-1}. The parameter δ_4 varied over the range 59 -71 cm^{-1}. Table 4.2 shows the values for δ_2 and δ_4 at

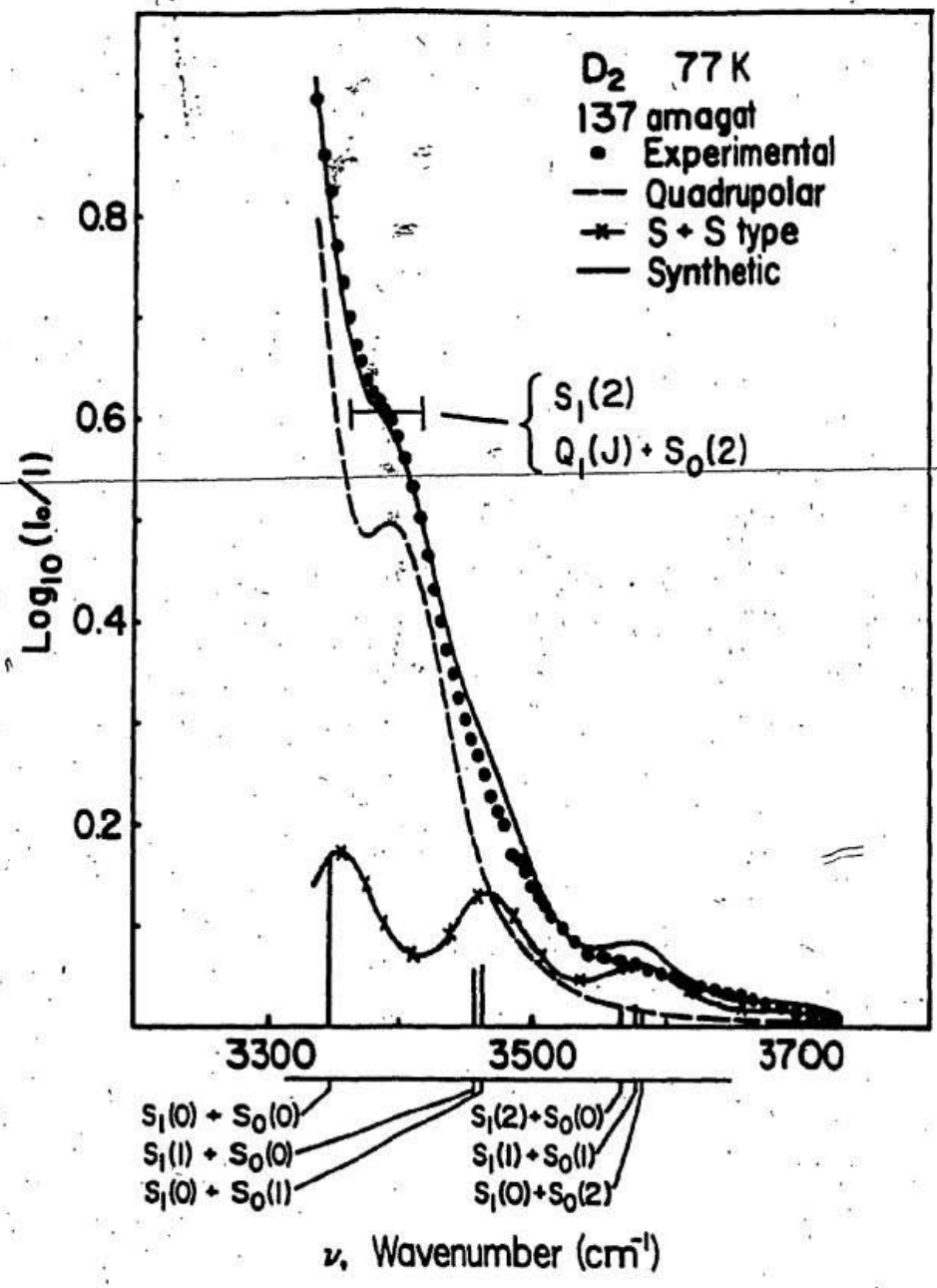

Figure 4.3 Analysis of the absorption profile of the fundamental band of normal D_2. The dots are the experimental points. The positions of the important transitions in this spectral region are indicated.

TABLE 4.2 Experimental data for each profile

Density (amagat)	δ_2 (cm^{-1})	δ_4 (cm^{-1})	Area (cm^{-2})
59.4	42.1	71.3	.9610e+01
64.2	42.4	68.3	.1080e+02
72.6	43.4	69.7	.1402e+02
76.9	43.2	66.5	.1529e+02
82.2	44.9	61.5	.1786e+02
87.9	42.6	68.4	.1965e+02
97.1	38.7	67.6	.2271e+02
101.7	41.7	64.3	.2571e+02
106.9	38.6	65.0	.2822e+02
112.4	41.0	61.7	.3330e+02
116.2	39.6	58.9	.3467e+02
124.6	41.1	59.7	.4067e+02
127.9	41.5	62.6	.4152e+02
137.2	39.0	65.3	.4831e+02

each density, together with the areas for the $S_1(0) + S_0(0)$ component.

The integrated absorption coefficient, $\int \alpha(\nu) d\nu$ for the transition $S_1(0) + S_0(0)$ was calculated from the fitted parameters for each experimental profile. Figure 4.4 shows a graph of $(1/\rho^2)\int \alpha(\nu) d\nu$ against density, ρ. A straight line was fitted to these points, and a value calculated for the binary and ternary absorption coefficients. Results of this analysis are presented in Table 4.3 together with the value of the binary absorption $\bar{\alpha}_{1a}$ calculated from the theory.

4.4. Conclusions

The S + S type double transitions in normal deuterium at 77 K were found to contribute significantly to the high wavenumber tail of the deuterium pressure-induced fundamental band, although nearby transitions of the main band arising from the rotational level J = 2 have sufficient intensity to obscure the direct observation of any structure for these components.

It should be noted that the data used to calculate the integrated absorptions were derived from Eq. (1.4), which is valid only for binary collisions. Since this model was used to extract the intensities for the S + S type double transitions from the broad structure, it may well be expected that some of the properties resulting from the analysis are strong functions of this model. This is particularly true of the ternary absorption coefficient which is found to be very small as would be expected from a model considering only binary collisions. In any case, the S + S type double transitions in deuterium are too well masked by nearby transitions to provide much more than a qualitative indication of the behavior of such double transitions.

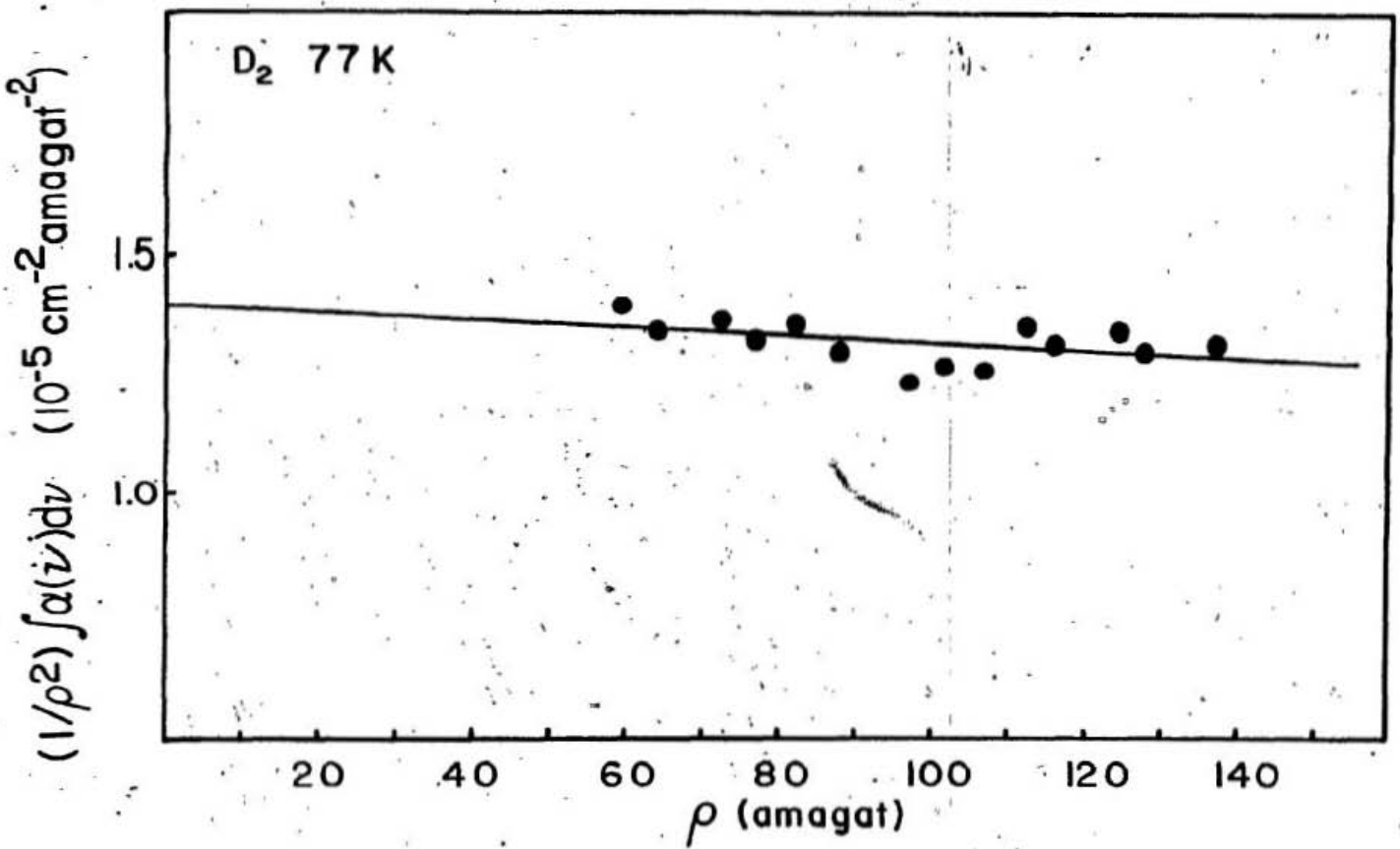

Figure 4.4 A plot of $(1/\rho^2)\int\alpha(\nu)d\nu$ against density ρ for the $S_1(0) + S_0(0)$ transition.

TABLE 4.3 Absorption Coefficients of the $S_1(0)+S_0(0)$ Transition of D_2 at 77 K

Binary Absorption Coefficient			Ternary Absorption Coefficient
Experiment		Theory	
α_{1a} (10^{-5} cm^{-2} $amagat^{-2}$)	$\bar{\alpha}_{1a}$ (10^{-37} cm^6 s^{-1})	$\bar{\alpha}_{1a}$ (10^{-37} cm^6 s^{-1})	α_{2a} (10^{-7} cm^{-2} $amagat^{-3}$)
1.37 ± .05	1.72 ± .06	1.27	-0.06 ± 0.05

The value calculated from Eq. (1.4) for the binary integrated absorption for the $S_1(0) + S_0(0)$ transition is $3.05 \times 10^{-9} cm^{-1} amagat^{-2}$. The corresponding value obtained by extrapolating the measured values to zero density is $(4.1 \pm 0.2) \times 10^{-9} cm^{-1} amagat^{-2}$. While this extrapolation may not be very accurate, it is representative of the measured values from the experiment. The experimental value is larger than the calculated value by 34 percent. For the quadrupolar contribution to the main part of the fundamental band, Penney et al. (1982) reported the value $1.8 \times 10^{-7} cm^{-1} amagat^{-2}$ for the binary integrated absorption, which was 19 percent larger than the theoretical value.

CHAPTER 5

ABSORPTION SPECTRA OF NORMAL D_2 IN THE FIRST OVERTONE REGION

5.1. Introduction

The collision-induced absorption spectrum of hydrogen in its first overtone region, first observed by Welsh et al. (1951), has been studied at room temperature and high densities by Hare and Welsh (1958) and at low temperatures by Watanabe, Hunt and Welsh (1971), Watanabe (1971) and McKellar and Welsh (1971). Silvaggio et al. (1981) have also studied this spectrum at low gas densities at 122, 273 and 275 K. Very recently in our laboratory van Nostrand (1983) has studied this spectrum in considerable detail at temperatures in the range 77 - 295 K. In all the work reported since 1971, profile analyses were carried out for the observed profiles with varying degrees of success. However, the corresponding spectrum of deuterium has been less well studied. The collision-induced spectrum of deuterium in its first overtone region was studied at room temperature by Reddy and Kuo (1971) in both the pure gas and for binary mixtures with argon and nitrogen; however, no profile analysis has been carried out for the absorption profiles of the pure gas.

In the present chapter, the collision-induced absorption spectra of the main band of deuterium in its first overtone region at 77, 201, and 295 K for a number of gas densities in the range 100 to 450 amagat are reported. Spectra of the relatively weaker S + S transitions in the the first overtone region, recorded for various gas densities in the range 500 - 850 amagat at 77 K are also presented. The absorption spectra have been analysed with respect to the calculated intensities from the theoretical matrix

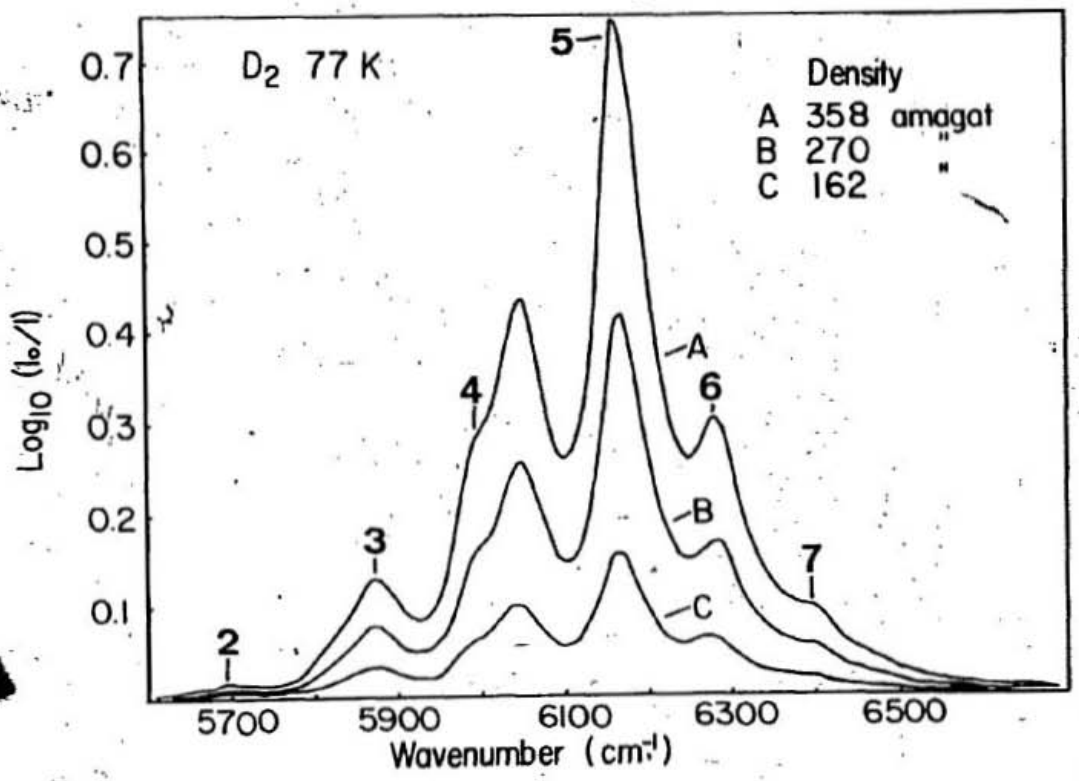

Figure 5.1 (a) Absorption profiles for the first overtone region of normal D_2 with an absorption path length of 194.6 cm. at 77 K. The numbered features are identified in Table 5.1.

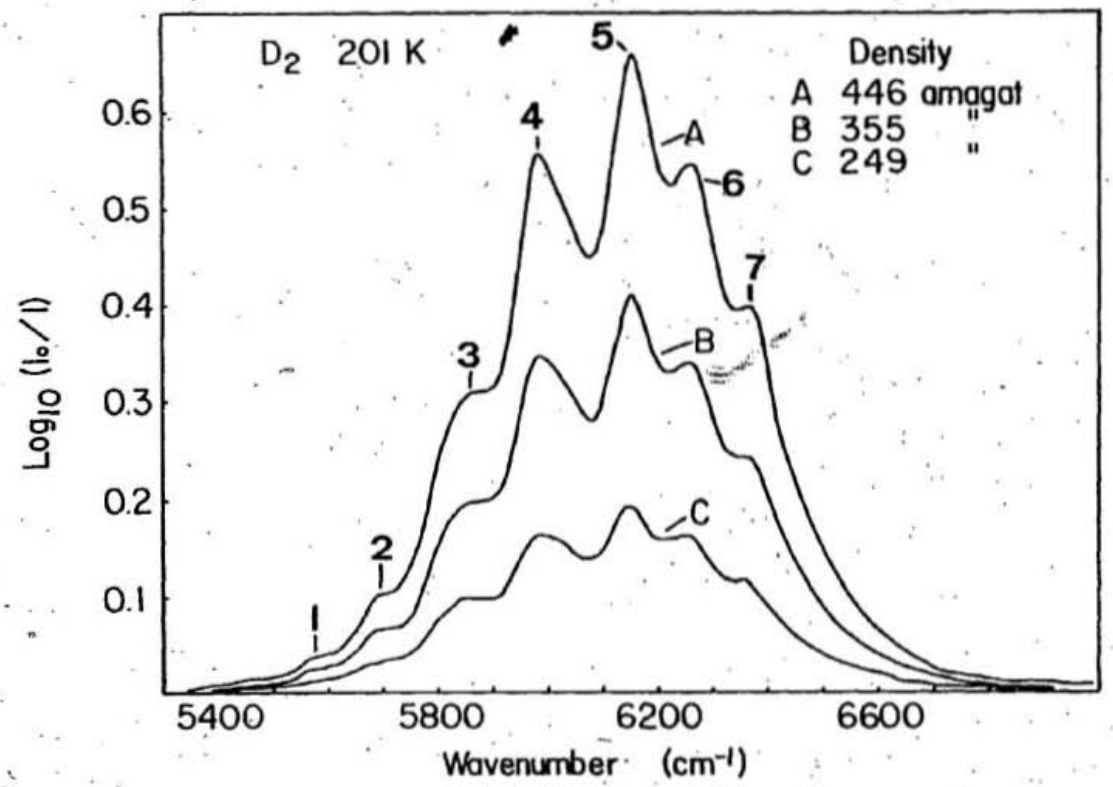

Figure 5.1 (b) Absorption profiles for the first overtone region of normal D_2 with an absorption path length of 194.8cm. The numbered features are identified in Table 5.1.

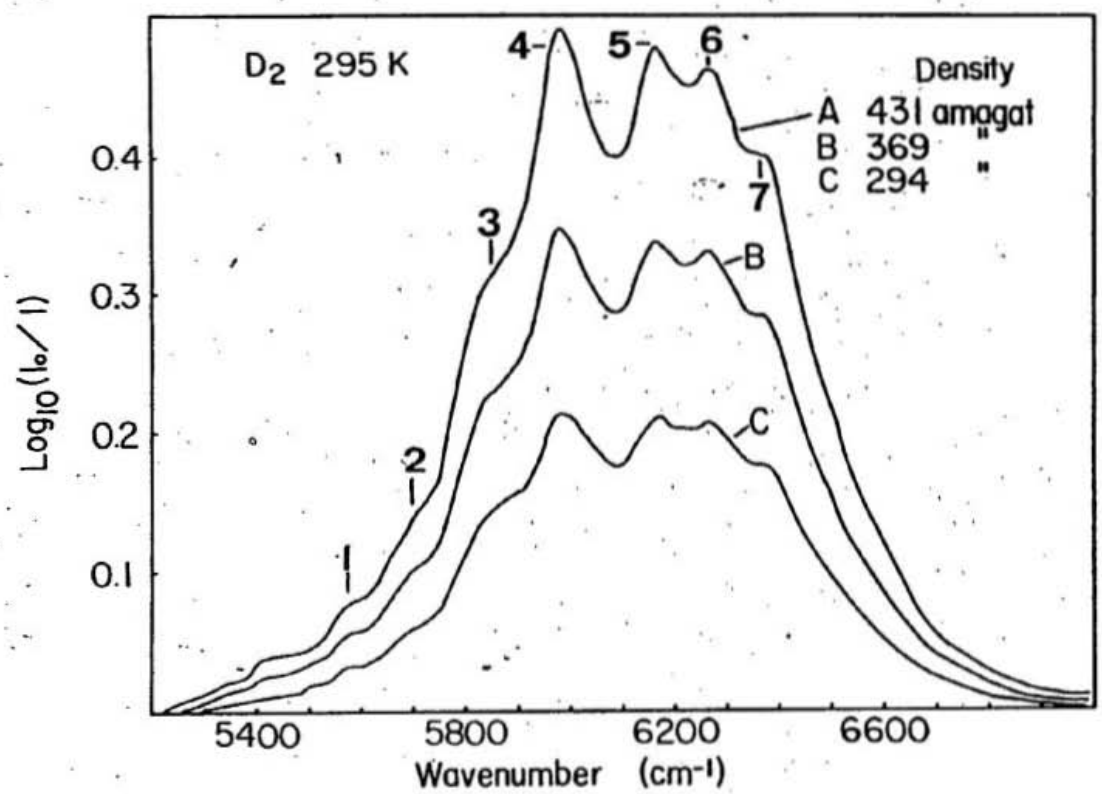

Figure 5.1 (c) Absorption profiles for the first overtone region of normal D_2 with an absorption path length of 195.0 cm. The numbered features are identified in Table 5.1.

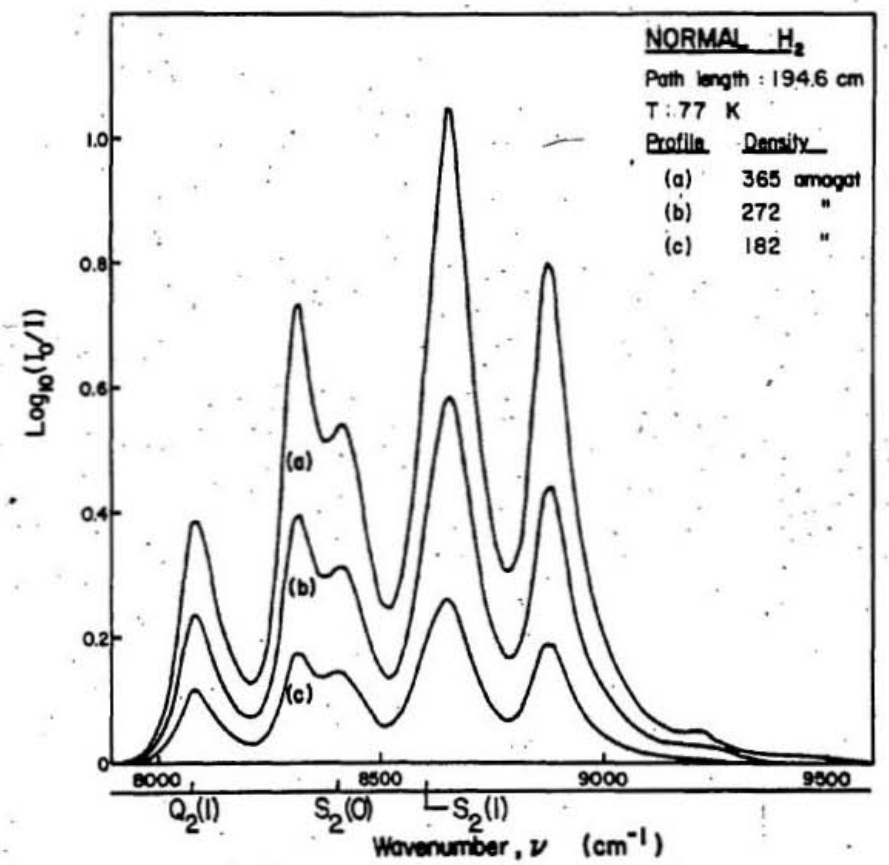

Figure 5.1 (d) Absorption profiles for the first overtone region of normal H_2.

TABLE 5.1 Assignment of the Observed Absorption Peaks of the D_2 First Overtone Region

Peak no.	Wavenumber of observed peak			Assignment
	77 K	201 K	295 K	
1		5575	5580	$O_2(3)$, $Q_1(J)+O_1(4)$
2	5695	5695	5705	$O_2(2)$, $Q_1(J)+O_1(3)$
3	5870	5850	5835	$Q_2(J)$, $Q_2(J)+Q_0(J)$
4	5990*	5980	5985	$Q_1(J)+Q_1(J)$
5	6165	6150	6160	$Q_2(J)+S_0(1)$, $Q_1(J)+S_1(0)$
6	6275	6260	6265	$Q_2(J)+S_0(2)$, $Q_1(J)+S_1(1)$
7	6380	6370	6365	$Q_2(J)+S_1(2)$, $Q_2(J)+S_0(3)$

* At 77 K, a peak has developed at about 6045 cm^{-1}, due to the strong $S_2(0)$ and $Q_2(J) + S_0(0)$ transitions. These transitions contribute to the peak at 5980 cm^{-1} at 201 and 295 K.

elements for the quadrupole moment, the polarizability and anisotropic polarizability for deuterium given by Poll (1983) and Kolos and Wolniewicz (1967). A modified symmetrized lineshape (Eq. 1.9) has been used for the quadrupolar components. No evidence is seen to indicate the presence of an electron overlap contribution to the intensity of the band.

The apparatus used to obtain these spectra has been described in detail in Chapter 2. The experimental gas was contained in the 2 m high pressure low temperature absorption cell. The source of infrared radiation was a General Electric FFJ 600 W projection lamp operated at approximately 300 W. The spectra were recorded with a modified Perkin-Elmer model 112 single-beam double-pass spectrometer equipped with an LiF prism, a 260 Hz tuning fork chopper, and an uncooled PbS detector. The spectrometer slit width maintained at 35 μm gave a spectral resolution of about 8 cm^{-1} at 5868 cm^{-1}, the position of the $Q_2(0)$ component of the first overtone band of deuterium.

5.2. Experimental absorption profiles of the main band

Three representative absorption profiles of normal deuterium for the pure gas in the first overtone region at each of the temperatures 77, 201 and 295 K are shown in Figs. 5.1 (a), (b) and (c) respectively. Observed absorption peaks of the profiles in these figures are marked with identification numbers and their measured wavenumbers together with the assignments of the transitions are listed in Table 5.1. The calculated wavenumbers of various components contributing to the spectrum, obtained from the constants for the free D_2 molecule are listed in Appendix B. One important difference between the collision-induced fundamental and first overtone bands

of deuterium should be pointed out. The fundamental band of deuterium contains a dip in the Q branch with associated high- and low-wavenumber maxima Q_P and Q_R, the separation between which varies linearly with density (see for example Penney et al., 1982). This dip is associated with the electron overlap contribution to the induced dipole moment; also the overlap components are in general broader than the quadrupolar components. There is no evidence of dips or components with greater breadth in the Q branches of the absorption profiles of D_2 in the first overtone region. As confirmed later by the profile analysis, there is no evidence for the presence of an overlap contribution to the intensities of the Q branches of the collision-induced absorption of deuterium in the first overtone region. It can be seen from Figs. 5.1 (a), (b) and (c) that the widths of the various components are relatively broader at higher temperature. This is because the relative translational energy of the colliding pair is large at higher temperature and hence the collision duration is relatively small. For comparison, a typical absorption profile of hydrogen in its first overtone region obtained at 77 K (van Nostrand, 1983) is shown in Fig. 5.1 (d). It is apparent from this figure that the various components of the absorption profile of hydrogen are better resolved than the corresponding components of the deuterium profiles. One of the reasons for this is that the rotational constant of H_2 is about twice that of D_2.

The area of each of the experimental profiles was measured to determine the integrated absorption coefficients $\int \alpha(\nu) d\nu$ as a function of density. Graphs of $1/(\rho^2)\int \alpha(\nu) d\nu$ against ρ are plotted in Fig. 5.2 (a), (b) and (c) for 77, 201 and 295 K respectively, and the binary and ternary coefficients obtained from the slopes and the intercepts respectively, (see Eq. 1.1) are

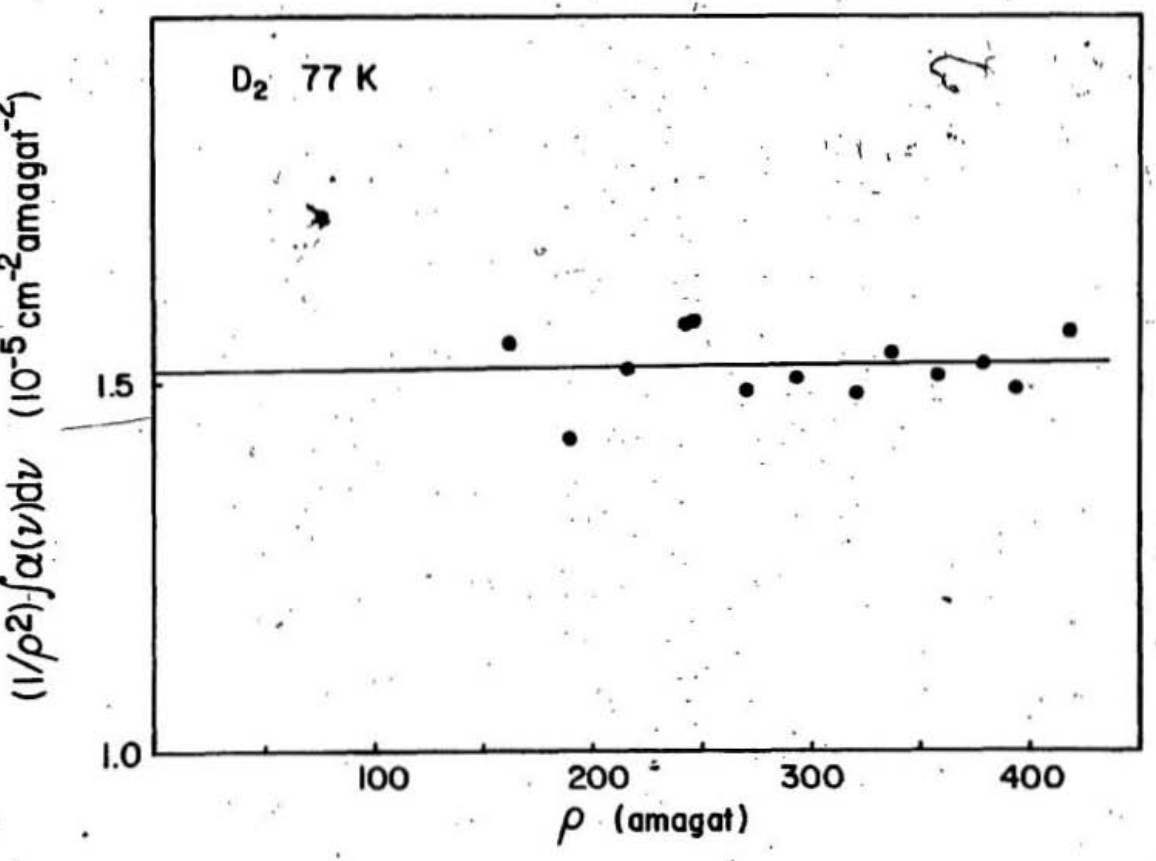

Figure 5.2 (a) A plot of $(1/\rho^2)\int\alpha(\nu)d\nu$ against density ρ for the first overtone region of normal D_2 at 77 K.

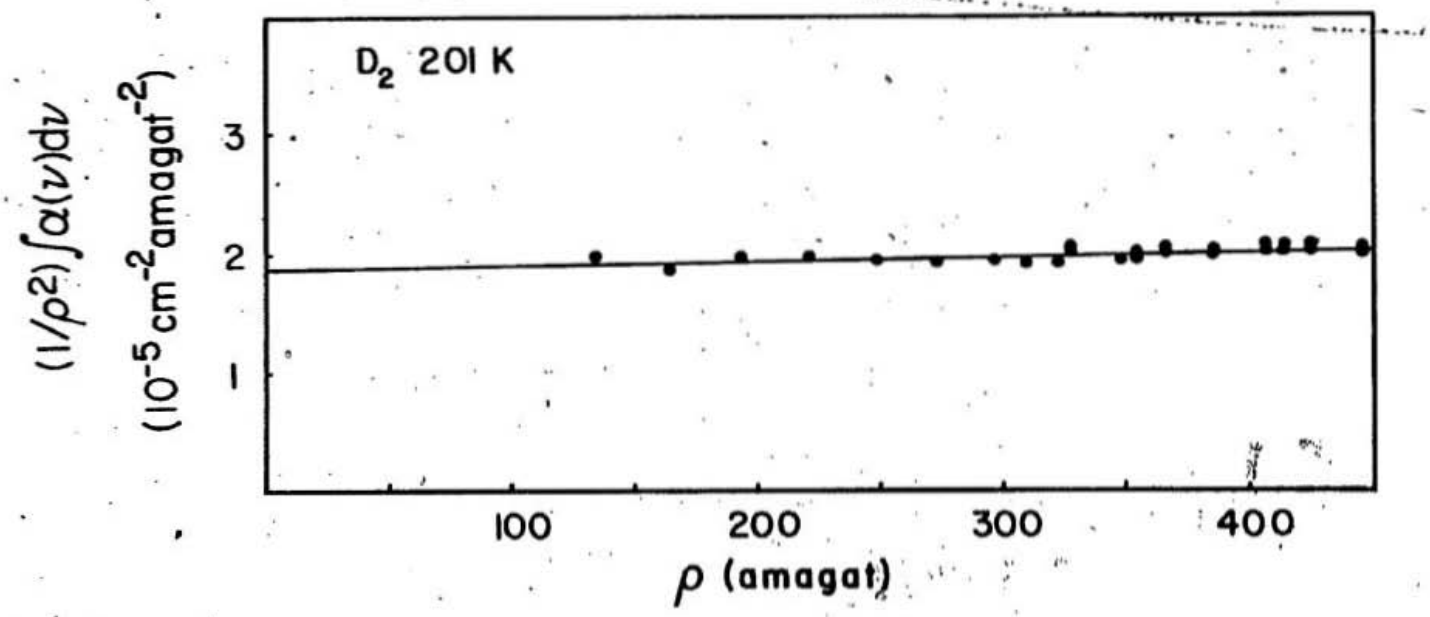

Figure 5.2 (b) A plot of $(1/\rho^2)\int\alpha(\nu)d\nu$ against density ρ for the first overtone of normal D_2 at 201 K.

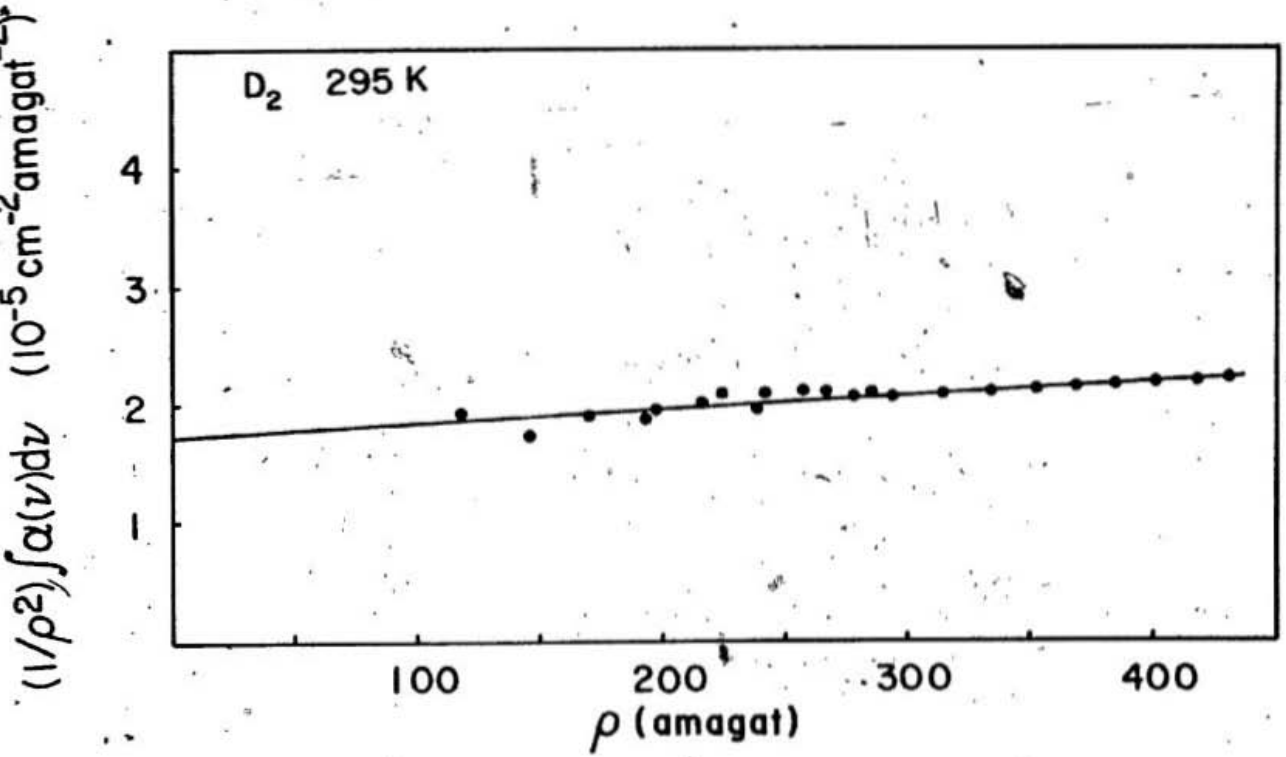

Figure 5.2 (c) A plot of $(1/\rho^2)\int\alpha(\nu)d\nu$ against density ρ for the first overtone of normal D_2 at 295 K.

tabulated in Table 5.2. Where appropriate, results of previous experiments are presented for comparison. The values calculated from the matrix elements of Poll (1983) for the binary absorption coefficient are also included for comparison.

5.3. Profile analysis of the main band

Initially, attempts were made to fit the observed profiles to a synthetic profile obtained using absolute intensities calculated from the matrix elements of Kolos and Wolniewicz (1967) and Poll (1983), and the modified symmetrized lineshape (Eq. 1.9). However, the fit between the observed and synthetic profiles was rather poor, as seen in Fig. 5.3 for deuterium at 77 K. It was noticed that the intensities of transitions involving the vibrational state v = 2 were consistently too high relative to the other transitions. This can be seen more clearly in Fig. 5.4 (a), where the observed profile is plotted together with a synthetic profile calculated for the gas at the same temperature and density, where the lineshape (Eq. 1.9) was used with parameters $\delta_2 = 35\ cm^{-1}$ and $\delta_4 = 120\ cm^{-1}$; as will be shown later, these values are consistent with the fitted values for these parameters. A similar discrepancy has also been observed in the hydrogen first overtone band (see McKellar and Welsh, 1971, Watanabe et al., 1971, Watanabe, 1971 and van Nostrand, 1983). Figure 5.4 (b) shows this effect in hydrogen.

In the hydrogen and deuterium fundamental bands, a better fit between the experimental and theoretical profiles is obtained when relative intensities rather than absolute intensities are fitted to the observed profiles; this effectively permits the theoretical and experimental profiles to differ by a constant multiplicative factor which is, in fact, an additional parameter to be fitted.

TABLE 5.2. Absorption Coefficients* of D_2 in the First Overtone Region

T	Binary Absorption Coefficient			Ternary Absorption Coefficient	
	Experiment		Theory		
K	α_{1a} ($10^{-5} cm^{-2} amagat^{-2}$)	$\bar{\alpha}_{1a}$ ($10^{-37} cm^6 s^{-1}$)	$\bar{\alpha}_{1a}$ ($10^{-37} cm^6 s^{-1}$)	α_{2a} ($10^{-8} cm^{-2} amagat^{-3}$)	
77	1.51 ± 0.05	1.04	1.17	0.05 ± 0.20	(a)
201	1.87 ± 0.04	1.27	1.24	0.38 ± 0.12	(a)
295	1.73 ± 0.05	1.18	1.30	1.20 ± 0.16	(a)
298	2.10	1.43	1.31	<1	(b)

* The errors quoted are standard deviations.

(a) Present work

(b) Reddy and Kuo (1971)

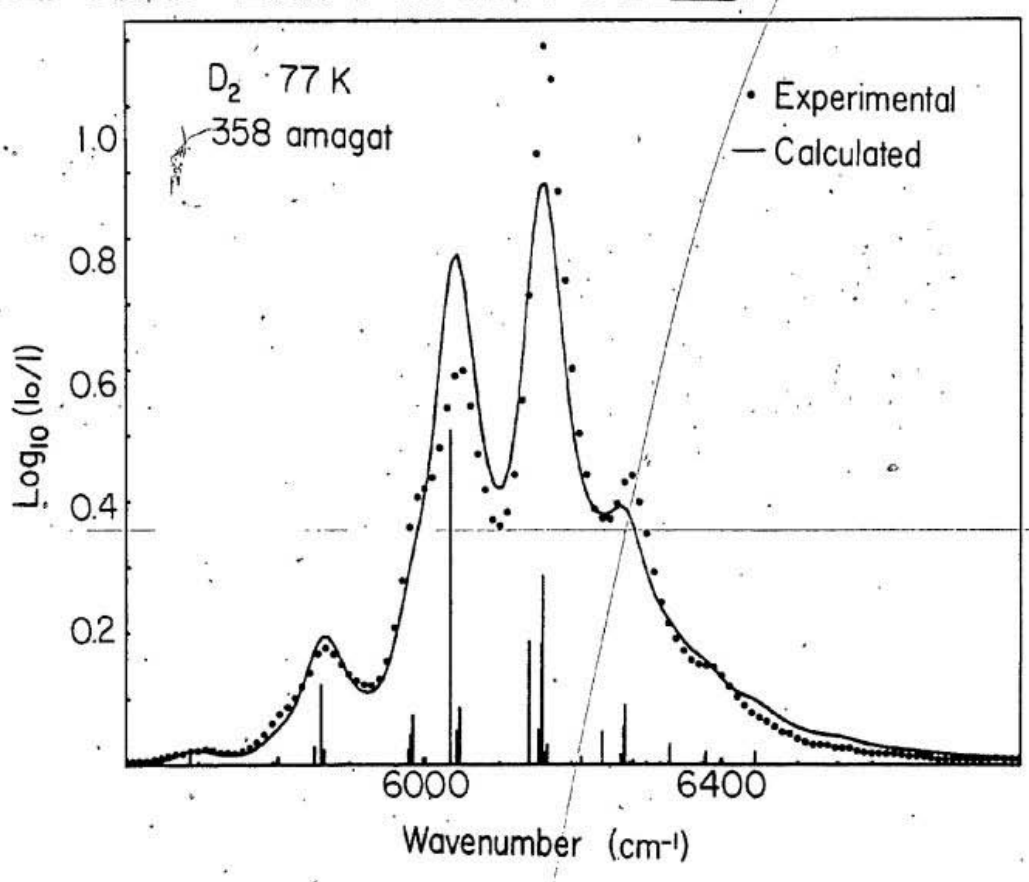

Figure 5.3 A plot of the experimental and fitted profile for the D_2 first overtone region at 77 K. The relative intensities used in the fit are tabulated in Appendix B.

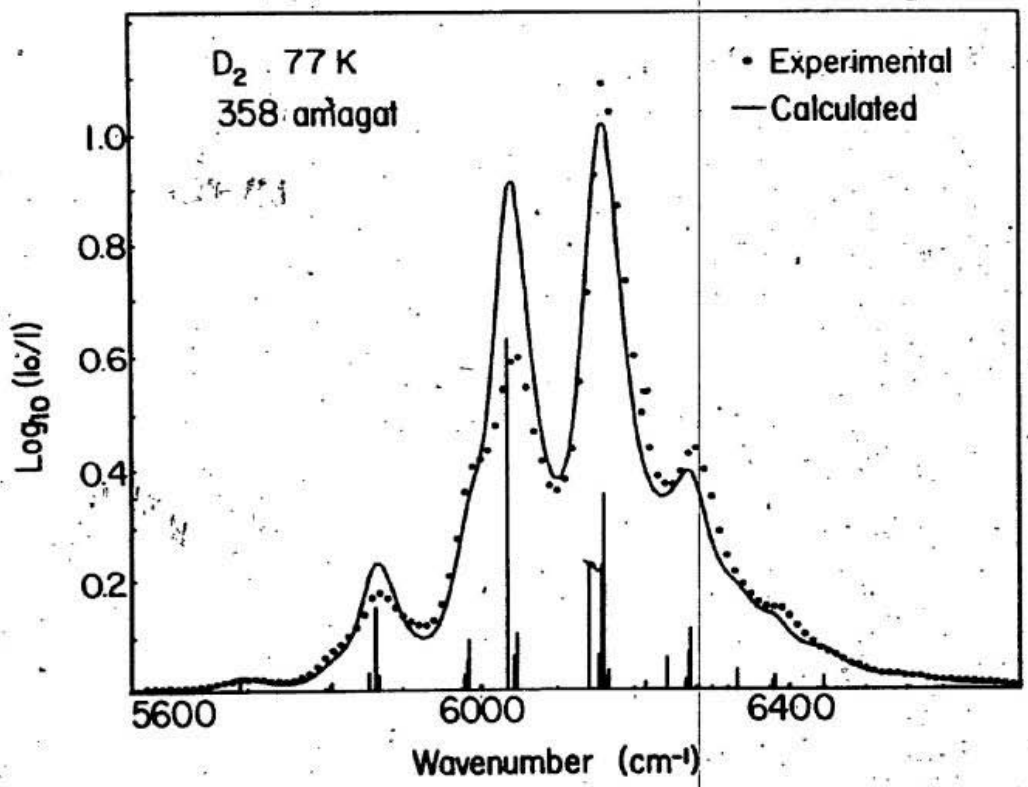

Figure 5.4 (a) A plot of the observed and theoretical profile for collision-induced absorption in the first overtone region of D_2.

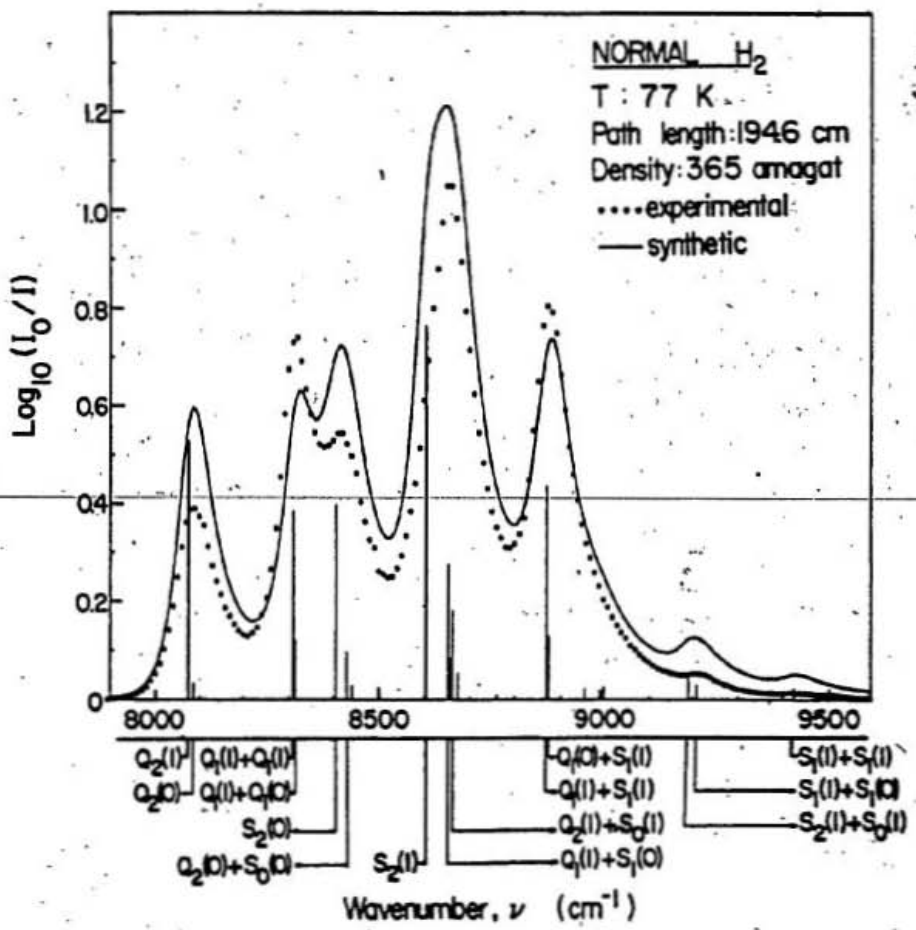

Figure 5.4 (b) A plot of the observed and theoretical profile for collision-induced absorption in the first overtone of H_2 at 77 K. The parameter δ_2 was fixed at 48 cm^{-1}, and δ_4 was fixed at 160 cm^{-1}.

The relative intensities are usually normalized so that the most intense component has a value of 1.0. For the first overtone spectrum, however, this procedure does not produce an adequate agreement between the fitted, or "synthetic", profiles and the experimental profiles.

Watanabe (1971) has suggested that for the hydrogen first overtone spectrum this difference may be explained by a different density dependence for the single and double transitions. This explanation does not appear to be consistent with our observations, however, because the double transitions involving the v = 2 state; i.e., transitions of the type $Q_2(J) + S_0(J)$, and $S_2(J) + S_0(J)$ also appear to be relatively too intense. It therefore appears that this discrepancy is present in all transitions which involve the v = 2 vibrational state. It was therefore decided to decrease the intensities of all of the transitions involving the v = 2 vibrational state by decreasing all of the v = 2 quadrupolar matrix elements by a constant factor which we will call an "improvement factor" to improve the fit between the observed and the synthetic profiles. An "improvement factor" of 0.68 was found to give the best agreement between the observed and fitted profiles, at the three experimental temperatures and over the range of densities studied. Typical fits to profiles at each temperature are shown in Figs. 5.5 (a), (b) and (c). This same "improvement factor" was also found to produce the best agreement between the observed and fitted profiles of hydrogen, as can be seen in Fig. 5.5 (d) for hydrogen at 77 K (van Nostrand, 1983). The fits of the calculated profiles to the experimental profiles are quite insensitive to changes in the polarizability matrix elements for the $\Delta v = 2$ transitions.

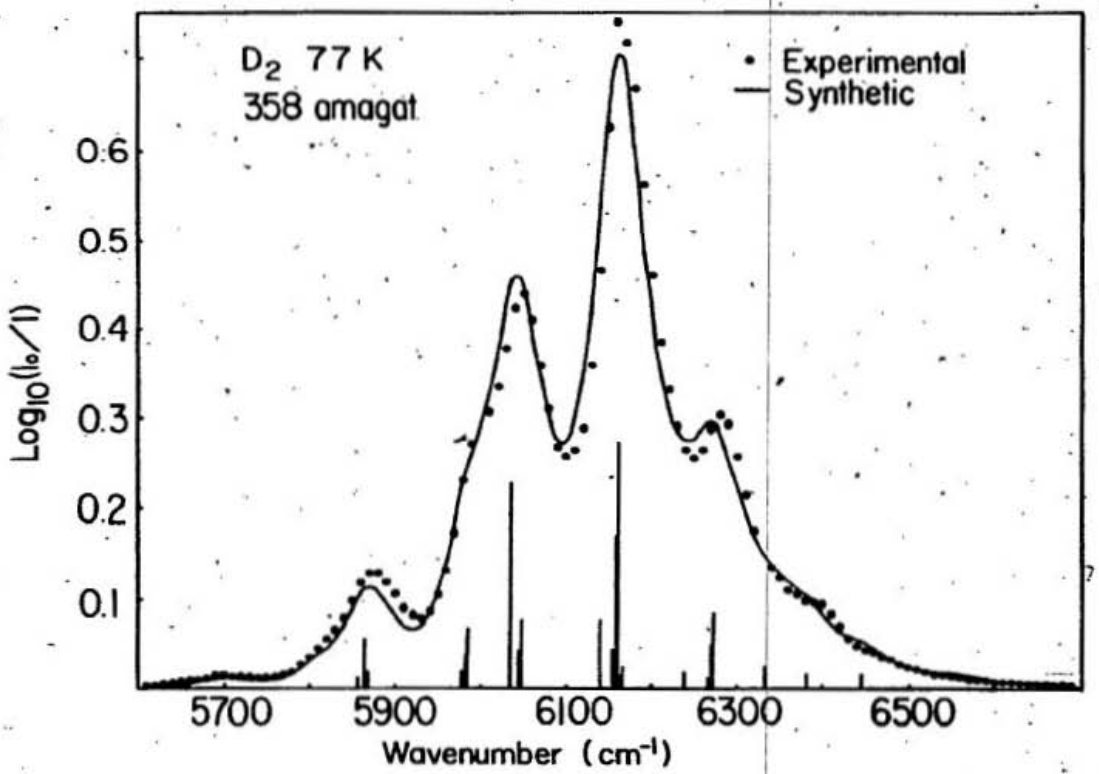

Figure 5.5 (a) A plot of the observed and fitted profile for the first overtone region of D_2 at 77 K. The fitted values were calculated from the "improved" relative intensities from Appendix B.

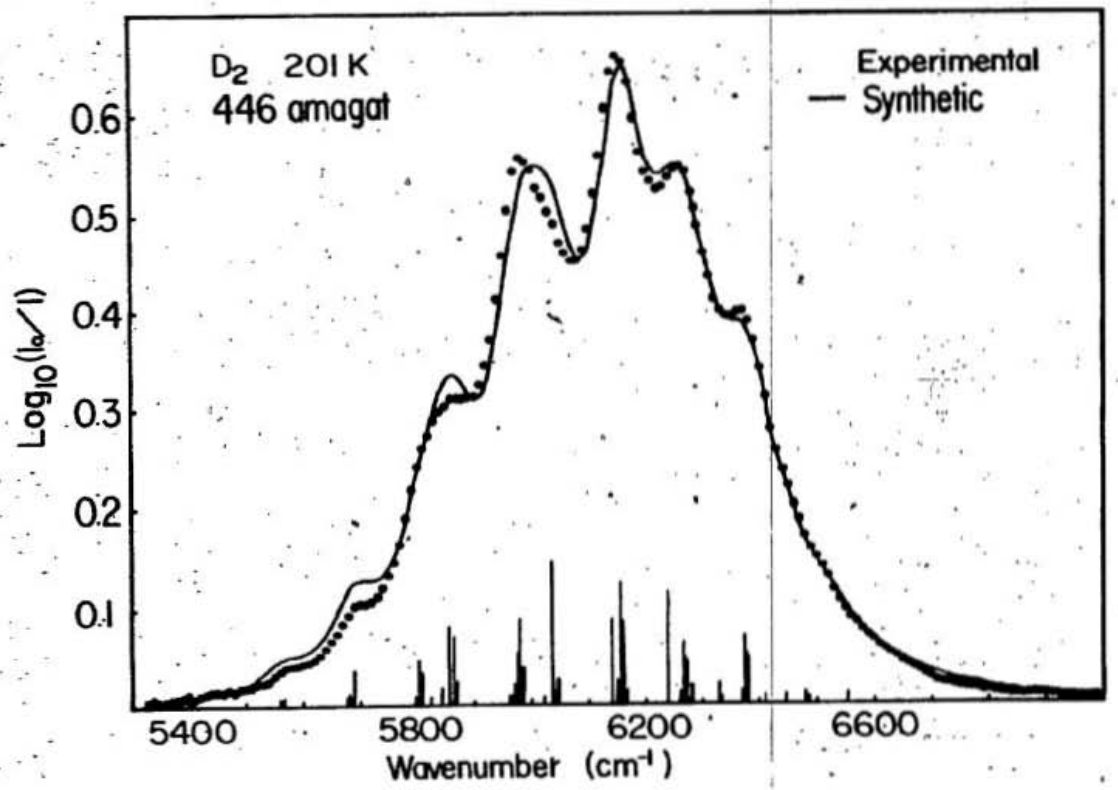

Figure 5.5 (b) A plot of the observed and fitted profile for the first overtone region of D_2 at 201 K. The fitted values were calculated from the "improved" relative intensities from Appendix B.

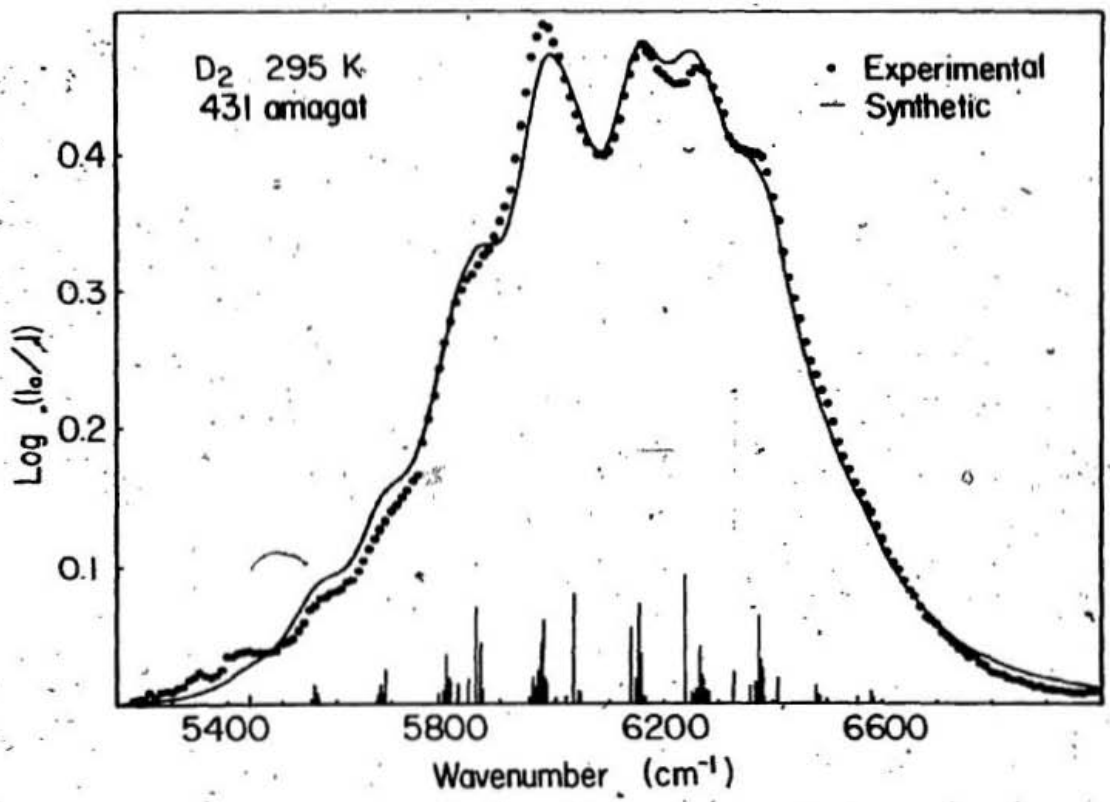

Figure 5.5 (c) A plot of the observed and fitted profile for the first overtone region of D_2 at 295 K. The fitted values were calculated from the "improved" relative intensities from Appendix B.

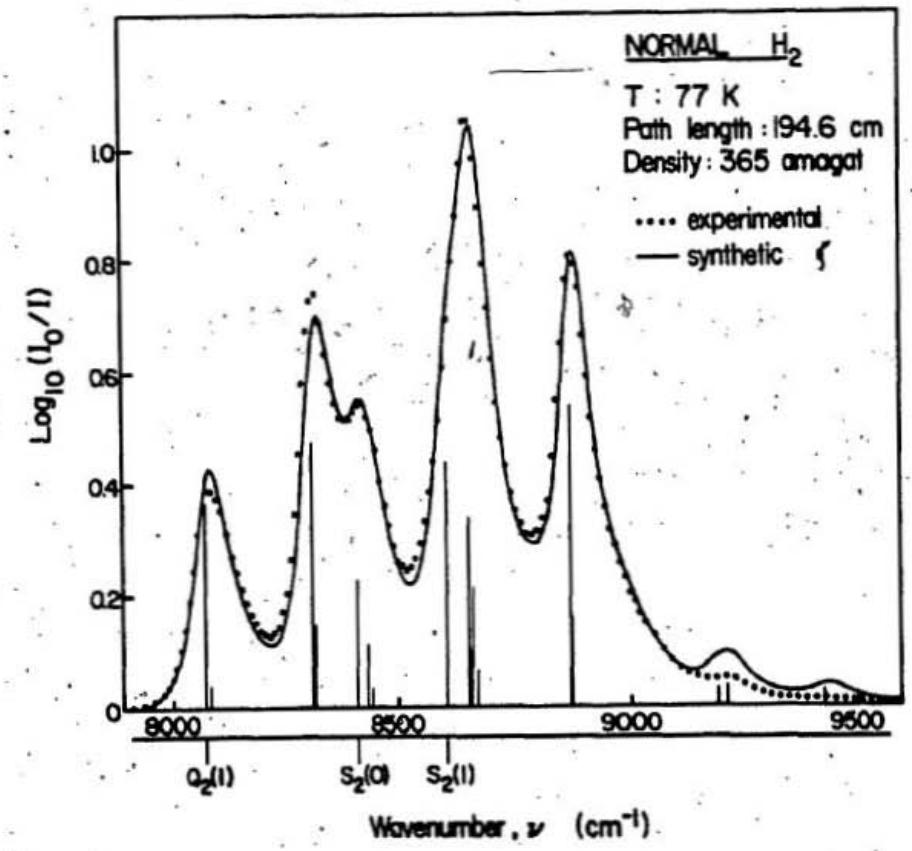

Figure 5.5 (d) A plot of the observed and fitted profile for the first overtone of H_2 at 77 K. The fitted values were calculated using relative intensities calculated with the same "improvement factor" as was used for the D_2 analysis.

Appendix B gives the relative and absolute intensities for the components of the band at temperatures 77, 201 and 295 K with relative intensities greater than 0.01; components with relative intensities as low as 0.001 were used in the analysis. The relative intensities for the transitions after application of the "improvement factor" to the v = 2 quadrupolar matrix elements are also included. The later relative intensities were used to generate the synthetic profiles of Fig. 5.5 (a), (b) and (c).

The lineshape parameters δ_2 and δ_4 are listed in Table 5.3. for the profiles at 77 K. The parameter δ_2 is relatively constant over the range of densities studied, but shows a slight tendency to decrease as the density of the gas is increased. There is significant variation in the parameter δ_4; this parameter shows a tendency to increase with density. Figure 5.6 shows a plot of the parameter δ_2 against the square root of temperature, in Kelvins. The straight line obtained from this plot gives the relation $\delta_2 = 4.26 T^{1/2}$, which compares favourably with the relation $\delta_2 = 4.30 T^{1/2}$ found by Penney et al. (1982) for the fundamental band.

5.4. S + S Type Transitions at 77 K

Two types of S + S type transitions arise in the high wavenumber tail of the first overtone region of deuterium; one type in which one of the molecules preforms a $\Delta v = 2$ vibrational transition, the other performs a $\Delta v = 0$ transition; in the other type, both molecules perform $\Delta v = 1$ transitions. Similar S + S type transitions in the first overtone region of hydrogen have been studied by van Nostrand (1983). As in the fundamental band, the S + S type transitions in the deuterium overtone band fall on the wing of other stronger quadrupolar transitions.

TABLE 5.3. Results of Profile Analysis of D_2 in the First Overtone Region

T (K)	Quadrupolar half-width δ_2 (cm^{-1})	δ_4 (cm^{-1})	Collision duration τ_q (10^{-13} s)
77	39 ± 3	76 ± 11	1.4
201	61 ± 2	114 ± 8	0.87
295	74.7 ± 0.8	173 ± 18	0.71

* $\tau_q = \frac{1}{2\pi c \delta_2}$

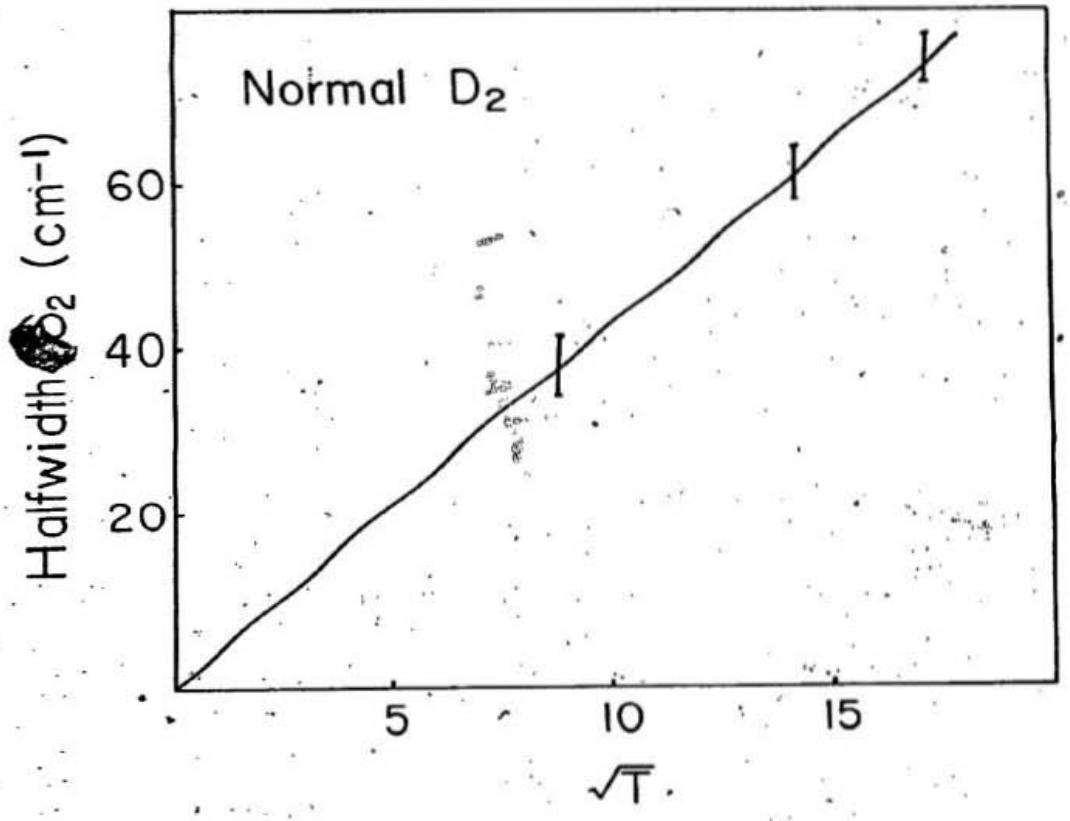

Figure 5.6 A plot of the halfwidth parameter δ_2 against $T^{\frac{1}{2}}$ ($K^{\frac{1}{2}}$). The errors indicated show the maximum experimental deviations.

A total of 15 profiles was recorded for gas densities in the range 500 - 930 amagat. Figure 5.7 shows typical absorption profiles at densities 678, 829 and 929 amagat at 77 K, and indicates the position of significant S + S type components in the region. At 77 K, there are ten S + S type components with relative intensities greater than 0.1 percent of the most intense quadrupolar transition in the range 6300 - 6750 cm^{-1}, but these are masked by the high wavenumber "tails" of nearby stronger isotropic quadrupolar transitions. Appendix B contains the relative intensities of all transitions in the band, including the S + S type transitions.

The experimental profiles were fitted to all of the quadrupolar lines; the intensity calculated for each line included the contribution from the anisotropic polarizability. The lineshape chosen was the "modified symmetrized lineshape" (Eq. 1.9). The relative intensities used in the fit were calculated with the "improvement factor" applied to the v = 2 quadrupolar matrix elements; when the "unimproved" matrix elements were used the fit was quite poor. Figure 5.8 shows a typical experimental and fitted profile, and indicates the relative intensity of each component. Although the transitions $S_0(J) + S_2(J)$ are not indicated in the diagrams since they do not occur in the range 6300 - 6750 cm^{-1} ($S_0(0) + S_2(0)$ occurs at 6214 cm^{-1}), they were taken into account in the analysis. The application of the "improvement factor" decreases the contribution of these terms. The lineshape parameters δ_2 and δ_4 in Eq. (1.9) were calculated for each profile; the parameter δ_2 showed a consistent tendency to decrease as the density increased. The parameter δ_4 varied significantly, again showing a tendency to increase with density.

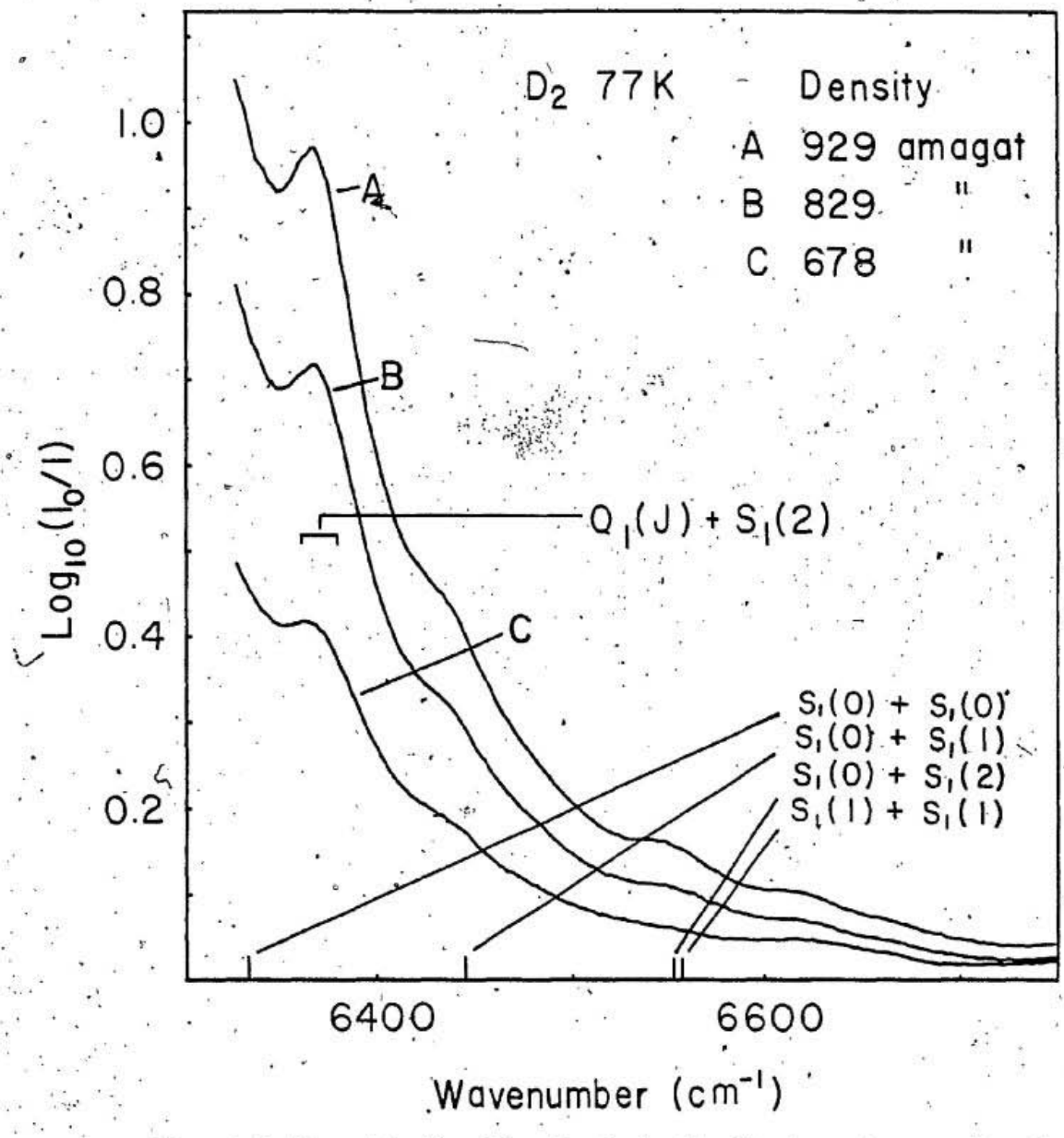

Figure5.7 Absorption profiles for D_2 in the first overtone region at 77 K in the range 6300 - 6750 cm^{-1}, where there is a contribution due to S + S type transitions.

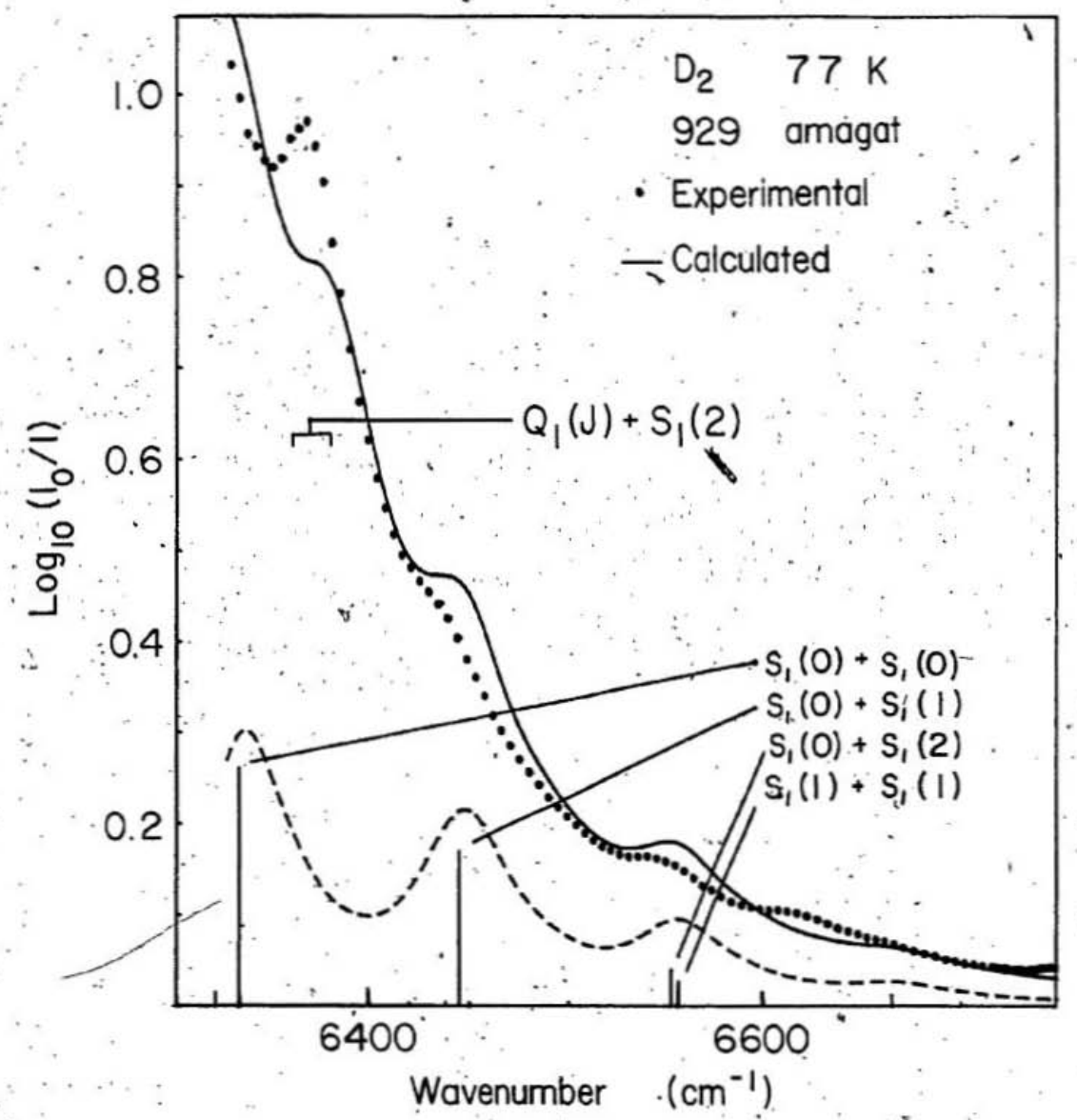

Figure 5.8 Experimental and fitted profiles in the D_2 first overtone region, showing the contribution of the S + S type transitions to the profile.

The integrated absorption coefficient, $\int \alpha(\nu) d\nu$, was calculated for the $S_1(0) + S_1(0)$ transition from the fitted parameters for each profile. Figure 5.9 shows a graph of $(1/\rho^2)\int \alpha(\nu) d\nu$ against ρ. A straight line was fitted to these points, and the values of the binary and ternary coefficients obtained are presented in Table 5.4. Table 5.4 also compares the value found for the binary integrated absorption extrapolated to zero density with the calculated value.

5.5. Density dependence of the lineshape

As mentioned earlier, a tendency for the halfwidth of the quadrupolar lines to decrease with density was noted in both the main band and the S + S transitions. This narrowing effect has been previously observed in the collision-induced absorption fundamental band of hydrogen in H_2 - inert gas mixtures at high density by De Remigis et al. (1971) and Mctaggart et al. (1973). This effect was explained by Zaidi and Van Kranendonk (1971) as a diffusional effect. The duration of a collision is effectively increased by the interactions with neighbouring molecules and the linewidth therefore decreases. In all cases the halfwidth of the quadrupolar lines remained constant for densities up to about 300 amagat, and then began to decrease sharply. The line width at high densities was predicted to be proportional to the diffusion constant. Recently, van Nostrand (1983), in this laboratory, has observed a distinct pressure narrowing of the hydrogen quadrupolar components in the pure gas in the first overtone region at 77 K; a graph of halfwidth against density for this experiment (van Nostrand, 1983) is shown in Fig. 5.10.

For the deuterium first overtone, the halfwidths δ_2 resulting from the

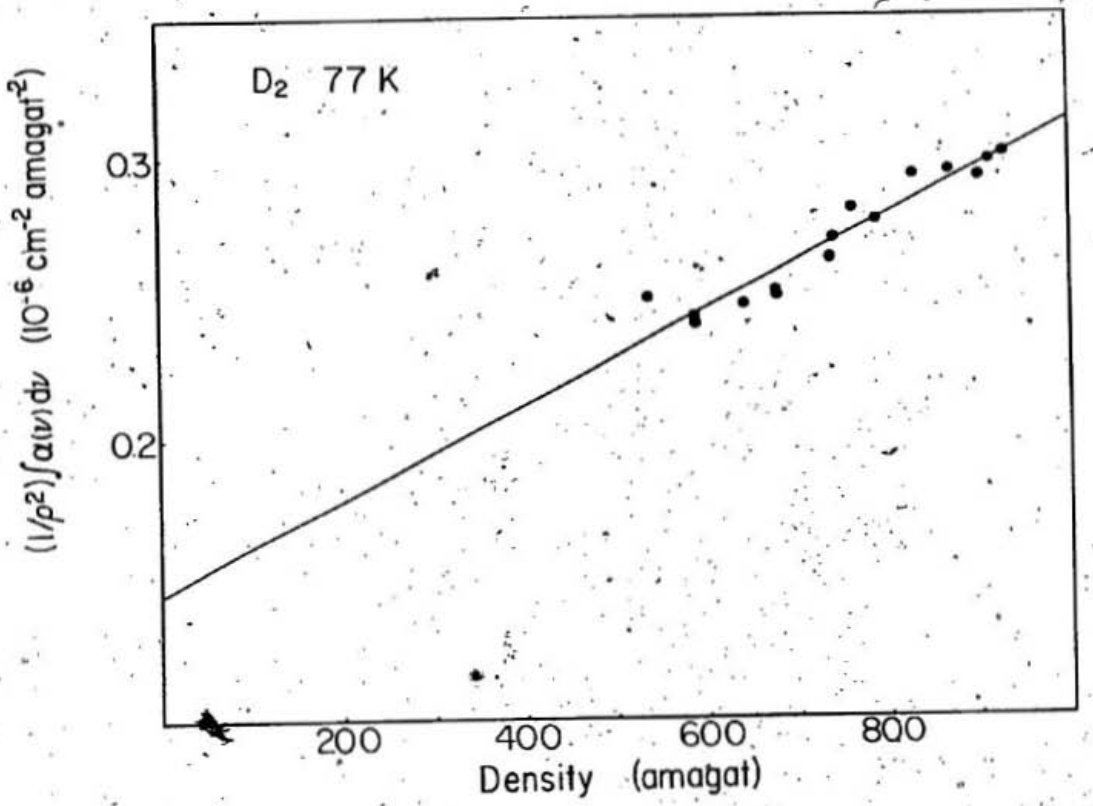

Figure 5.9 A plot of $(1/\rho^2)\int\alpha(\nu)d\nu$ against ρ for the $S_1(0) + S_1(0)$ transition in normal D_2 at 77 K.

TABLE 5.4 Absorption Coefficients of the $S_1(0)+S_1(0)$ Transition of D_2 at 77 K

Binary Absorption Coefficient			Ternary Absorption Coefficient
Experiment		Theory	
α_{1a} $(10^{-7} cm^{-2} amagat^{-2})$	$\bar{\alpha}_{1a}$ $(10^{-39} cm^6 s^{-1})$	$\bar{\alpha}_{1a}$ $(10^{-39} cm^6 s^{-1})$	α_{2a} $(10^{-10} cm^{-2} amagat^{-3})$
1.4 ± .1	0.95 ± .07	1.62	1.7 ± .1

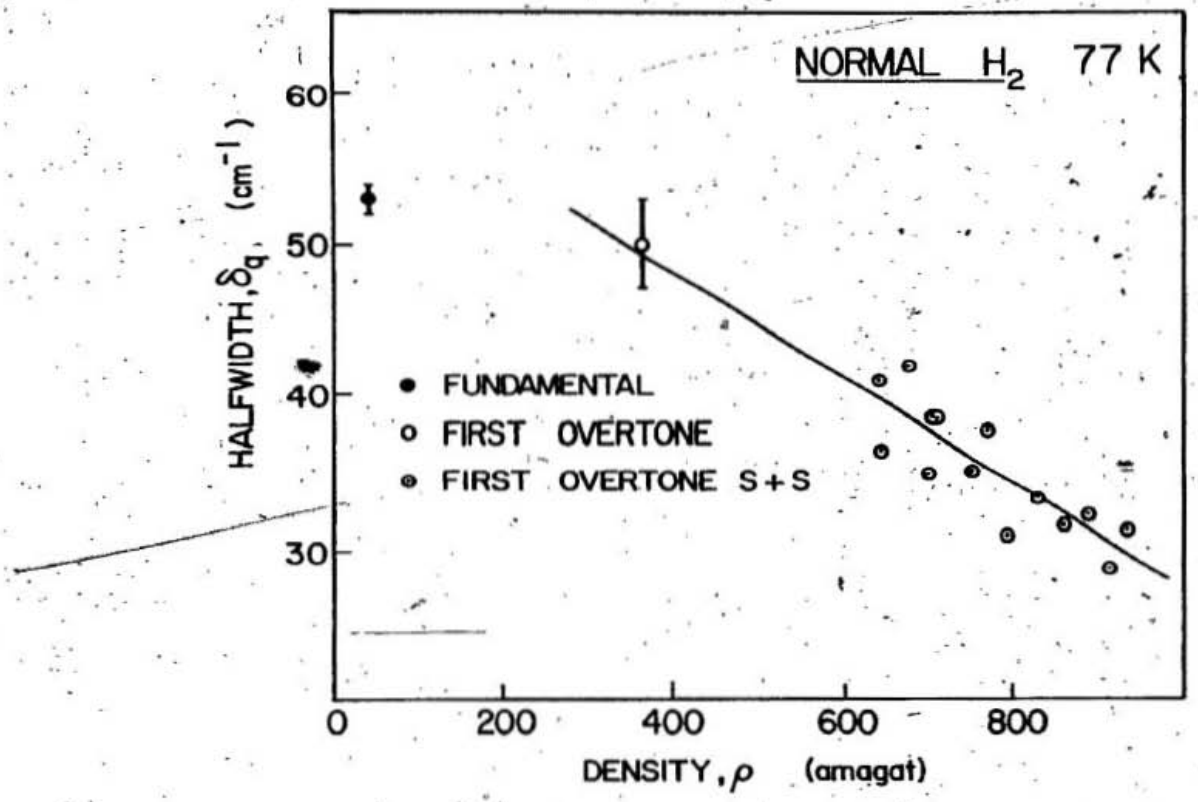

Figure 5.10 A plot of the variation of the halfwidth δ_2 as a function of density for H_2 at 77 K.

analysis of the main first overtone band and the S + S analysis discussed above are together plotted against density in Fig. 5.11. Over the range of densities used in these experiments, there is a distinct decrease in the observed halfwidth of the quadrupolar components of the spectrum. The decrease with density is linear, over the range of densities used in these experiments. As noted earlier, there is also a consistent increase in the parameter δ_4 as the density increases. This parameter has little effect on the shape of the central part of the line, but has a strong effect on the far wings of the line. The fact that this parameter consistently increases implies that although the halfwidth of the lines decreases with density, the base width of the line increases with density. The increase of the base width of the line with density was predicted in collision-induced absorption by Lewis and Tjon (1978).

5.6. Conclusions

There is a significant discrepancy between the observed and calculated quadrupolar intensities for both hydrogen and deuterium in the first overtone spectrum at the densities studied. The quadrupole matrix elements used in the calculation of the absolute intensities, calculated by Karl and Poll (1967) are in reasonable agreement with the experimental intensities found by Fink et al. (1965) for the pure quadrupolar spectrum of hydrogen, where molecules undergo collision-free absorption (see Karl and Poll, 1967 for a comparison of theory and experiment). It should be noted, however, that for some of the V = 1 quadrupolar matrix elements the experimental results produced values (Fink et al., 1965) which were approximately 10 % less than the corresponding theoretical values. Even this discrepancy, however,

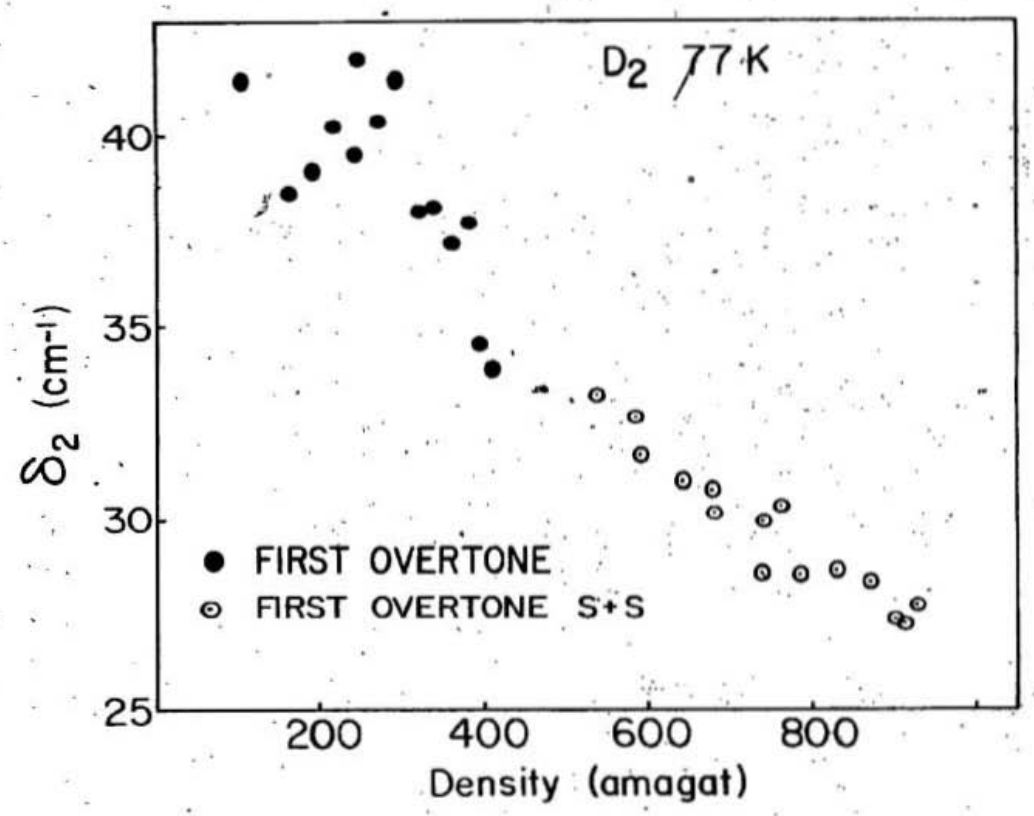

Figure 5.11 A plot of the variation of the halfwidth δ_2 as a function of density for D_2 in the first overtone region.

is not sufficient to account for the observed differences between the experimental and theoretical profiles in the present study.

A simple "improvement factor" applied to the V = 2 quadrupolar matrix elements gives agreement between the observed and fitted profiles. No quantitative explanation for this factor is available. It is interesting to note that a similar effect was observed at much lower densities by McKellar and Welsh (1971) and Watanabe (1971); Watanabe (1971) attributed this effect to a different density dependence for single and double transitions.

There is no observable shift in the transition wavenumbers of the collision-induced spectra in the pure gas, so it would appear that the effects of the collision do not perturb the energy levels of the interacting molecules. This suggests that the observed reduction in intensity for the 2 - 0 vibrational transition relative to transitions where both molecules undergo a 1 - 0 vibrational transition is due to the intermolecular interaction itself. There is, however, a clear and consistent decrease in the halfwidth parameter δ_2 with density for densities greater than about 300 amagat. This is consistent with the observations of van Nostrand (1983) in the hydrogen first overtone band, and with De Remigis et al. (1971) in the fundamental band for hydrogen-argon mixtures. There is also some evidence that the base of the line is broadened as the density increases.

CHAPTER 6

ABSORPTION SPECTRA OF THE SECOND OVERTONE REGION OF NORMAL H_2 AND D_2

6.1. Introduction

The collision-induced absorption spectrum of hydrogen in the second overtone region was first observed in the laboratory by Herzberg (1952) who photographed the band at a gas pressure of 100 atm at 77 K with a path length of 80 m. He interpreted the spectrum as consisting of a pure second overtone band, in which one of the two colliding molecules makes a vibrational transition $\Delta v = 3$, and a double vibrational band in which one molecule makes a vibrational transition $\Delta v = 2$ while its collision partner simultaneously makes a vibrational transition $\Delta v = 1$. Prior to this observation in the laboratory, Herzberg (1951) identified a diffuse feature at 8267 Å (12,093 cm^{-1}), observed in the spectra of Uranus and Neptune by Kuiper (1949) as the pressure-induced $S_3(0)$ component of the 3 - 0 band of hydrogen. The first quantitative measurement of the absorption spectrum of hydrogen in its second overtone region has been made by McKellar and Welsh (1971) who recorded the spectra for gas densities of about 37 amagat at 85 K with a path length of 137 m and performed a profile analysis of the recorded spectra. No collision-induced spectra of deuterium in its second overtone region has been reported prior to the present work.

In the present work, the collision-induced absorption spectra of both hydrogen and deuterium in the second overtone regions were recorded for gas densities in the range 500 - 930 amagat at 77 K with the 2 m absorption cell. The observed absorption peaks in the spectra have been

interpreted satisfactorily and the binary and ternary absorption coefficients have been derived from the measured integrated absorption. However, the profile analysis carried out with the available values of the matrix elements of the quadrupole moment, polarizability and anisotropy of the polarizability of hydrogen and deuterium are far from satisfactory.

A description of the apparatus used to record the spectra is given in Chapter 2. Normal hydrogen or deuterium gas was contained in the 2 m absorption cell immersed in liquid nitrogen. For the deuterium experiments, a Perkin-Elmer model 112 single-beam double-pass spectrometer equipped with a 260 Hz tuning fork chopper and an uncooled PbS detector was used together with the associated electronics to record the spectrum. The slit width maintained at 35 μm gave a spectral slit width of about 18 cm^{-1} at 8626 cm^{-1}, the position of the $Q_3(0)$ component of deuterium. For the hydrogen experiments, a Perkin Elmer model 112G single-beam double-pass spectrometer equipped with a plane grating with 300 grooves/mm and a Hamamatsu model R758 photomultiplier tube together with a Princeton Applied Research model 124A lock-in amplifier and associated electronics were used to record the spectra. The slit width maintained at 10 μm gave a linear resolution of about 2 cm^{-1} at 11782 cm^{-1}, the position of the $Q_3(0)$ transition. The sensitivity of the PMT was several orders of magnitude greater than that of the PbS detector in this spectral region.

6.2. Experimental Absorption Profiles

Three typical absorption profiles of normal hydrogen in the pure gas at 77 K and at 647, 775 and 894 amagat in the second overtone region are shown in Fig. 6.1. A characteristic dip at 11775 cm^{-1} with its low- and

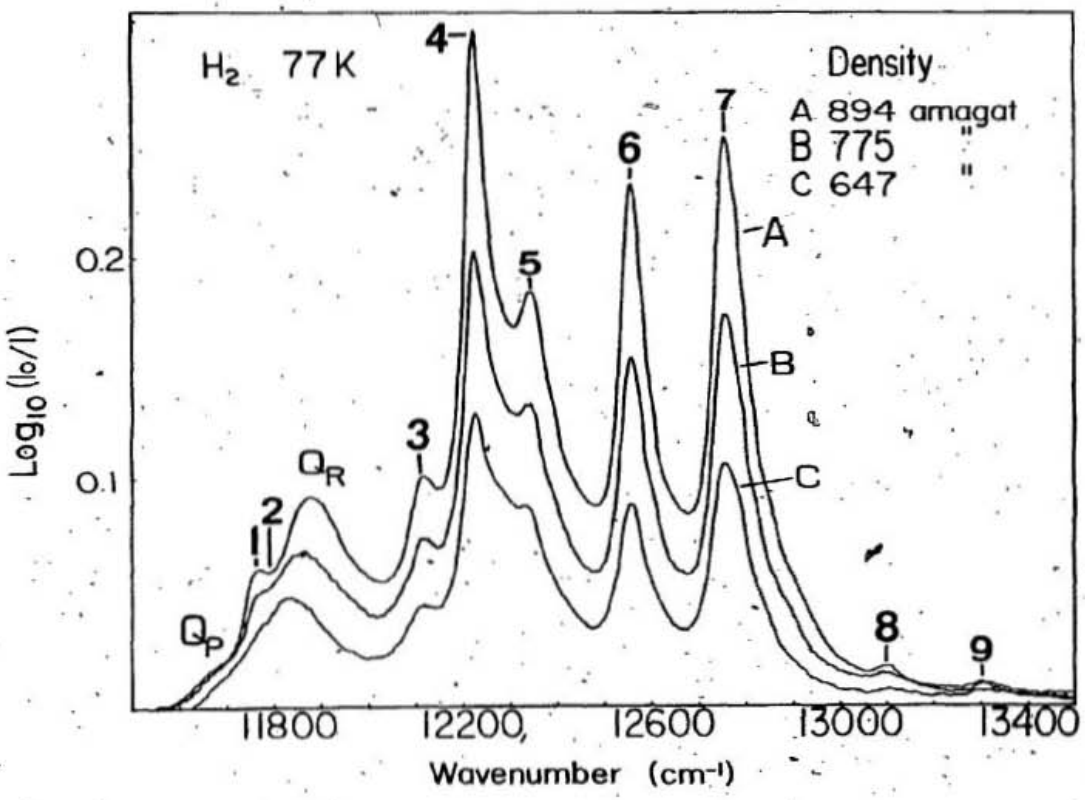

Figure 6.1 Absorption profiles of the second overtone region of H_2 at 77 K with a path length of 194.6 cm. The numbered features correspond to the assignments in Table 6.1.

high-wavenumber maxima Q_P and Q_R respectively and seven other distinct peaks are clearly seen in this figure. The occurrence of the dip in the Q branch of the collision-induced fundamental band of hydrogen has been interpreted in terms of the density-dependent intercollisional interference effect which arises from the negative correlations existing between the short-range overlap dipole moment induced in successive collisions (see van Kranendonk, 1968, Mcataggart and Welsh, 1973 and Reddy et al. 1977). The presence of the dip in the Q branch of the 3-0 band of hydrogen is a positive indication of the overlap contribution to the intensity of the band. The positions of the dip and of the absorption peaks are marked with identification numbers in Fig. 6.1. Their measured wavenumbers and assignments of the transitions are listed in Table 6.1. The calculated wavenumbers of various transitions in the 3-0 band region of hydrogen, obtained from the constants of the free hydrogen molecule, are listed in Appendix B. It may be mentioned that the absorption profiles of the hydrogen 3-0 band at 85 K show five peaks. The profiles reported here show three new peaks at 12,345, 13,100 and 13,310 cm^{-1} in addition to the dip and the associated Q_P and Q_R maxima. The peak at 12,345 cm^{-1} is attributed to the transition $Q_3(J) + S_0(J)$, the one at 13,100 cm^{-1} is assigned to $S_2(1) + S_1(0)$ and $S_2(0) + S_1(1)$ and the 13,310 peak is assigned to $S_2(1) + S_1(1)$. It is also apparent from the profiles in Fig. 6.1 that the separation between the Q_P and Q_R maxima increases with increasing density of the gas. For the profile at 894 amagat, $\Delta\nu_{PR}$ between the Q_P and Q_R maxima is about 170 cm^{-1}. The quadrupolar lines in the profiles shown in Fig. 6.1 appear to be somewhat narrower than the corresponding lines in the fundamental and first overtone regions. This is attributed to the diffusional narrowing which

TABLE 6.1 Assignment of the Observed Features in the H_2 Second Overtone Region

Peak no.	Wavenumber of observed peak (cm^{-1})	Assignment
1	11775	$Q_0(J) + Q_3(J)$
2	11793	$Q_3(J)$ *overlap*
3	12120	$S_3(0)$, $Q_3(J) + S_0(0)$
4	12227	$Q_1(J) + Q_2(J)$, $S_3(1)$
5	12345	$Q_3(J) + S_0(1)$
6	12562	$Q_1(J) + S_2(0)$, $Q_2(J) + S_1(0)$
7	12760	$Q_1(J) + S_2(1)$, $Q_2(J) + S_1(1)$
8	13100	$S_1(0) + S_2(1)$, $S_1(1) + S_2(0)$
9	13310	$S_1(1) + S_2(1)$

occurs at the high gas densities used in the present experiment.

The second overtone spectrum of deuterium was recorded at 7 densities in the range 500 to 950 amagat at a temperature of 77 K. Typical profiles are shown in Fig. 6.2. Although the features are less clearly resolved than in the hydrogen profiles, the electron overlap contribution to the Q branch is apparent, and the Q_P and Q_R maxima can be identified. The characteristic dip is less obvious, but can be distinguished as well. Again, there appears to be some pressure narrowing but it is less obvious in this case because the overall intensity of the absorption is smaller than in the hydrogen profiles. The wavenumbers of the absorption peaks and an identification of the more intense components which contribute to the features are given in Table 6.2.

The area of each experimental profile was measured to determine the integrated absorption coefficients $\int \alpha(\nu) d\nu$ as a function of density. Figure 6.3 shows a graph of $(1/\rho^2)\int \alpha(\nu) d\nu$ as a function of density for the hydrogen profiles. A similar graph for deuterium is shown if Fig. 6.4. In each case, a straight line was fitted to these points, and the resulting binary and ternary coefficients are tabulated in Table 6.3.

Attempts were made to fit the observed profiles to the theoretical relative intensities calculated for the quadrupolar and overlap components for both hydrogen and deuterium. In both cases it was found that the calculated quadrupolar relative intensities are quite different from the observed intensities. This can readily be seen in Fig. 6.5, where an observed profile for hydrogen is plotted together with the corresponding quadrupole profile calculated from the theoretical absolute intensities assuming a value of 35 cm^{-1} for δ_2 and 100 cm^{-1} for δ_4 in Eq. 1.9. These assumed values are the

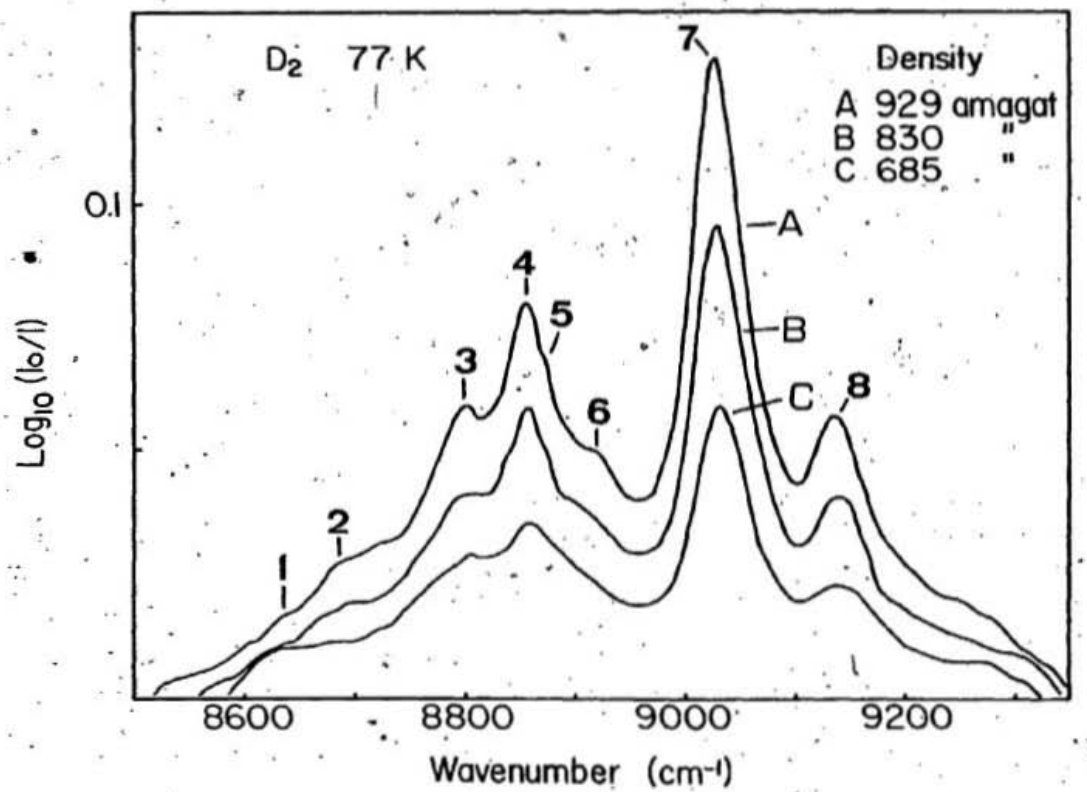

Figure 6.2 Absorption profiles of the D_2 second overtone region at 77 K with a path length of 194.6 cm. The numbered features correspond to the assignments in Table 6.2.

TABLE 6.2 Assignment of the Observed Features in the D_2 Second Overtone Region

Peak no.	Wavenumber of observed peak (cm^{-1})	Assignment
1	8630	$Q_0(J)+Q_3(J)$
2	8680	$Q_1(J)+O_2(2)$
3	8790	$S_3(0)$, $S_3(0)$, $Q_3(J)+S_0(0)$
4	8860	$Q_1(J)+Q_2(1)$, $Q_2(0)+Q_1(J)$
5	8880	$S_3(1)$
6	8920	$Q_3(J)+S_0(1)$
7	9030	$Q_1(J)+S_2(0)$, $Q_2(J)+S_1(0)$
8	9130	$Q_1(J)+S_2(1)$, $Q_2(J)+S_1(1)$

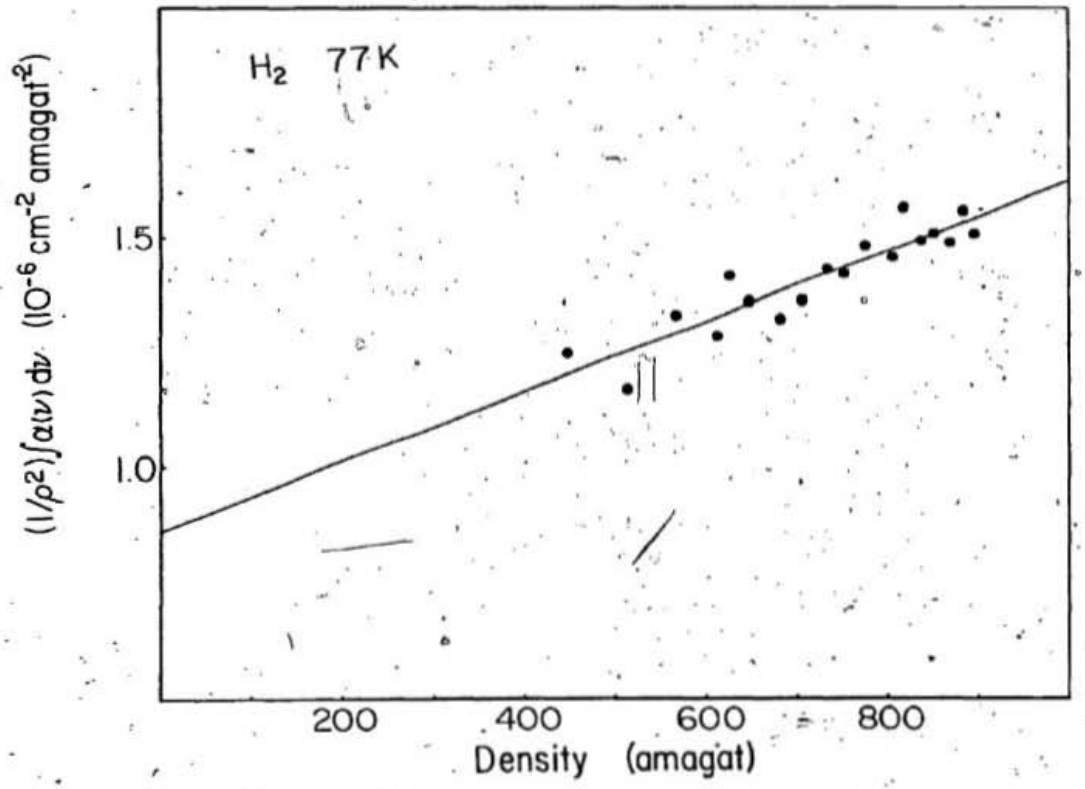

Figure 6.3 A plot of $(1/\rho^2)\int\alpha(\nu)d\nu$ against density, ρ, for the second overtone region of H_2 at 77 K.

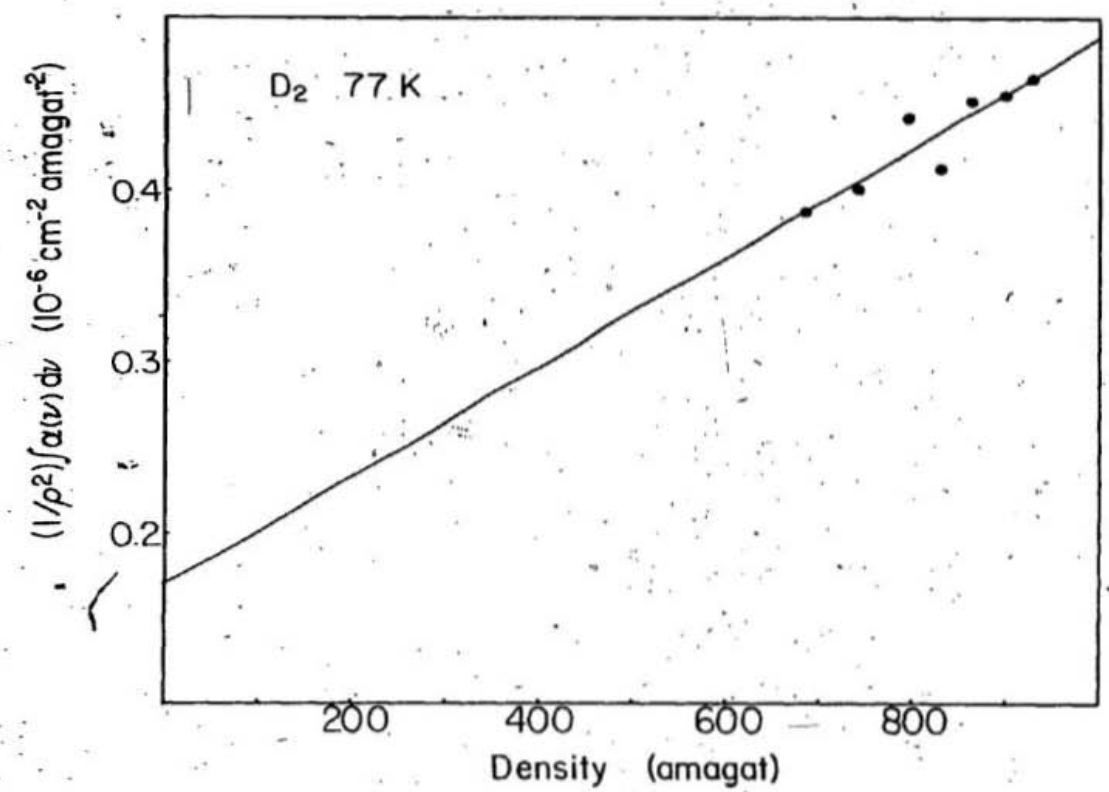

Figure 6.4 A plot of $(1/\rho^2)\int\alpha(\nu)d\nu$ against density, ρ, for the second overtone region of D_2 at 77 K.

Table 6.3. Absorption Coefficients* in the Second Overtone Region

Gas	Binary Absorption Coefficient			Ternary Absorption Coefficient	
		Experiment	Theory		
	α_{1a} $(10^{-7} cm^{-2} amagat^{-2})$	α_{1a} $(10^{-39} cm^{6} s^{-1})$	α_{1a} $(10^{-39} cm^{6} s^{-1})$	α_{2a} $(10^{-10} cm^{-2} amagat^{-3})$	
H_2	8.6 ± 0.6	4.4 ± .3	7.18	7.6 ± 0.8	(a)
H_2		5.4			(b)
D_2	1.7 ± 0.5	.78 ± .24	2.14	3.2 ± 0.6	(a)

* The errors indicated are standard deviations.

(a) Present work, at 77K.

(b) McKellar and Welsh (1971), at 85 K.

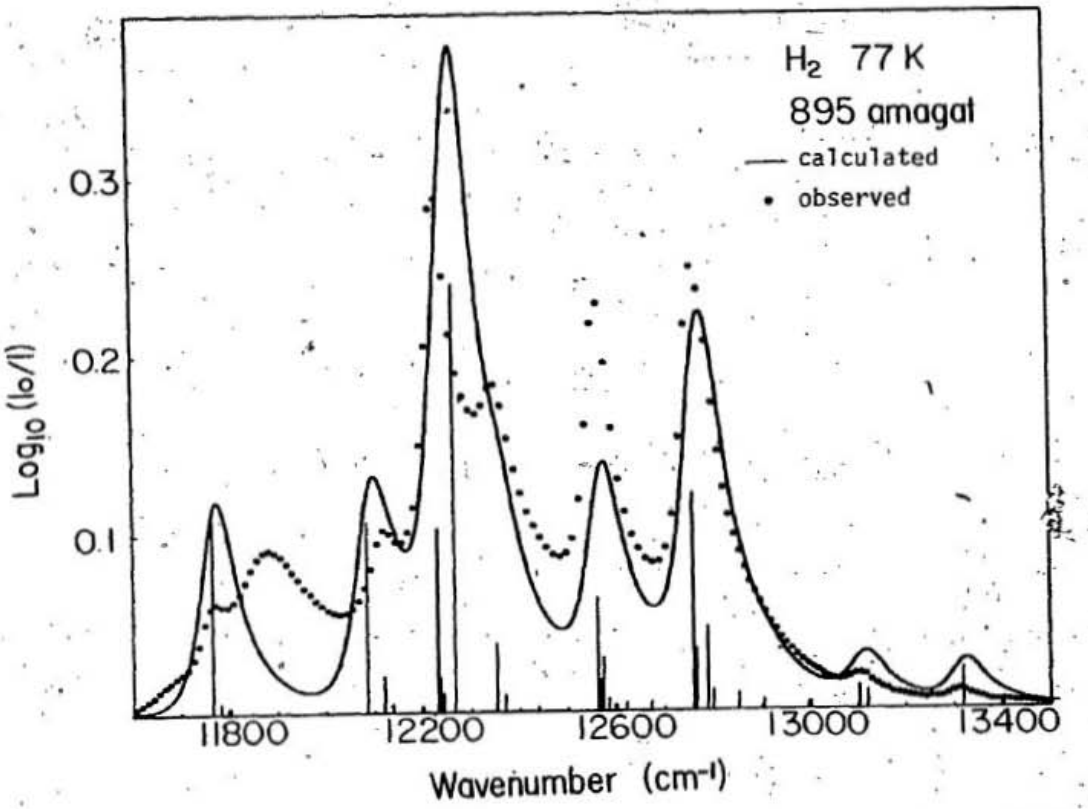

Figure 6.5 A plot of an observed profile for the H_2 second overtone region at 77 K with a path length of 194.6 cm., and a theoretically calculated profile for the quadrupolar components.

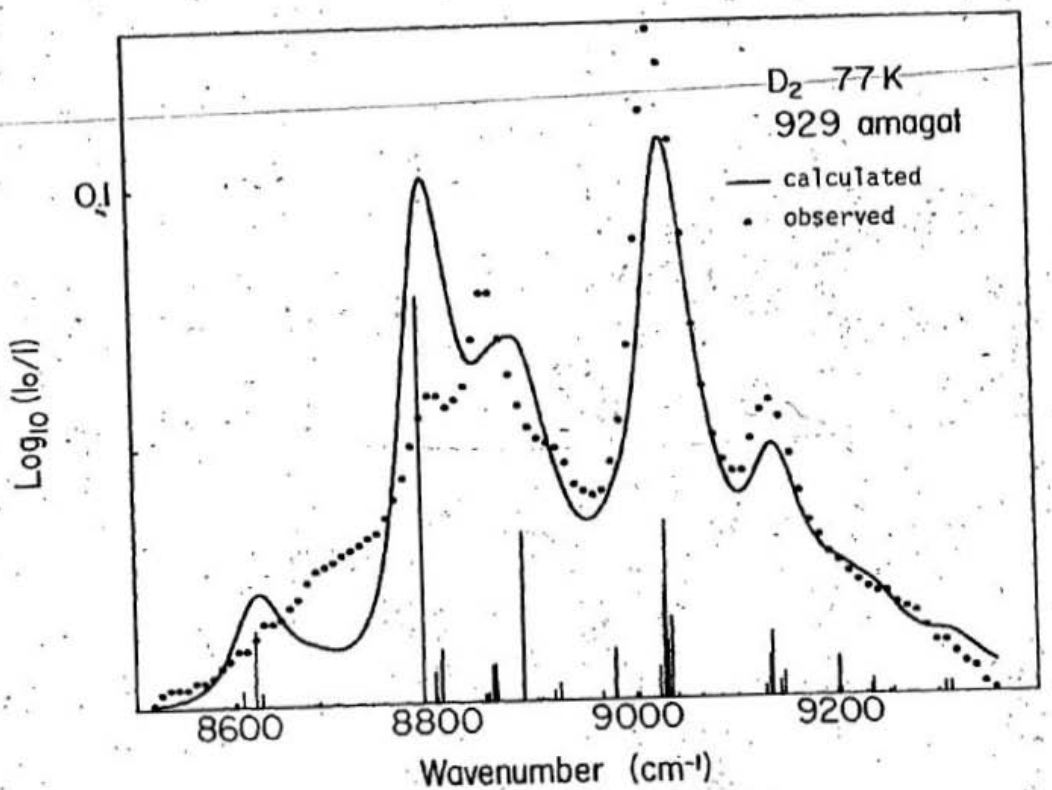

Figure 6.6 A plot of an observed profile for the D_2 second overtone region at 77 K with a path length of 194.6 cm., and a theoretically calculated profile for the quadrupolar components.

ones obtained for the 2-0 band of H_2 at 77 K (van Nostrand, 1983). The positions and calculated relative intensities of the important components are also shown. A similar profile is plotted for deuterium in Fig. 6.6, where $\delta_2 = 20\ cm^{-1}$ and $\delta_4 = 80\ cm^{-1}$. It is noted from Figs. 6.5 and 6.6 that similar transitions in hydrogen and deuterium appear to differ from the observed profiles by approximately the same factor.

As was the case for the first overtone spectrum, the calculated intensities involving the highest vibrational level appear to be too intense. In this case, however, no simple "improvement factor" applied to the v = 3 quadrupolar matrix elements results in an appreciable improvement in the quality of the fit to the experimental profiles. Even if the "improvement factor" for the v = 2 matrix elements found in the analysis of the first overtone profiles is retained, no satisfactory fit to the experimental profiles could be obtained.

6.3. Conclusions

The collision induced absorption spectra of the second overtone region of hydrogen and deuterium were measured at 77 K, and over a range of densities approaching the liquid density for both gases. At these high densities, at least, the theoretical absolute intensities for the quadrupolar lines do not agree with the observed intensities. The relative intensities so calculated also do not agree with experiment, and it appears that there is no simple relationship between the observed and calculated quadrupolar intensities as there is in the fundamental and first overtone spectra.

The individual lines appear to be narrower than the quadrupolar lines in the first overtone region, having a halfwidth δ_2 of about 35 cm^{-1}. From the shape of the lines, it appears that there is significant pressure narrowing at

these high densities.

In the 3-0 band, there is definite evidence of an overlap contribution to the second overtone spectrum in both hydrogen and deuterium. In each case there is a characteristic dip and a significant intensity in the Q branch of the spectrum. This dip is a characteristic of the overlap transitions, and is a result of "intercollisional interference". Unfortunately, the overlap contribution to both spectra cannot be satisfactorily analysed because the quadrupolar and overlap components are intermixed, and the quadrupolar components cannot be satisfactorily accounted for. It is therefore difficult to ascertain whether there are similar problems with the relative intensities of the overlap components.

APPENDIX A

Programs for data acquisition and analysis

of the experimental data.

PROGRAM TO LOG DATA FROM MICROPROCESSOR

```
110 REM DATA LOGGER
120 INPUT "INITIAL TRACE NO.";G
130 REM READ FILENAME,NO. OF POINTS,TEMP
140 READ F$,H$,N,T,P
150 PRINT "SWITCH TO VAX,THEN PRESS RETURN" : INPUT A$
160 GOSUB 1900
170 PRINT "sed -f ed.file ";F$+MID$(STR$(G),2)
180 GOSUB 1900
190 REM GET INITIAL DATA
200 PRINT H$
210 PRINT "NO. OF POINTS ";N
220 PRINT "TRACE NO. ";G
230 INPUT "PRESSURE ";P
235 PRINT "DENSITY     ";0
240 PRINT "PATH LENGTH ";P
250 PRINT "TEMPERATURE ";T
260 REM INITIALIZE PPI
270 OUT 11,147
280 REM DISABLE ADC OUTPUT
290 OUT 10,255
300 REM SET UP TIMERS FOR 0 AVERAGE
310 OUT 7,54 : OUT 7,116
320 INPUT "BLOCK LIGHT FOR 0 AVERAGE";A$
330 REM START FAST TIMER
340 OUT 4,24 : OUT 4,0
350 REM START 0.5 SEC TIMER
360 OUT 5,0 : OUT 5,125
370 S=0
380 FOR I = 1 TO 40
390 GOSUB 1400
400 S = S + E
410 NEXT I
420 S = INT(S/40+.5)
430 PRINT "0 AVERAGE ";S
440 INPUT "START TRACE-PRESS CR";A$
500 REM WAIT FOR SIGNAL TO START SAMPLING
510 WAIT 8,128
520 OUT 7,116 : OUT 7,176
530 REM START 0.5 SEC. INTERVAL TIMER
540 OUT 5,0 : OUT 5,125
550 REM SET UP COUNTER FOR INTERVALS
```

```
560 OUT 6,0 : OUT 6,250
600 REM START SAMPLING EVERY INTERVAL
610 FOR I = 1 TO N
620 REM GET DIGITIZED VALUE AS E
630 GOSUB 1400
640 PRINT K;E-S
650 NEXT I
700 PRINT "COMMENT/2 LINES"
710 INPUT A$
720 INPUT A$
730 INPUT "REFERENCE POSITION";A$
740 INPUT "more";A$
800 REM PLACE DATA IN FILE
810 PRINT CHR$(4)
820 GOSUB 1900
830 REM START NEXT RUN
840 G = G+1
850 GOTO 170
900 DATA "file"
910 DATA "TITLE"
920 DATA 632
930 DATA 77
940 DATA 186.1
990 END
1400 REM READ ADC , RETURNS A
1420 OUT 7,64
1430 X=INP(5) : X=INP(5)
1440 Y=X
1450 OUT 7,64
1460 X=INP(5) : X=INP(5)
1470 IF X<>Y THEN 1440
1500 REM ONE INTERVAL HAS PASSED
1510 WAIT 8,64
1520 OUT 10,0
1530 Z=INP(8)
1540 A=Z-INT(Z/16)*16
1550 OUT 10,16
1560 Z=INP(8)
1570 B=Z-INT(Z/16)*16
1580 OUT 10,32
1590 Z=INP(8)
1600 C=Z-INT(Z/16)*16
1610 OUT 10,48
1620 Z=INP(8)
1630 D=Z-INT(Z/16)*16
1640 OUT 7,128
1650 L=INP(6)+256*INP(6)
1660 K=64000-L
1670 E=A+10*B+100*C+1000*D
1690 RETURN
1900 REM APPROX. 3 SEC. TIME DELAY
```

```
1910 FOR J = 1 TO 3000
1920 NEXT J
1930 RETURN
1990 END
```

PROGRAM TO CALCULATE RELATIVE INTENSITIES FOR
MULTIPOLE INDUCTION

```
c       calculate relative and absolute intensities for normal D2
        integer vh,vl,v2,dj,djl,dj2
        real*8 maxin,Jstar,iso
        implicit real *8 (a-h,o-z)
        real*8 B(5),D(5),H(5),V(5),ff(5),A(5,5),Q(5,5,5),gamma(5,5,5)
        real*8 x(5,5,5,5,5),x1(2000,7),p(2),eng(2)
        character*20 fname
        write (0,*) 'highest vibrational state'
        read *,n
        write (0,*) 'temperature ? (remember decimal point)'
        read *,t
c
c       evaluate constant for absolute intensities
c       constant const = 8 * pi**3 * e ** 2 * n0**2 / (3 * h * c)
c
c       const = 8.0 * 3.14159265**3 * 4.80325e-10**2 * 2.687e19**2
c       const = const / (3.0 * 6.626196e-27 * 2.997925e10)
c       to avoid overflow , we quote  const in (Angstrom)**-5 ;
c       we divide the above by 10**40
c
        const = 6.93328e-03
c
c       evaluate multiplier for absolute intensities
c       the following values are assumed
c       ao , sigma are given in Angstroms
c       eps is in ergs
c       rmass is the reduced mass of the interacting pair in AMU
c
        a0 = 0.52917
        sigma = 2.928
        eps = 5.11e-15
        rmass = 2.00
c
c       L is the order of the inducing moment
c       L = 2 for quadrupole moment
c       L = 4 for hexadecapole moment
c
        write (0,*) 'enter multipole order (2 - quad. , 4 - hex.)'
        read *,L
        L1 = L / 2 + 1
c
```

```
c     abfact is the factor const * a0**5 * J* , where J* is
c     as 4 * pi * (L + 1) * integral(g(x) * x**-(2*L + 2) dx)
c     The subroutine Jstar includes the factor 4 * pi * (L + 1)
c
      abfact = const * a0**5 * Jstar(eps,a0,sigma,rmass,t,L)
c
      write (0,*) 'enter cutoff value for relative intensity'
      read *,maxin
    5 format (a20)
      write (0,*) 'enter name of matrix element file'
      read (*,5) fname
c
c     nl is the no. of v levels in the input data
      nl = 4
c
      open (unit =8,file = fname,status = 'old')
      rewind 8
  100 format ('      SPECTROSCOPIC CONSTANTS'///)
      read (8,100)
  101 format ('  v = ',i2,4(2x,e15.8))
  102 format (5f12.8)
  103 format (11x,'B',11X,'D',11X,'H',11X,'v')
  104 format (' ')
      do 110 v1 = 0,nl
        read (8,101) i,B(v1+1),D(v1+1),H(v1+1),V(v1+1)
  110 continue
      read (8,104)
  105 format(/'      polarizability matrix elements'/)
      read (8,105)
      do 140 v1 = 0 , nl
        read (8,102) (a(v1+1,j+1),j=0,4)
  140 continue
  106 format(/'       quadrupole matrix elements .      '/)
      read (8,106)
      do 170 dj = -L , L , 2
        do 160 v1 = 0 , nl
              read (8,102) (q(dj/2+L1,v1+1,j+1),j = 0,4)
  160   continue
        read (8,104)
  170 continue
  107 format(/'      anisotropic polarizability matrix elements
     1 (gamma)'/)
      read (8,107)
      do 200 dj = -L , L , 2
        do 190 v1 = 0 , nl
              read (8,102) (gamma(dj/2+L1,v1+1,j+1),j = 0,4)
  190   continue
        read (8,104)
  200 continue
  201 format ('enter quadrupole V = ',i2,' fudge factor ',$)
      do 205 v1 = 1 , n
```

```
        write (0,201) v1
        read *,ff(v1+1)
  205   continue
        do 225 v1 = 1 , n
        do 220 dj = -L , L , 2
          do 210 j = 0 , 4
            q(dj/2+L1,v1+1,j+1) = ff(v1+1) * q(dj/2+L1,v1+1,j+1)
  210     continue
  220   continue
  225   continue
c
c       calculate rotational partitional function (rpf)
c       and effective statistical weights for normal D2
c
        y = 0.0
        rt = 1.438832042 / t
        w = 0.0
        do 380 j = 0 , 4 , 2
          w = w + (2 * j + 1) * exp(-termv1(B(1),D(1),H(1),V(1),j)*rt)
          y = y + (2 * j + 3) * exp(-termv1(B(1),D(1),H(1),V(1),j+1)*rt)
  380   continue
        rpf = 3.0 * y
        hh =  abfact / rpf**2
        w = 2.0 * y / w
  391   format (' normal deuterium')
        write (6,391)
  392   format ('quadrupolar fudge factors  ',$)
        write (6,392)
  393   format (f9.2,$)
        do 390 v1 = 1 , n
          write (6,393) ff(v1+1)
  390   continue
  394   format (/' temperature = ',f7.2)
        write (6,394) t
        n1 = 0
        do 450 dj1 = -L , L , 2
          do 440 v1 = 0 , n
          v2 = n-v1
             do 430 j1 = max(-dj1,0) , 4
               eng(1) = termv1(B(1),D(1),H(1),V(1),j1)
               e1 = termv1(B(v1+1),D(v1+1),H(v1+1),V(v1+1),j1+dj1)-
     1         eng(1)
               if ( mod(j1,2) .eq. 0 ) then
                 g = w
               else
                 g = 1
               end if
               p(1) = g * (2 * j1 + 1 ) * exp(-eng(1)*rt) * hh
                 do 420 dj2 = -L , L , 2
                do 410 j2 = 0 , 4
                  eng(2) = termv1(B(1),D(1),H(1),V(1),j2)
```

```
      e2 = termv1(B(v2+1),D(v2+1),H(v2+1),V(v2+1),j2+dj2)-
     1 eng(2)
      if ( mod(j2,2) .eq. 0 ) then
        g = w
      else
        g = 1
      end if
      p(2) = g * (2.0 * j2 + 1.0 ) * exp(-eng(2)*rt)
      pp = p(1) * p(2)
c
c     anisotropic calculation
c
      t1=(q(dj1/2+L1,v1+1,j1+1)*gamma(dj2/2+L1,v2+1,j2+1))**2
      t2=(q(dj2/2+L1,v2+1,j2+1)*gamma(dj1/2+L1,v1+1,j1+1))**2
      tt1 = (2.0/9.0) * ( t1 + t2 )
      t3=q(dj1/2+L1,v1+1,j1+1)*q(dj2/2+L1,v2+1,j2+1)
      t4=gamma(dj1/2+L1,v1+1,j1+1)*gamma(dj2/2+L1,v2+1,j2+1)
      tt2 = (4.0/15.0) * ( t3 * t4 )
      anis = cg(j1,L,j1+dj1)*cg(j2,L,j2+dj2)*( tt1 - tt2 )
c
c     isotropic calculation
c
      iso = 0.0
      if (dj2 .eq. 0) then
        iso = (q(dj1/2+L1,v1+1,j1+1)*a(v2+1,j2+1))**2
        iso = iso * cg(j1,L,j1+dj1)
      end if
c
      z = anis + iso
      if (v1 .le. v2) then
        iv = v1 +1
        idj1 = dj1/2+L1
        ij1 = j1 + 1
        idj2 = dj2/2+L1
        ij2 = j2 + 1
      else
        iv = v2 + 1
        idj1 = dj2/2+L1
        ij1 = j2 + 1
        idj2 = dj1/2+L1
        ij2 = j1 + 1
      end if
      zz = x(idj1,iv,ij1,idj2,ij2)
      x(idj1,iv,ij1,idj2,ij2) = zz + z * pp
410   continue
420   continue
430 continue
440 continue
450 continue
c
c     sum all v = 0 transitions with dj1 = 0 , since these are
```

```
c       orientational transitions
c
        do 500 dj2 = -L , L , 2
          do 490 j2 = 0 , 4
               do 480 j1 = 1 , 4
                  x(L1,1,1,dj2/2+L1,j2+1)=x(L1,1,1,dj2/2+L1,j2+1) +
     1            x(L1,1,j1+1,dj2/2+L1,j2+1)
                  x(L1,1,j1+1,dj2/2+L1,j2+1) = 0.0
  480          continue
  490     continue
  500   continue
c
c       collect identical terms when v = n/2
c
        vh = n/2
        if (vh * 2 .eq. n) then
        vh = vh + 1
            do 600 dj1 = -L , L , 2
          do 590 j1 = max(-dj1,0) , 4
              do 580 dj2 = -L , L , 2
                j2s = j1
                if (dj1 .eq. dj2) j2s = j1 + 1
                  do 570 j2 = j2s , 4
                    y = x(dj1/2+L1,vh,j1+1,dj2/2+L1,j2+1)
                    x(dj1/2+L1,vh,j1+1,dj2/2+L1,j2+1) = y +
     1              x(dj2/2+L1,vh,j2+1,dj1/2+L1,j1+1)
                    x(dj2/2+L1,vh,j2+1,dj1/2+L1,j1+1) = 0.0
  570           continue
  580         continue
  590     continue
  600       continue
        end if
c
c       find normalization factor and integrated absorption coefficient
c
        absc = 0.0
        y = 0.0
        do 840 dj1 = -L , L , 2
            do 830 v1 = 0 , n
          do 820 j1 = max(-dj1,0) , 4
              do 810 dj2 = -L , L , 2
                do 800 j2 = max(-dj2,0) , 4
                    absc = absc + x(dj1/2+L1,v1+1,j1+1,dj2/2+L1,j2+1)
                  if (x(dj1/2+L1,v1+1,j1+1,dj2/2+L1,j2+1) .gt.y) then
                    y = x(dj1/2+L1,v1+1,j1+1,dj2/2+L1,j2+1)
                  end if
  800           continue
  810         continue
  820     continue
  830       continue
  840   continue
```

```
      nval = 0
      do 890 dj1 = -L , L , 2
         do 880 v1 = 0 , n
        v2 = n - v1
        do 870 j1 = max(-dj1,0) , 4
           e1 = termv1(B(v1+1),D(v1+1),H(v1+1),V(v1+1),j1+dj1)-
     1     termv1(B(1),D(1),H(1),V(1),j1)
           do 860 dj2 = -L , L , 2
             do 850 j2 = max(-dj2,0) , 4
               e2 = termv1(B(v2+1),D(v2+1),H(v2+1),V(v2+1),j2+dj2)-
     1         termv1(B(1),D(1),H(1),V(1),j2)
               x1 = x(dj1/2+L1,v1+1,j1+1,dj2/2+L1,j2+1)
               if (x1 / y .gt. maxin ) then
                 nval = nval + 1
                 x1(nval,1)=dj1
                 x1(nval,2)=v1
                 x1(nval,3)=j1
                 x1(nval,4)=dj2
                 x1(nval,5)=j2
                 x1(nval,6)=e1+e2
                 x1(nval,7)=x1
               end if
850          continue
860        continue
870     continue
880       continue
890   continue
909   format (' no. of values greater than ',e10.3,' = ',i5/)
      write (6,909) maxin,nval
911   format (' largest absolute intensity        = ',e15.7)
      write (6,911) y
912   format (' integrated absorption coefficient = ',e15.7/)
      write (6,912) absc
913   format ('       molecule 1     molecule 2'/)
914   format ('     dj1  dv1   j1  dj2  dv2   j2'/)
      write (6,913)
      write (6,914)
915   format (3x,6i5,2x,f12.3,2x,2e15.8)
      do 920 i = 1 , nval
        dj1 = x1(i,1)
        v1 = x1(i,2)
        j1 = x1(i,3)
        dj2 = x1(i,4)
        j2 = x1(i,5)
        e = x1(i,6)
        x1 = x1(i,7)
        xx = x1 / y
        v2 = n - v1
        write (6,915) dj1,v1,j1,dj2,v2,j2,e,xx,x1
920   continue
      end
```

```
c
c
      double precision function termvl(B,D,H,V,j)
      jj = j * (j + 1)
      termvl = B * jj - D * jj ** 2 + H * jj ** 3 + V
      return
      end
c
c
      double precision function cg(l1,l2,l3)
c     evaluates squares of Clebsh-Gordan coefficients for M = m = 0
c
      integer l1,l2,l3
      real*8 c
      real t
      if (mod((l1+l2+l3),2) .ne. 0) then
        cg = 0.0
      else
      if (((l1-l2+l3).lt.0).or.((l1+l2-l3).lt.0).or.
     1 ((-l1+l2+l3).lt.0)) then
        cg = 0.0
      else
        c = (2. * l3 + 1) / (l1 + l2 +l3 + 1.)
        cg = c * t(l1+l2+l3) / (t(l1+l2-l3) *
     1  t(l1-l2+l3) * t(-l1+l2+l3))
      end if
      end if
      return
      end
c
      real function t(i)
        t = fact(i/2)**2 / fact(i)
      return
      end
c
      real function fact(i)
      integer i,j
      if (i .le. 0) then
        fact = 1.0
      else
        fact = 1.0
        do 40 j = 1 , i
             fact = fact * j
 40     continue
      end if
      return
      end
c
c     function to evaluate the integral J*
      real function Jstar(eps,a0,sigma,rmass,t,L)
c     rmass is the reduced mass of the interacting pair , in AMU
```

```
c     sigma is in angstroms
c     eps is in ergs
      real jstar0,jstar1,jstar2,lambda,k
      n = 2 * L + 2
c     k = 1.380622e-16 erg/K
      k = 1.380622e-16
c
c     lambda = h**2 * N / (2 * rmass * eps * sigma**2)
c
      lambda = 2.64409e-13 / (2.0 * rmass * eps * sigma**2)
      pi = 3.14159265
      ts = t/(eps/k)
      jstar0 = 0.0
      jstar1 = 0.0
      jstar2 = 0.0
      hh = .005
      do 50 x = 0.5 , 20.0 , hh
      v0 = 4.0 * (x**-12 - x**-6)
      v1 = -24.0 * (2.0 * x**-13 - x**-7)
      v2 = 24.0 * (26.0 * x**-14 - 7.0 * x**-8)
      v3 = -672.0 * (13.0 * x**-15 - 2.0 * x**-9)
      v4 = 2016.0 * (65.0 * x**-16 - 6.0 * x**-10)
      g0 = exp(-v0/ts)
      g1 = g0 / (24.0*pi**2*ts**2) * (-(v2+2.0*v1/x) + v1**2/(2.0*ts))
      zz = -(v4 + 4.0*v3/x) / 5.0
      zz = zz +(9.0*v2**2 +12.0*v1*v3 +44.0*v1*v2/x
     1 +(2.0*v1/x)**2) /(30.0*ts)
      zz = zz -(11.0*v2*v1**2 +10.0*v1**3/x) /(30.0*ts**2)
     1 +v1**4/(24.0*ts**3)
      g2 = g0 / (192.0 * pi**4 * ts**3) * zz
      vjn0 = x**-n * g0
      vjn1 = x**-n * g1
      vjn2 = x**-n * g2
      jstar0 = jstar0 + vjn0*hh
      jstar1 = jstar1 + vjn1*hh
      jstar2 = jstar2 + vjn2*hh
   50 continue
      jstar = 4.0 * pi *(L+1) * (a0 / sigma)**(n-1)
      jstar = jstar * (jstar0 + lambda * jstar1 + lambda**2 * jstar2)
      return
      end
```

PROGRAM TO FIT LINESHAPES TO OBSERVED SPECTRA

```
c     non-linear least squares fit to experimental profile of a
c     synthetic quadrupolar and overlap spectrum
c
c     to do overlap spectrum only :
c     1. enter no quadrupolar lines
c     2. set np=3
c
c     to do overlap and unshifted quadrupolar ;
c     1. set np=5 (=6 if a 1/v**4 tail is used)
c
c       to do quadrupolar spectrum only
c       1. enter no overlap lines
c       2. enter appropriate no. of parameters (2 or 3)
c
        implicit real*8 (a-h,o-z)
        real *8 rs(10),sdf(10,11),df(10),a,eps,af,daf,afot,afqt,r
        common sq(250),sqf(250),so(50),sof(50),a(10),afq(250),afo(50),
     1  nlq,nlo,r,afqt,afot
        real*8 x(2000),y(2000)
        integer v
        character*20 calfil,obsfil,outfil
        character*60 head
   15   format (a20)
        v = 4
        a(1) = 0.0
        a(2) = 1.0
        a(3) = 1.0
c
c     read intensities (sq) and frequencies (sqf) of quad. lines
c
        write (0,*) 'enter filename for calculated data'
        read (5,15) calfil
        open (unit = 8,file = calfil,status = "old")
        rewind (8)
   51   format (a60)
   52   format (' temperature = ',f7.2)
   53   format (' no. of values greater than ',e10.4,' = ',i6)
   55   format (3x,6i5,2x,f12.3,2x,2e15.8)
        do 56 i = 1 , 2
          read (8,51) head
   56   continue
        read (8,52) t
```

```
      r=1.438832042d0/t
      read (8,53) cutoff,nlq
      do 60 i = 1 , 8
        read (8,51) head
   60 continue
      qinten = 0.0
      do 70 i = 1 , nlq
        read (8,55) i1,i2,i3,i4,i5,i6,sqf(i),sq(i),xx
        qinten = qinten + xx
   70 continue
   71 format (/' quadrupolar integrated absorption = ',e14.7/)
c
c     read intensities (so) and frequencies (sof) for overlap
c
      do 80 i = 1 , 5
        read (8,51,end = 100) head
   80 continue
      read (8,53,end = 100) cutoff,nlo
      read (8,51,end = 100) head
      do 90 i = 1 , nlo
        read (8,55) i1,i2,i3,i4,i5,i6,sof(i),so(i)
   90 continue
      v = 1
      if (nlo .eq. 0) v = 4
  100 continue
c
c     np is the no. of parameters
c     the a(np) are the adjustable parameters, h is the increment,
c     eps is the allowable fractional error in the constants
c
  111 format ('no. of parameters          ',$)
  112 format ('increment for derivative   ',$)
  113 format ('allowable fractional error ',$)
  114 format ('a(',i1,') = ',$)
      write (0,111)
      read *, np
      np = np + v - 1
      write (0,112)
      read *, h
      write (0,113)
      read *, eps
      do 120 i = v , np
        write (0,114) i-v+1
        read *, a(i)
  120 continue
      do 130 i = np + 1 , 10
        a(i) = 0.0
  130 continue
c
c     read frequencies(x) and log(intensities ratios) (y) for the
c     experimental profile
```

```
c
    2  continue
       write (0,*) 'enter filename for observed data'
       read (5,15,end = 990) obsfil
       if ((obsfil .eq. 'none') .or. (obsfil .eq. 'q')) go to 990
       open (unit = 9,file = obsfil,status = "old")
       rewind (9)
       write (0,*) 'enter output filename'
       read (5,15,end = 990) outfil
       if ((outfil .eq. 'none') .or. (outfil .eq. 'q')) go to 990
       open (unit = 4,file = outfil,status = "new")
       rewind (4)
       write (4,*) 'data file for theoretical intensities ',calfil
  135  format(//1h ,'increment= ',f9.5,4x,'error= ',f9.5/)
       write (4,135) h,eps
  101 format (14x,i4)
  102 format (12x,f10.2)
  105 format (3x,'temperature ',f10.2/3x,'pressure    ',f10.2/
     1'   density     ',f10.2,/3x,'path length ',f10.2//)
  106  format ('sequence error at line ',2i5)
       read (9,101) n
       read (9,102) press
       read (9,102) dens
       read (9,102) path
       read (9,102) temp
       write (4,105) temp,press,dens,path
       write (0,105) temp,press,dens,path
       write (1,105) temp,press,dens,path
       factor = path * dens**2
       do 110 i = 1 , n
         read (9,*) iseq,x(i),y(i)
         if (iseq .ne. i) then
               write (0,106) iseq,i
               go to 100
         end if
         y(i)=y(i)/x(i)
  110  continue
       if (temp .ne. t) then
         write (0,*) 'temperatures do not match'
         go to 990
       end if
c
       kj=0
  131  format(//2x,'fitted parameters'/)
       write(4,131)
       write (4,132) kj,(a(i),i=v,np)
       write (0,132) kj,(a(i),i=v,np)
  132  format (1h ,i2,3x,10g12.5)
c
c      this fills the matrix to be solved
c
```

```
      do 300 kj=1,25
        aerr = 0.
        do 140 i = 1 , n
          call cal(x(i),af)
          aerr = aerr + ((y(i)-af)*x(i))**2
  140   continue
  141   format (' standard error = ',e14.7/)
        write (4,141) sqrt(aerr)/(n-np+v-1)
        write (0,141) sqrt(aerr)/(n-np+v-1)
        do 160 i=1,np
          do 150 j=1 , np + 1
  150     sdf(i,j) = 0.
  160   rs(i)=0.
        do 200 i=1,n
          xi=x(i)
          call cal(xi,af)
          do 170 j=v,np
                ha=a(j)*h
                a(j)=a(j)+ha
                call cal(xi,daf)
                a(j)=a(j)-ha
                df(j)=(daf-af)/ha
  170     continue
          do 190 j=v,np
                do 180 jj=v,np
            sdf(j,jj)=sdf(j,jj)+df(j)*df(jj)
  180           continue
                rs(j)=rs(j)+(y(i)-af)*df(j)
  190     continue
  200   continue
c
c     a routine to solve the above lin. equations
c
        do 210 k = v , np
          sdf(k,np+1) = rs(k)
  210   continue
        do 240 k=v,np
          kk=k+1
          do 230 j=kk,np + 1
                if (sdf(k,k) .eq. 0.0) then
                  write (0,*) 'matrix is singular'
                  write (4,*) 'matrix is singular'
                  go to 990
                end if
                sdf(k,j)=sdf(k,j)/sdf(k,k)
                do 220 i=v,np
           if(k .ne. i) sdf(i,j)=sdf(i,j)-sdf(i,k)*sdf(k,j)
  220           continue
  230     continue
  240   continue
        do 250 i=v,np
```

```
        rs(i)=sdf(i,np+1)
  250   continue
c
c     here we add the correction terms just evaluated
c
        do 260 i=v,np
          a(i)=a(i)+rs(i)
  260   continue
        write (4,132) kj,(a(i),i=v,np)
        write (0,132) kj,(a(i),i=v,np)
        do 270 i=v,np
          if(dabs(rs(i)/a(i)) .ge. eps) go to 300
  270   continue
        go to 301
  300 continue
  301   continue
        aerr = 0.0
        do 305 i = 1 , n
          call cal(x(i),af)
          aerr = aerr + ((y(i)-af)*x(i))**2
  305   continue
        write (4,141) sqrt(aerr)/(n-np+v-1)
        write (0,141) sqrt(aerr)/(n-np+v-1)
        write (1,132) kj,(a(i),i=v,np)
        write (1,141) sqrt(aerr)/(n-np+v-1)
        write (4,309)
c
  306   format(///4x9hfrequency,4x8hobserved,3x9hpredicted,2x
     1  10hdifference,5x7hoverlap,1x11hquadrupolar/)
        write (4,306)
        ax = x(1)
        ay = y(1)
        call cal(ax,af)
        dff = 0.5 * (x(2) - x(1))
        diff = ay-af
        aerr = (ay - af)**2
        areao = afot * dff
        areaq = afqt * dff
        areaf = af * dff
        areay = ay * dff
        areavo = afot * ax * dff
        areavq = afqt * ax * dff
        areavf = af * ax * dff
        areavy = ay * ax * dff
        afotm1 = afot
        afqtm1 = afqt
        afm1 = af
        aym1 = ay
        axm1 = ax
        write (4,309) ax,ay*ax,af*ax,diff*ax,afot,afqt
  309   format (1h ,10f12.4)
```

```
      do 310 i = 2 , n
            ax=x(i)
            ay=y(i)
            dff=0.5*(ax-axml)
            call cal(ax,af)
            diff=ay-af
            aerr=aerr+diff*diff
            areao=areao+(afot+afotml)*dff
            areaq=areaq+(afqt+afqtml)*dff
            areaf=areaf+(af+afml)*dff
            areay=areay+(ay+ayml)*dff
            areavo=areavo+(afot*ax+afotml*axml)*dff
            areavq=areavq+(afqt*ax+afqtml*axml)*dff
            areavf=areavf+(af*ax+afml*axml)*dff
            areavy=areavy+(ay*ax+ayml*axml)*dff
            afqtml=afqt
            afotml=afot
            afml=af
            ayml=ay
            axml = ax
      write (4,309) ax,ay*ax,af*ax,diff*ax,afot,afqt
310   continue
      aerr=sqrt(aerr)/(n-np+v-1)
312   format (/a14,5e13.5)
      write (4,312) 'areas          ',areavy,areavf,
     1 areavy-areavf,areavo,areavq
      write (4,312) '1/(1*p^2)*area',areavy/factor,areavf/factor,
     1 (areavy-areavf)/factor,areavo/factor,areavq/factor
      write (4,312) 'int abs        ',areay,areaf,areay-areaf,
     1 areao,areaq
      write (4,312) 'int abs coeff ',areay/factor,areaf/factor,
     1 (areay-areaf)/factor,areao/factor,areaq/factor
      write (4,*) ' '
      write (4,141) aerr
      write (4,71) qinten
      go to 2
990   stop
      end
c
c
      subroutine cal(xi,af)
      implicit real*8 (a-h,o-z)
      double precision a,xt,af,afot,afqt,r
      common sq(250),sqf(250),so(50),sof(50),a(10),afq(250),afo(50),
     1 nlq,nlo,r,afqt,afot
      ick=0
      go to 300
      entry call(xi)
      ick=1
c
c     overlap contribution
```

```
c
  300   afot=0.d0
        if (nlo .le. 0) go to 401
  301   do 400 j=1,nlo
          xt=xi-sof(j)
          rn=a(1)*so(j)*over(xt,r,a(2),a(3))
          afo(j)=rn
          afot=afot+rn
  400   continue
  401   if(ick .eq. 0) go to 850
c
c       quadrupolar contribution
c
        entry cal2(xi)
  850   afqt=0.d0
        if (nlq .le. 0)  go to 221
  851   do 220 j=1,nlq
          xt=xi-sqf(j) + a(7)
          rn = a(4) * sq(j) * quad(xt,r,a(5),a(6))
  200     afq(j)=rn
          afqt=afqt+rn
  220   continue
  221   af=afot+afqt
 1000   return
        end
c
        real*8 function quad(dv,r,a1,a2)
        implicit real*8 (a-h,o-z)
        if (a2 . gt. 0.0) then
              rn=1.0/(1.+(dv/a1)**2+(dv/a2)**4)
        else
          rn=1.0/(1.+(dv/a1)**2)
        end if
        quad = rn/(1.+dexp(-r*dv))
        return
        end
c
        real*8 function over(dv,r,a1,a2)
        implicit real*8 (a-h,o-z)
        xt = dv
        rn=(1.-1./(1.+(xt/a1)**2))/(1.+dexp(-r*xt))
        xt=2.*xt/a2
c
c       routine to calculate mod. bessel fn of the 2nd kind order2
c
        xt=dabs(xt)
        if(xt.gt.0.) go to 600
        res=2.0000000
        go to 250
  600   if(xt.gt.2.) go to 800
        t=xt/3.75
```

```
      ai=1.+3.5156229*t**2+3.0899424*t**4+1.2067492*t**6+
     1  .2659732*t**8+.0360768*t**10+.0045813*t**12
      ai1=.5+.87890594*t**2+.51498869*t**4+.15084934*t**6+
     1  .02658733*t**8+.00301532*t**10+.00032411*t**12
      xr=xt/2.
      ab1=1.+.15443144*xr**2-.67278579*xr**4-.18156897*xr**6
     1  -.01919402*xr**8-.00110404*xr**10-.00004686*xr**12+
     1  xt**2*dlog(xr) *ai1
      ab1=ab1*2.
      ab2=-ai*dlog(xr)-.57721566+.42278420*xr**2+.23069756*xr**4
     1  +.03488590*xr**6+.00262698*xr**8+.00010750*xr**10+
     1  .00000740*xr**12
      res=ab1+ab2*xt**2
      go to 250
  800 xr=2./xt
      ab1=1.25331414+.23498619*xr-.03655620*xr**2+.01504268*xr**3
     1  -.00780353*xr**4+.00325614*xr**5-.00068245*xr**6
      ab1=2.*ab1*xt**.5*dexp(-1.*xt)
      ab2=1.25331414-.07832358*xr+.02189568*xr**2-.01062446*xr**3
     1  +.00587872*xr**4-.00251540*xr**5+.00053208*xr**6
      ab2=ab2*xt**1.5*dexp(-1.*xt)
      res=ab1+ab2
  250 rn=rn*res
      over = rn
      return
      end
```

SUBROUTINE FOR U TRANSITIONS

```
      subroutine cal(xi,af)
      implicit real*8 (a-h,o-z)
      double precision a,xt,af,afot,afqt,r
      common sq(250),sqf(250),so(50),sof(50),a(10),afq(250),afo(50),
     1 nlq,nlo,r,afqt,afot
      afot=0.d0
c
c     quadrupolar contribution
c
      entry cal2(xi)
  850 afqt=0.d0
      if (nlq .le. 0) go to 221
      dx = xi - 5299.9
      r1 = a(4) / (1.0 +(dx/a(5))**2 + (dx/a(6))**4)
  851 do 220 j=1,nlq
c             xt=xi-sqf(j)+a(10)
              xt=xi-sqf(j)
              rn = quad(r,xt,a(7),a(8),a(9))
              rn = a(7) * sq(j) * quad(xt,r,a(8),a(9))
              afq(j)=rn
              afqt=afqt+rn
  220 continue
  221 af= r1 + afqt
 1000 return
      end
c
      real*8 function quad(dv,r,a1,a2)
      implicit real*8 (a-h,o-z)
      if (a2 . .gt. 0.0) then
              rn=1.0/(1.+(dv/a1)**2+(dv/a2)**4)
      else
              rn=1.0/(1.+(dv/a1)**2)
      end if
      quad = rn/(1.+dexp(-r*dv))
      return
      end
```

APPPENDIX B

Theoretically calculated relative and absolute intensities for quadrupolar transitions in the collision-induced spectra studied in this work.

TABLE B.1 Calculated Intensities for D_2 Transitions in the First Overtone Region at 77 K

Transition	Wavenumber (cm^{-1})	Relative Intensity	Absolute Intensity ($cm^{-1} amagat^{-2}$)	"Improved" Relative Intensity
$O_2(2)$	5689.4	.0309	.2048e-10	.0259
$O_0(2) + Q_2(0)$	5689.4	.0059	.3937e-11	.0108
$Q_1(1) + O_1(2)$	5806.1	.0172	.1142e-10	.0312
$Q_1(0) + O_1(2)$	5808.2	.0264	.1747e-10	.0477
$Q_0(J) + Q_2(2)$	5856.0	.0560	.3710e-10	.0551
$Q_0(J) + Q_2(1)$	5864.3	.2470	.1635e-09	.2338
$Q_0(J) + Q_2(0)$	5868.5	.0481	.3184e-10	.0870
$Q_1(2) + Q_1(2)$	5974.6	.0060	.3959e-11	.0108
$Q_1(1) + Q_1(2)$	5978.8	.0476	.3155e-10	.0862
$Q_1(0) + Q_1(2)$	5980.9	.0326	.2161e-10	.0590
$S_1(0) + O_1(2)$	5980.9	.0070	.4666e-11	.0127
$Q_1(1) + Q_1(1)$	5983.0	.0925	.6120e-10	.1672
$Q_1(0) + Q_1(1)$	5985.1	.1510	.9998e-10	.2731
$S_2(0)$	6035.0	1.0000	.6620e-09	.8357
$S_0(0) + Q_2(2)$	6035.0	.0313	.2072e-10	.0553
$S_0(0) + Q_2(1)$	6043.4	.1046	.6927e-10	.1831
$S_0(0) + Q_2(0)$	6047.5	.1688	.1118e-09	.3053
$S_2(1)$	6141.1	.3620	.2397e-09	.3026
$S_0(1) + Q_2(2)$	6153.5	.0110	.7282e-11	.0194
$S_1(0) + Q_1(2)$	6153.7	.1048	.6939e-10	.1895
$S_1(0) + Q_1(1)$	6157.9	.3547	.2348e-09	.6414
$S_1(0) + Q_1(0)$	6160.0	.5530	.3661e-09	1.0000
$S_0(1) + Q_2(1)$	6161.8	.0368	.2434e-10	.0643
$S_0(1) + Q_2(0)$	6166.0	.0593	.3927e-10	.1073
$S_0(0) + S_2(0)$	6214.1	.0241	.1596e-10	.0184
$S_2(2)$	6241.6	.0961	.6361e-10	.0803
$S_1(1) + Q_1(2)$	6265.8	.0328	.2170e-10	.0593
$S_1(1) + Q_1(1)$	6270.0	.1110	.7348e-10	.2007
$Q_1(0) + S_1(1)$	6272.1	.1726	.1143e-09	.3121
$S_0(2) + Q_2(1)$	6278.9	.0096	.6349e-11	.0168
$S_0(2) + Q_2(0)$	6283.1	.0155	.1024e-10	.0280
$S_1(0) + S_1(0)$	6332.7	.0591	.3911e-10	.1068
$S_1(2) + Q_1(2)$	6374.6	.0076	.5029e-11	.0137
$Q_1(1) + S_1(2)$	6378.8	.0257	.1704e-10	.0465
$Q_1(0) + S_1(2)$	6380.9	.0399	.2643e-10	.0722
$S_1(0) + S_1(1)$	6444.9	.0379	.2508e-10	.0685
$S_1(0) + S_1(2)$	6553.6	.0090	.5973e-11	.0163
$S_1(1) + S_1(1)$	6557.0	.0061	.4015e-11	.0110

TABLE B.2 . Calculated Intensities for D_2 Transitions in the First Overtone Region at 201 K

Transition	Wavenumber (cm^{-1})	Relative Intensity	Absolute Intensity ($cm^{-1} amagat^{-2}$)	"Improved" Relative Intensity
$O_2(4)$	5441.3	.0299	.9772e-11	.0299
$O_0(3) + Q_2(2)$	5558.4	.0080	.2633e-11	.0170
$Q_1(2) + O_1(4)$	5559.9	.0232	.7596e-11	.0503
$Q_1(1) + O_1(4)$	5564.1	.0168	.5497e-11	.0364
$Q_1(0) + O_1(4)$	5566.3	.0153	.5018e-11	.0332
$O_0(3) + Q_2(1)$	5566.8	.0057	.1873e-11	.0120
$O_2(3)$	5566.8	.0587	.1920e-10	.0587
$O_0(3) + Q_2(0)$	5570.9	.0055	.1802e-11	.0119
$O_0(2) + Q_2(3)$	5664.5	.0062	.2043e-11	.0132
$Q_1(3) + O_1(3)$	5675.0	.0079	.2578e-11	.0170
$O_0(2) + Q_2(2)$	5676.9	.0319	.1044e-10	.0674
$Q_1(2) + O_1(3)$	5681.3	.0404	.1322e-10	.0874
$O_0(2) + Q_2(1)$	5685.2	.0227	.7424e-11	.0475
$Q_1(1) + O_1(3)$	5685.5	.0292	.9565e-11	.0633
$Q_1(0) + O_1(3)$	5687.6	.0267	.8732e-11	.0578
$O_0(2) + Q_2(0)$	5689.4	.0218	.7145e-11	.0473
$Q_0(J) + O_2(2)$	5689.4	.2440	.7984e-10	.2442
$O_1(2) + Q_1(4)$	5787.2	.0136	.4441e-11	.0294
$O_1(2) + Q_1(3)$	5795.5	.0286	.9362e-11	.0619
$Q_1(2) + O_1(2)$	5801.8	.1467	.4800e-10	.3175
$Q_1(1) + O_1(2)$	5806.1	.1061	.3473e-10	.2297
$Q_1(0) + O_1(2)$	5808.2	.0969	.3171e-10	.2097
$Q_0(J) + Q_2(4)$	5827.0	.0411	.1344e-10	.0518
$Q_0(J) + Q_2(3)$	5843.5	.0880	.2879e-10	.1105
$Q_0(J) + Q_2(2)$	5856.0	.4730	.1548e-09	.5879
$S_1(0) + O_1(3)$	5860.3	.0071	.2332e-11	.0154
$Q_0(J) + Q_2(1)$	5864.3	.4362	.1428e-09	.5167
$Q_0(J) + Q_2(0)$	5868.5	.0705	.2306e-10	.1525
$Q_1(3) + Q_1(4)$	5953.6	.0058	.1899e-11	.0126
$Q_1(2) + Q_1(4)$	5959.9	.0307	.1005e-10	.0665
$Q_1(3) + Q_1(3)$	5962.0	.0062	.2024e-11	.0134
$Q_1(1) + Q_1(4)$	5964.1	.0262	.8585e-11	.0568
$Q_1(0) + Q_1(4)$	5966.2	.0102	.3321e-11	.0220
$Q_1(2) + Q_1(3)$	5968.3	.0655	.2142e-10	.1417
$Q_1(1) + Q_1(3)$	5972.5	.0558	.1826e-10	.1208
$Q_1(2) + Q_1(2)$	5974.6	.1730	.5661e-10	.3745
$Q_1(0) + Q_1(3)$	5974.6	.0219	.7169e-11	.0474
$Q_1(1) + Q_1(2)$	5978.8	.2933	.9599e-10	.6349

TABLE B.2 (continued)

$Q_1(0)+Q_1(2)$	5980.9	.1198	.3922e-10	.2594
$S_1(0)+Q_1(2)$	5980.9	.0259	.8468e-11	.0560
$Q_1(1)+Q_1(1)$	5983.0	.1211	.3963e-10	.2621
$Q_1(0)+Q_1(1)$	5985.1	.1180	.3861e-10	.2554
$S_0(0)+Q_2(4)$	6006.1	.0107	.3511e-11	.0227
$S_0(0)+Q_2(3)$	6022.6	.0225	.7363e-11	.0476
$S_2(0)$	6035.0	1.0000	.3272e-09	1.0000
$S_0(0)+Q_2(2)$	6035.0	.1149	.3761e-10	.2429
$S_0(0)+Q_2(1)$	6043.4	.0817	.2675e-10	.1712
$S_0(0)+Q_2(0)$	6047.5	.0787	.2574e-10	.1703
$S_1(1)+Q_1(2)$	6093.1	.0143	.4671e-11	.0309
$S_0(1)+Q_2(4)$	6124.5	.0063	.2069e-11	.0134
$S_1(0)+Q_1(4)$	6139.0	.0356	.1166e-10	.0771
$S_0(1)+Q_2(3)$	6141.1	.0133	.4338e-11	.0281
$S_2(1)$	6141.1	.6070	.1986e-09	.6072
$S_1(0)+Q_1(3)$	6147.4	.0751	.2457e-10	.1625
$S_1(1)+Q_2(2)$	6153.5	.0677	.2216e-10	.1431
$S_0(0)+Q_2(2)$	6153.7	.3848	.1259e-09	.8328
$S_1(0)+Q_1(1)$	6157.9	.2771	.9068e-10	.5998
$S_1(0)+Q_1(0)$	6160.0	.2577	.8432e-10	.5577
$S_0(1)+Q_2(1)$	6161.8	.0482	.1576e-10	.1009
$S_0(1)+Q_2(0)$	6166.0	.0463	.1516e-10	.1003
$S_1(2)+Q_1(2)$	6201.8	.0164	.5353e-11	.0354
$S_0(0)+S_2(0)$	6214.1	.0112	.3675e-11	.0103
$S_2(2)$	6241.6	.7568	.2477e-09	.7574
$S_0(2)+Q_2(4)$	6241.6	.0077	.2535e-11	.0164
$S_1(1)+Q_1(4)$	6251.1	.0187	.6111e-11	.0404
$S_0(2)+Q_2(3)$	6258.2	.0162	.5316e-11	.0344
$S_1(1)+Q_1(3)$	6259.5	.0394	.1288e-10	.0852
$S_1(1)+Q_1(2)$	6265.8	.2017	.6602e-10	.4367
$S_1(1)+Q_1(1)$	6270.0	.1454	.4758e-10	.3147
$S_0(2)+Q_2(2)$	6270.6	.0830	.2715e-10	.1754
$Q_1(0)+S_1(1)$	6272.1	.1348	.4413e-10	.2919
$S_0(2)+Q_2(1)$	6278.9	.0590	.1932e-10	.1236
$S_0(2)+Q_2(0)$	6283.1	.0568	.1858e-10	.1229
$S_1(0)+S_1(0)$	6332.7	.0275	.9007e-11	.0596
$S_2(3)$	6336.3	.1392	.4555e-10	.1394
$S_1(2)+Q_1(4)$	6359.9	.0203	.6654e-11	.0440
$S_1(2)+Q_1(3)$	6368.3	.0429	.1403e-10	.0928
$S_1(2)+Q_1(2)$	6374.6	.2197	.7190e-10	.4756
$Q_1(1)+S_1(2)$	6378.8	.1585	.5186e-10	.3430
$Q_1(0)+S_1(2)$	6380.9	.1465	.4795e-10	.3172
$S_0(3)+Q_2(2)$	6385.9	.0152	.4957e-11	.0320
$S_0(3)+Q_2(1)$	6394.2	.0108	.3527e-11	.0226
$S_0(3)+Q_2(0)$	6398.4	.0104	.3391e-11	.0224
$S_2(4)$	6424.7	.0648	.2120e-10	.0649
$S_1(0)+S_1(1)$	6444.9	.0296	.9687e-11	.0641
$S_1(3)+Q_1(3)$	6473.1	.0069	.2265e-11	.0150
$Q_1(2)+S_1(3)$	6479.4	.0355	.1162e-10	.0768

TABLE B.2 (continued)

$Q_1(1) + S_1(3)$	6483.6	.0257	.8409e-11	.0556
$Q_1(0) + S_1(3)$	6485.7	.0235	.7677e-11	.0508
$S_0(4) + Q_2(2)$	6498.8	.0069	.2265e-11	.0146
$S_0(4) + Q_2(1)$	6507.1	.0049	.1612e-11	.0103
$S_0(4) + Q_2(0)$	6511.3	.0047	.1550e-11	.0103
$S_1(0) + S_1(2)$	6553.6	.0331	.1084e-10	.0717
$S_1(1) + S_1(1)$	6557.0	.0079	.2600e-11	.0172
$Q_1(2) + S_1(4)$	6579.9	.0141	.4622e-11	.0306
$Q_1(1) + S_1(4)$	6584.1	.0102	.3345e-11	.0221
$Q_1(0) + S_1(4)$	6586.2	.0093	.3053e-11	.0202
$S_1(0) + S_1(3)$	6658.5	.0060	.1962e-11	.0130
$S_1(1) + S_1(2)$	6665.8	.0178	.5808e-11	.0384
$S_1(2) + S_1(2)$	6774.5	.0099	.3238e-11	.0214

TABLE B.3 Calculated Intensities for D_2 Transitions in the First Overtone Region at 295 K

Transition	Wavenumber (cm^{-1})	Relative Intensity	Absolute Intensity ($cm^{-1} amagat^{-2}$)	"Improved" Relative Intensity
$O_2(4)$	5441.3	.1016	.2823e-10	.1016
$O_0(4) + Q_2(2)$	5441.3	.0155	.4293e-11	.0326
$O_0(4) + Q_2(1)$	5449.6	.0083	.2310e-11	.0174
$O_0(4) + Q_2(0)$	5453.8	.0070	.1953e-11	.0152
$Q_1(4) + O_1(4)$	5545.3	.0200	.5567e-11	.0433
$O_0(3) + Q_2(3)$	5546.0	.0049	.1370e-11	.0104
$Q_1(3) + O_1(4)$	5553.6	.0245	.6797e-11	.0529
$O_0(3) + Q_2(2)$	5558.4	.0169	.4692e-11	.0357
$Q_1(2) + O_1(4)$	5559.9	.0841	.2337e-10	.1820
$Q_1(1) + O_1(4)$	5564.1	.0461	.1279e-10	.0996
$Q_1(0) + O_1(4)$	5566.3	.0369	.1026e-10	.0799
$O_2(3)$	5566.8	.1156	.3212e-10	.1156
$O_0(3) + Q_2(1)$	5566.8	.0091	.2525e-11	.0190
$O_0(3) + Q_2(0)$	5570.9	.0077	.2134e-11	.0166
$O_0(2) + Q_2(4)$	5647.9	.0108	.2998e-11	.0228
$O_0(2) + Q_2(3)$	5664.5	.0131	.3641e-11	.0277
$Q_1(3) + O_1(4)$	5666.6	.0202	.5610e-11	.0437
$Q_1(3) + O_1(3)$	5675.0	.0247	.6849e-11	.0533
$O_0(2) + Q_2(2)$	5676.9	.0449	.1247e-10	.0948
$Q_1(2) + O_1(3)$	5681.3	.0848	.2355e-10	.1834
$O_0(2) + Q_2(1)$	5685.2	.0242	.6710e-11	.0505
$Q_1(1) + O_1(3)$	5685.5	.0464	.1289e-10	.1004
$Q_1(0) + O_1(3)$	5687.6	.0372	.1034e-10	.0805
$O_0(2) + Q_2(0)$	5689.4	.0204	.5674e-11	.0442
$O_2(2)$	5689.4	.3225	.8958e-10	.3225
$S_1(0) + O_1(4)$	5739.0	.0099	.2740e-11	.0213
$O_1(2) + Q_1(4)$	5787.2	.0492	.1366e-10	.1064
$O_1(2) + Q_1(3)$	5795.5	.0600	.1668e-10	.1299
$Q_1(2) + O_1(2)$	5801.8	.2065	.5735e-10	.4465
$Q_1(1) + O_1(2)$	5806.1	.1130	.3139e-10	.2444
$Q_1(0) + O_1(2)$	5808.2	.0906	.2518e-10	.1961
$Q_0(J) + Q_2(4)$	5827.0	.1415	.3932e-10	.1802
$Q_0(J) + Q_2(3)$	5843.5	.1756	.4877e-10	.2225
$S_1(1) + O_1(4)$	5851.2	.0062	.1720e-11	.0134
$Q_0(J) + Q_2(2)$	5856.0	.6327	.1757e-09	.7928
$S_1(0) + O_1(3)$	5860.3	.0099	.2761e-11	.0215
$Q_0(J) + Q_2(1)$	5864.3	.4401	.1223e-09	.5248
$Q_0(J) + Q_2(0)$	5868.5	.0655	.1820e-10	.1417

TABLE B.3 (continued)

$Q_1(4) + Q_1(4)$	5945.2	.0127	.3527e-11	.0275
$Q_1(3) + Q_1(4)$	5953.6	.0314	.8710e-11	.0678
$Q_1(2) + Q_1(4)$	5959.9	.1113	.3092e-10	.2408
$S_1(2) + O_1(4)$	5959.9	.0094	.2606e-11	.0203
$Q_1(3) + Q_1(3)$	5962.0	.0194	.5377e-11	.0419
$Q_1(1) + Q_1(4)$	5964.1	.0719	.1998e-10	.1556
$Q_1(0) + Q_1(4)$	5966.2	.0245	.6792e-11	.0529
$Q_1(2) + Q_1(3)$	5968.3	.1374	.3816e-10	.2972
$S_1(1) + O_1(3)$	5972.5	.0062	.1734e-11	.0135
$Q_1(1) + Q_1(3)$	5972.5	.0886	.2461e-10	.1916
$Q_1(2) + Q_1(2)$	5974.6	.2435	.6764e-10	.5267
$Q_1(0) + Q_1(3)$	5974.6	.0306	.8490e-11	.0661
$Q_1(1) + Q_1(2)$	5978.8	.3123	.8676e-10	.6755
$Q_1(0) + Q_1(2)$	5980.9	.1121	.3114e-10	.2425
$S_1(0) + O_1(2)$	5980.9	.0242	.6725e-11	.0524
$Q_1(1) + Q_1(1)$	5983.0	.0975	.2710e-10	.2110
$Q_1(0) + Q_1(1)$	5985.1	.0835	.2319e-10	.1806
$S_0(0) + Q_2(4)$	6006.1	.0258	.7180e-11	.0547
$S_0(0) + Q_2(3)$	6022.6	.0314	.8720e-11	.0664
$S_0(0) + Q_2(2)$	6035.0	.1075	.2986e-10	.2271
$S_2(0)$	6035.0	.8783	.2440e-09	.8776
$S_0(0) + Q_2(1)$	6043.4	.0578	.1607e-10	.1211
$S_0(0) + Q_2(0)$	6047.5	.0489	.1359e-10	.1058
$S_1(2) + O_1(3)$	6081.2	.0095	.2626e-11	.0204
$S_1(1) + O_1(2)$	6093.1	.0152	.4221e-11	.0329
$S_0(1) + Q_2(4)$	6124.5	.0173	.4814e-11	.0367
$S_1(0) + Q_1(4)$	6139.0	.0858	.2384e-10	.1856
$S_0(1) + Q_2(3)$	6141.1	.0211	.5847e-11	.0445
$S_2(1)$	6141.1	.6067	.1685e-09	.6064
$S_1(0) + Q_1(3)$	6147.4	.1048	.2910e-10	.2266
$S_0(1) + Q_2(2)$	6153.5	.0721	.2002e-10	.1522
$S_1(0) + Q_1(2)$	6153.7	.3600	.9999e-10	.7785
$S_1(0) + Q_1(1)$	6157.9	.1961	.5448e-10	.4242
$S_1(0) + Q_1(0)$	6160.0	.1602	.4451e-10	.3465
$S_0(1) + Q_2(1)$	6161.8	.0388	.1078e-10	.0812
$S_0(1) + Q_2(0)$	6166.0	.0328	.9110e-11	.0709
$S_1(2) + O_1(2)$	6201.8	.0230	.6395e-11	.0498
$S_2(2)$	6241.6	1.0000	.2778e-09	1.0000
$S_0(2) + Q_2(4)$	6241.6	.0281	.7799e-11	.0594
$S_1(1) + Q_1(4)$	6251.1	.0512	.1422e-10	.1107
$S_0(2) + Q_2(3)$	6258.2	.0341	.9472e-11	.0721
$S_1(1) + Q_1(3)$	6259.5	.0625	.1736e-10	.1352
$S_1(1) + Q_1(2)$	6265.8	.2148	.5967e-10	.4646
$S_1(1) + Q_1(1)$	6270.0	.1171	.3253e-10	.2533
$S_0(2) + Q_2(2)$	6270.6	.1168	.3244e-10	.2466
$Q_1(0) + S_1(1)$	6272.1	.0954	.2651e-10	.2064
$S_0(2) + Q_2(1)$	6278.9	.0628	.1746e-10	.1315
$S_0(2) + Q_2(0)$	6283.1	.0531	.1476e-10	.1149
$O_1(2) + S_1(3)$	6306.6	.0067	.1858e-11	.0145

TABLE B.3 (continued)

$S_1(0)+S_1(0)$	6332.7	.0171	.4754e-11	.0370
$S_2(3)$	6336.3	.2743	.7619e-10	.2745
$S_0(3)+Q_2(4)$	6356.9	.0076	.2123e-11	.0162
$S_1(2)+Q_1(4)$	6359.9	.0737	.2047e-10	.1594
$S_1(2)+Q_1(3)$	6368.3	.0900	.2499e-10	.1946
$S_0(3)+Q_1(3)$	6373.4	.0093	.2578e-11	.0196
$S_1(2)+Q_1^2(2)$	6374.6	.3093	.8590e-10	.6689
$Q_1(1)+S_1(2)$	6378.8	.1687	.4687e-10	.3649
$Q_1(0)+S_1(2)$	6380.9	.1371	.3808e-10	.2965
$S_0(3)+Q_2(2)$	6385.9	.0318	.8832e-11	.0671
$S_0(3)+Q_2^2(1)$	6394.2	.0171	.4753e-11	.0358
$S_0(3)+Q_2^2(0)$	6398.4	.0145	.4016e-11	.0313
$S_2(4)$	6424.7	.2204	.6122e-10	.2208
$S_1(0)+S_1(1)$	6444.9	.0210	.5819e-11	.0453
$S_1(3)+Q_1(4)$	6464.7	.0178	.4929e-11	.0384
$S_0(4)+Q_2(4)$	6469.8	.0060	.1675e-11	.0128
$S_1(3)+Q_1(3)$	6473.1	.0217	.6019e-11	.0469
$Q_1(2)+S_1(3)$	6479.4	.0745	.2070e-10	.1612
$Q_1(1)+S_1(3)$	6483.6	.0408	.1133e-10	.0882
$Q_1(0)+S_1(3)$	6485.7	.0327	.9091e-11	.0708
$S_0(4)+Q_2(3)$	6486.4	.0073	.2035e-11	.0155
$S_0(4)+Q_2^2(2)$	6498.8	.0251	.6969e-11	.0530
$S_0(4)+Q_2^2(1)$	6507.1	.0135	.3750e-11	.0282
$S_0(4)+Q_2^2(0)$	6511.3	.0114	.3170e-11	.0247
$S_0(0)+S_1^2(2)$	6553.6	.0310	.8608e-11	.0670
$S_1(1)+S_1(1)$	6557.0	.0064	.1778e-11	.0138
$S_1(4)+Q_1(4)$	6565.2	.0122	.3387e-11	.0264
$Q_1(3)+S_1(4)$	6573.6	.0149	.4136e-11	.0322
$Q_1(2)+S_1(4)$	6579.9	.0512	.1422e-10	.1107
$Q_1(1)+S_1(4)$	6584.1	.0280	.7784e-11	.0606
$Q_1(0)+S_1(4)$	6586.2	.0225	.6244e-11	.0486
$S_1(0)+S_1(3)$	6658.5	.0084	.2323e-11	.0181
$S_1(1)+S_1(2)$	6665.8	.0189	.5250e-11	.0409
$S_1(0)+S_1(4)$	6758.9	.0060	.1667e-11	.0130
$S_1(1)+S_1(3)$	6770.6	.0051	.1408e-11	.0110
$S_1(2)+S_1(2)$	6774.5	.0139	.3869e-11	.0301
$S_1(2)+S_1(3)$	6879.4	.0074	.2062e-11	.0161
$S_1(2)+S_1(4)$	6979.8	.0057	.1586e-11	.0124

TABLE B.4 Calculated Intensities for H_2 Transitions in the Second Overtone Region at 77 K

Transition	Wavenumber (cm^{-1})	Relative Intensity	Absolute Intensity ($cm^{-1}amagat^{-2}$)
$Q_0(J)+Q_3(1)$	11764.9	.4722	.1812e-10
$Q_0(J)+Q_3(0)$	11782.4	.0278	.1068e-11
$Q_0(J)+S_3(0)$	12084.6	.4558	.1749e-10
$S_0(0)+Q_3(1)$	12119.3	.0866	.3325e-11
$S_0(0)+Q_3(0)$	12136.7	.0230	.8843e-12
$Q_1(1)+Q_2(1)$	12230.6	.4330	.1662e-10
$Q_1(0)+Q_2(1)$	12236.5	.0831	.3189e-11
$Q_1(1)+Q_2(0)$	12242.3	.0475	.1821e-11
$S_3(1)$	12265.5	1.0000	.3838e-10
$S_0(1)+Q_3(1)$	12352.0	.1584	.6080e-11
$S_0(1)+Q_3(0)$	12369.4	.0421	.1616e-11
$S_0(0)+S_3(0)$	12439.0	.0121	.4653e-12
$Q_1(1)+S_2(0)$	12561.6	.2616	.1004e-10
$Q_1(0)+S_2(0)$	12567.5	.0740	.2839e-11
$S_1(0)+Q_2(1)$	12573.1	.1212	.4652e-11
$S_1(0)+Q_2(0)$	12584.8	.0311	.1195e-11
$S_0(0)+S_3(1)$	12619.9	.0212	.8142e-12
$S_0(1)+S_3(0)$	12671.7	.0223	.8541e-12
$Q_1(1)+S_2(1)$	12759.5	.4945	.1898e-10
$Q_1(0)+S_2(1)$	12765.4	.1383	.5308e-11
$S_1(1)+Q_2(1)$	12788.2	.1889	.7248e-11
$S_1(1)+Q_2(0)$	12799.9	.0477	.1832e-11
$S_0(1)+S_3(1)$	12852.6	.0390	.1495e-11
$S_1(0)+S_2(0)$	12904.2	.0266	.1022e-11
$S_1(0)+S_2(1)$	13102.1	.0536	.2056e-11
$S_1(1)+S_2(0)$	13119.3	.0437	.1676e-11
$S_1(1)+S_2(1)$	13317.1	.0876	.3361e-11

TABLE B.5 Calculated Intensities for D_2 Transitions in the Second Overtone Region at 77 K

Transition	Wavenumber (cm^{-1})	Relative Intensity	Absolute Intensity ($cm^{-1} amagat^{-2}$)
$Q_0(J) + Q_3(2)$	8607.0	.0445	.5153e-12
$Q_0(J) + Q_3(1)$	8619.5	.1935	.2239e-11
$Q_0(J) + Q_3(0)$	8625.7	.0377	.4357e-12
$Q_1(0) + Q_2(2)$	8683.0	.0132	.1525e-12
$S_3(0)$	8786.1	1.0000	.1157e-10
$S_0(0) + Q_3(2)$	8786.1	.0245	.2834e-12
$S_0(0) + Q_3(1)$	8798.5	.0818	.9459e-12
$S_0(0) + Q_3(0)$	8804.8	.1322	.1529e-11
$Q_1(1) + Q_2(2)$	8847.5	.0227	.2623e-12
$Q_1(0) + Q_2(2)$	8849.6	.0203	.2345e-12
$Q_1(2) + Q_2(1)$	8851.6	.0246	.2847e-12
$Q_1(2) + Q_2(0)$	8855.8	.0117	.1352e-12
$Q_1(1) + Q_2(1)$	8855.8	.0918	.1062e-11
$Q_1(0) + Q_2(1)$	8857.9	.0934	.1081e-11
$Q_1(1) + Q_2(0)$	8860.0	.0541	.6257e-12
$S_3(1)$	8886.0	.4123	.4770e-11
$S_0(1) + Q_3(1)$	8917.0	.0287	.3323e-12
$S_0(1) + Q_3(0)$	8923.2	.0464	.5373e-12
$S_0(0) + S_3(0)$	8965.2	.0217	.2506e-12
$S_3(2)$	8978.3	.1224	.1416e-11
$S_1(0) + Q_2(2)$	9022.3	.0399	.4619e-12
$Q_1(2) + S_2(0)$	9022.3	.0808	.9352e-12
$Q_1(1) + S_2(0)$	9026.5	.2733	.3162e-11
$Q_1(0) + S_2(0)$	9028.7	.4273	.4943e-11
$S_1(0) + Q_2(1)$	9030.7	.1376	.1592e-11
$S_1(0) + Q_2(0)$	9034.8	.1980	.2291e-11
$S_0(2) + Q_3(0)$	9040.4	.0121	.1401e-12
$Q_1(2) + S_2(1)$	9128.4	.0292	.3378e-12
$Q_1(1) + S_2(1)$	9132.6	.0986	.1141e-11
$S_1(1) + Q_2(2)$	9134.5	.0125	.1452e-12
$Q_1(0) + S_2(1)$	9134.7	.1547	.1790e-11
$S_1(1) + Q_2(1)$	9142.8	.0433	.5013e-12
$S_1(1) + Q_2(0)$	9147.0	.0618	.7151e-12
$S_1(0) + S_2(0)$	9201.4	.0920	.1064e-11
$Q_1(1) + S_2(2)$	9233.1	.0261	.3018e-12
$Q_1(0) + S_2(2)$	9235.3	.0411	.4752e-12
$S_1(2) + Q_2(1)$	9251.6	.0101	.1170e-12
$S_1(2) + Q_2(0)$	9255.7	.0143	.1654e-12

TABLE B.5 (continued)

$S_1(0)+S_2(1)$	9307.4	.0319	.3687e-12
$S_1(1)+S_2(0)$	9313.6	.0304	.3518e-12
$S_1(1)+S_2(1)$	9419.6	.0105	.1220e-12

REFERENCES

Birnbaum, A. and Poll, J. D., J. Atmos. Sci. **26** , 943 (1969).

Birnbaum, G., and Cohen, E.R., Can. J. Phys. **54** , 593 (1976).

Birnbaum, G., Gulliot, B. and Bratos, S., Adv. Chem. Phys. **51** , 49 (1982).

Chang, K.S., Ph.D Thesis, Memorial University of Newfoundland, St. John's, Newfoundland (1974).

Chisholm, D.A., MacDonald, J.C.F., Crawford, M.F. and Welsh, H.L., Phys. Rev. **88** , 957 (1952).

Crawford, M.F., Welsh, H.L. and Locke, J.L., Phys. Rev. **75** , 1607 (1949).

Crawford, M.F., Welsh, H.L., MacDonald, J.C.F. and Locke, J.L., Phys. Rev. **80** , 469 (1950).

De Remigis, J., MacTaggart, J.W. and Welsh, H.L., Can. J. Phys. **49** , 381 (1971).

Downie, A.R., Magoon, M.C., Purcell, T. and Crawford, B., J. Opt. Soc. Amer. **43** , 941 (1953).

Fink, U., Wiggins T.A. and Rank D.A., J. Mol. Spect. **18** , 384 (1965).

Foltz, J.V., Rank, D.H. and Wiggins, T.A., J. Mol. Spect. **21** , 203 (1966).

Gibbs, P.W., Gray, C.G., Hunt, J.L., Reddy, S.P., Tipping, R.H. and Chang, K.S., Phys. Rev. Lett. **33** , 256 (1974).

Goorvitch, D., Silvaggio, P.M., and Boese, R.W. J. Quant. Spectrosc. Radiat. Transfer **25** , 237 (1981).

Hare, W.F.J. and Welsh, H.L., Can. J. Phys. **36** , 88 (1958).

Herzberg, G., J. Roy. Astron. Soc. Can. **45** ,100 (1951).

Herzberg, G., Astrophysics J. **109** ,115 (1952).

Humphreys, C. J., J. Opt. Soc. Amer. **43** ,1027 (1953).

Hunt, J. L. and Welsh, H. L., Can. J. Phys. **42** , 873 (1964).

IUPC Tables of Wavenumbers for Calibration of Infrared Spectrometers 2nd. ed., edited by A. R. H. Cole, Pergamon (1977).

Karl, G. and Poll, J.D., J. Chem. Phys. **46** , 2944 (1967).

Karl, G., Poll, J. D. and Wolniewicz, L., Can. J. Phys. **19** , 1781 (1975).

Kiss, Z.K. and Welsh, H.L., Can. J. Phys. **37** , 1249 (1959).

Kuiper, G. P., Astrophysics J. **109** , 540 (1949).

Levine, H.B. and Birnbaum, G., Phys. Rev. **154** , 172 (1967).

Lewis, J. C. and Van Kranendonk, J., Phys. Rev. Lett. **24** , 802, (1971).

Lewis, J. C. and Van Kranendonk, J., Can. J. Phys. **50** , 2881, (1972).

Lewis, J. C. and Van Kranendonk, J., Can. J. Phys. **50** , 2902, (1972).

Lewis, J. C. and Van Kranendonk, J., Can. J. Phys. **50** , 352, (1972).

Lewis, J.C., Physica A **82** , 500 (1976).

Lewis, J. C. and Tjon, J. A., Physica A **91** ,161 (1978).

Lewis, J.C., Private communication (1983).

Mactaggart, J.W. and Hunt, J.L., Can. J. Phys. **47** , 65 (1969).

Mactaggart, J.W., De Remegis, J. and Welsh, H.L., Can. J. Phys. **51** , 1971 (1973).

Mactaggart, J.W. and Welsh, H.L., Can. J. Phys. **51** , 158 (1973).

McCarty, R.D., Hord, J. and Roder, H.M., Natl. Bur. Standards Monograph **168** (1981).

McKellar, A.R.W. and Welsh, H.L., Proc. Roy. Soc. London **A322** , 421 (1971).

McKellar, A.R.W. and Oka, T., Can. J. Phys. **56** , 1315 (1978).

Michels, A., De Graaff, W., Wassennaar, T., Levelt, J.M.H., and Louwerse, P., Physica **25** , 25 (1959).

Penney, R.J., M.Sc. Thesis, Memorial University of Newfoundland, St. John's, Newfoundland (1980).

Penney, R.J., Prasad, R.D.G. and Reddy, S.P., J. Chem. Phys. **77** , 131 (1982).

Plyler, E.K., Gallar, N.M. and Wiggins, T.A., J. Res. Natl. Bur. Standards, **48** , 221 (1952).

Poll, J.D., **Proceedings I.A.U. Symposium 40 on Planetary Atmospheres** (Reidel, Dordrecht), 384 (1971).

Poll, J. D., Ph.D. thesis, University of Toronto (1960).

Poll, J. D., Hunt, J. L. and Mactaggart, J. W., Can. J. Phys. **53**, 954 (1975).

Poll, J.D. and Wolniewicz, L., J. Chem. Phys. **68**, 3053 (1978).

Poll, J. D., 1983 private communication

Prasad, R. D. G., Clouter, M. J. and Reddy, S. P., Phys. Rev. **A17**, 1690 (1978).

Prasad, R.D.G., Ph.D. Thesis, Memorial University of Newfoundland, St. John's Newfoundland (1976).

Rao, K. N., Humphreys, C. J. and Rank, D. H., **Wavelength Standards in the Infrared** A. P., New York (1966).

Reddy, S.P. and Kuo, C.Z., J. Mol. Spectrosc. **37**, 327 (1971).

Reddy, S.P., Varghese, G. and Prasad R.D.G., Phys. Rev. A **15**, 975 (1977).

Reddy, S.P. and Prasad, R.D.G., J. Chem. Phys. **66**, 5259 (1977).

Reddy, S.P., Sen, A. and Prasad, R.D.G., J. Chem. Phys. **72**, 6102 (1980).

Rich, N.H. and McKellar, A.R.W., Can. J. Phys. **54**, 486 (1976).

Sen, A., Prasad, R.D.G. and Reddy, S.P., J. Chem. Phys. **72**, 1716 (1980).

Silvaggio, P.M., Goorvitch, D. and Boese, R.W., J. Quant. Spectrosc Radiat. Transfer **26**, 103 (1981).

Van Kranendonk, J., Physica **23**, 825 (1957).

Van Kranendonk, J., Physica **24**, 347 (1958).

Van Kranendonk, J., Physica **25**, 337 (1959).

Van Kranendonk, J., Can. J. Phys. **46**, 1173 (1968).

Van Kranendonk, J., Physica **73**, 156 (1974).

van Nostrand, E. M.Sc. Thesis, Memorial University of Newfoundland (1983).

Watanabe, A. and Welsh, H.L., Can. J. Phys. **43**, 818 (1965).

Watanabe, A. and Welsh, H.L., Can. J. Phys. **45**, 2859 (1967).

Watanabe, A., Can. J. Phys. **49**, 1320 (1971).

Watanabe, A., Hunt, J.L. and Welsh, H.L., Can. J. Phys. **49**, 860 (1971).

Welsh, H. L. and Hunt, J. L., J. Quant. Spect. Rad. Trans. **3**, 385 (1963).

Welsh, H.L., Crawford, M.F. and Locke, J.L., Phys. Rev. **76**, 580 (1949).

Welsh, H.L., Crawford, M.F., MacDonald, J.C.F. and Chishlom, D.A., Phys. Rev. **83**, 1264 (1951).

Welsh, H.L., **MTP International Review of Science, Physical Chemistry, Vol. 3, Spectroscopy**, edited by D.A. Ramsay (Butterworths, London) (1972) and references therein.

Zaidel, A.N., Prokofer, V.K., Raisku, S.M., Slavnyi, V.A. and Shreider, E.Ya., **Tables of Spectral Lines** (IFI/Plenum, New York-London.) (1970).

Zaidi, H.R. and Van Kranendonk, J., Can. J. Phys. **49**, 385 (1971).